NASA TECHNICAL NOTE

NASA TN D-4815

DETAILED DESCRIPTION AND RESULTS OF A METHOD FOR COMPUTING MEAN AND FLUCTUATING QUANTITIES IN TURBULENT BOUNDARY LAYERS

by Ivan E. Beckwith and Dennis M. Bushnell

Langley Research Center
Langley Station, Hampton, Va.

DETAILED DESCRIPTION AND RESULTS OF A METHOD

FOR COMPUTING MEAN AND FLUCTUATING QUANTITIES IN

TURBULENT BOUNDARY LAYERS

By Ivan E. Beckwith and Dennis M. Bushnell

Langley Research Center
Langley Station, Hampton, Va.

NATIONAL AERONAUTICS AND SPACE ADMINISTRATION

DETAILED DESCRIPTION AND RESULTS OF A METHOD

FOR COMPUTING MEAN AND FLUCTUATING QUANTITIES IN

TURBULENT BOUNDARY LAYERS

By Ivan E. Beckwith and Dennis M. Bushnell
Langley Research Center

SUMMARY

The conservation equations for mass, mean momentum, and turbulent kinetic energy for the incompressible turbulent boundary layer have been solved by an implicit finite-difference procedure. Mathematical models developed by Glushko (Bull. Acad. Sci. USSR, Mech. Ser., no. 4, 1965) for the production, dissipation, and diffusion of the turbulent kinetic energy in the flat-plate turbulent boundary layer have been modified and used to calculate a nonequilibrium turbulent boundary layer subjected initially to a large adverse pressure gradient followed by a run of constant pressure.

Comparisons of both mean and fluctuating flow properties have indicated generally good agreement between the calculated results and experimental measurements of Goldberg (MIT Rep. No. 85, 1966). The best overall agreement with data was obtained by reducing the scale of turbulence in the outer part of the boundary layer to about 70 percent of the flat-plate values as used by Glushko. The calculations have indicated that further simple modifications to the turbulence scale function and to some of the mathematical models for the turbulence correlation terms should improve the accuracy of predictions for the Goldberg data. The present authors have shown (paper presented at 1968 Conference on Computation Methods in Turbulent Boundary Layers at Stanford University, Aug. 1968) that predictions in good agreement with data were obtained for other arbitrary pressure distributions.

INTRODUCTION

The basic assumption in conventional methods for the calculation of turbulent flows is that the mean values of products of the fluctuating characteristics of the flow are related in some unique manner to the mean flow properties. Such relations between these correlations of fluctuating flow quantities and the mean flow cannot be determined solely from theoretical analysis. In the Reynolds equations of mean motion, this problem of relating the correlations to the mean flow has generally been met by introducing more or less arbitrary assumptions for the Reynolds stress terms (ref. 1, pp. 277-293). In 1945, Prandtl, Nevzgljadov, and Chou (refs. 2 to 5) reported on independent investigations

intended to develop a more rigorous approach to this problem. These investigations were based on the idea of using independent differential equations to describe the dynamics of the correlations for the turbulent velocity fluctuations. The correlation equations are derived (ref. 1, pp. 250-260, for example) from the Navier-Stokes equations of motion and contain terms for double velocity correlations (Reynolds stress and turbulence kinetic energy terms), triple velocity correlations, and correlations of velocity and pressure fluctuations.

In 1951 Rotta (ref. 6) extended the work of Prandtl (ref. 2), and, in particular, that of Chou (refs. 4 and 5), in considerable detail; his work was based on advances in theory and new data not available during the earlier investigations of 1945. (See also discussion in ref. 7, pp. 43-54.) These methods were developed further and applied to various types of simple flows as described in references 8 to 11. An integral form of the turbulence energy equation was utilized by McDonald (ref. 12) to compute the mean profiles by an integral method.

Kovasznay and Nee (refs. 13 and 14) assumed that the effective total viscosity obeys a "rate equation" expressing the "conservation" of the total viscosity. Harlow and Nakayama (ref. 15) gave a more formal derivation (based on the equation for the turbulence kinetic energy) of a rate equation for the eddy viscosity and also constructed a "transport" equation for the scale of turbulence by analogy with Brownian motion. The same authors (ref. 16) have since derived a new transport equation for the dissipation function. Since this function depends on the scale of turbulence, their new equation and their previous rate equation for the eddy viscosity were proposed as the basic equations for a general method of computing turbulent shear flows.

In all the investigations mentioned, except the integral method of McDonald, assumptions regarding the relative magnitudes of the various fluctuating quantities were made in order to simplify and obtain solutions to the nonlinear equations involved. Consequently, these methods were applied mostly to simple flows or portions of simple flows where some terms in the correlation equations could be neglected. Hence, the mathematical formulations of remaining terms representing the fluctuating quantities could not be tested for their degree of generality. In the integral method of McDonald, it is still not possible to test the detailed spatial variations of these formulations and the turbulent diffusion terms drop out completely upon integration across a shear layer.

The answer to these difficulties is, of course, to obtain numerical solutions of the complete equations with automatic computing machines. Such solutions have been given recently by Glushko (ref. 17), Bradshaw, Ferriss, and Atwell (ref. 18), and Nash (ref. 19). In the methods of references 18 and 19, the molecular shear is neglected; it was therefore necessary to provide the correct wall boundary condition by incorporating the "law-of-the-wall" relation between velocity and wall shear. Glushko, on the other hand, kept all the

viscous terms and used formulations with essentially correct limiting forms at the wall. It might be expected that this latter approach would therefore be somewhat more general than that of Bradshaw in that sudden changes in wall-boundary conditions could be negotiated and the extension to compressible flows where the law-of-the-wall relation may not be generally applicable should give better results. The only computation presented by Glushko, however, was for the flat plate; again, the degree of generality of his assumptions for the fluctuating flow parameters could not be determined.

The primary purpose of the present paper is to test the method of Glushko in a non-equilibrium adverse-pressure-gradient flow and to determine whether his formulations of the turbulence quantities based primarily on flat-plate data result in satisfactory predictions for the mean properties of this more complex flow. Since the ultimate success of these methods depends on the assumptions for the fluctuating properties, comparisons of values from numerical solutions for these quantities with experimental data are also made. Except for shear profiles in references 14, 18, and 19, and turbulent kinetic energy profiles in reference 17, such comparisons for boundary-layer flows have not been published yet. The work reported herein is part of a general investigation intended to develop these methods for application to compressible flows.

This paper includes an appendix by Carolyn C. Thomas, of the Langley Research Center. This appendix presents a description and listing of the digital computer program.

SYMBOLS

A_n, B_n, C_n, D_n functions in linearized finite-difference form of momentum equation (eq. (B13))

$\hat{A}_n, \hat{B}_n, \hat{C}_n, \hat{D}_n$ functions in linearized finite-difference form of energy equation (eq. (B27))

C constant in model of turbulent dissipation term (eq. (12))

$\left.\begin{array}{l} C_1, C_2, C_3, C_4, C_5, C_6 \\ C', C_1', C_2', C_3', C_6' \end{array}\right\}$ constants used in appendix A

C_f local skin friction, $\dfrac{\mu \left(\dfrac{\partial \bar{u}_1}{\partial x_2}\right)_w}{\dfrac{1}{2}\rho U_e^2}$

3

D   dimensionless diffusion and dissipation function $1 + \alpha \kappa R H(\kappa R)$ (eq. (19))

E   turbulent kinetic-energy profile function, $\bar{e}/U_e^2$

E_0^* constant in expression used for initial E profile (eq. (31a))

e   instantaneous turbulent kinetic energy per unit mass, $\frac{1}{2}\left(u_1'^2 + u_2'^2 + u_3'^2\right)$

$\bar{e}$ mean turbulent kinetic energy per unit mass, $\frac{1}{2}\left(\overline{u_1'^2} + \overline{u_2'^2} + \overline{u_3'^2}\right)$

F   velocity profile function, $\bar{u}_1/U_e$

f   factor in $\Delta\xi$ expression used for flat-plate solutions (see expression (31b))

G_n, g_n functions required to calculate F_{m+1} (eq. (B16))

H(R)   eddy viscosity function (eq. (9b))

H^* shape factor, δ^*/θ

K   factor for variable $\Delta\eta$ step size, $\Delta\eta_n/\Delta\eta_{n-1}$

$$\bar{K} = \frac{2}{1 + K}$$

$$K^* = \frac{2K}{1 + K}$$

k   exponent in $\Delta\xi$ expression used for flat-plate solutions (see expression (31b))

l characteristic mean scales of turbulent motion

M   dimensionless total viscosity function $1 + \alpha R H(R)$ (eq. (19))

m,n   computing grid location (see sketch in appendix B)

N   maximum value of n

$\bar{n}$ exponent in definition of η (eq. (22))

p   pressure

4

p' fluctuation in pressure, $p - \bar{p}$

$\bar{p}$ mean pressure

R turbulent Reynolds number, $\dfrac{\sqrt{\bar{e}}\,l}{\nu}$

R_0 constant in models of turbulent terms (eq. (9))

R_{x_1} Reynolds number based on x_1, $\dfrac{U_e x_1}{\nu}$

R_δ Reynolds number based on δ, $\dfrac{U_e \delta}{\nu}$

R_θ Reynolds number based on θ, $\dfrac{U_e \theta}{\nu}$

t time

U_e local free-stream velocity in x_1 direction at edge of boundary layer

u_i instantaneous velocity in x_i direction

$\bar{u}_i$ mean velocity in x_i direction

u_i' fluctuation in velocity in x_i direction, $u_i - \bar{u}_i$

u^* friction velocity, $\sqrt{\tau_w / \rho}$

V transformed normal velocity (eq. (26))

x_i Cartesian coordinates in tensor notation (i = 1, 2, 3)

α constant in models of turbulent terms (eqs. (9) and (10))

δ boundary-layer thickness $\left(\text{taken at some specified value of } \dfrac{\bar{u}_1}{U_e}\right)$

δ^* displacement thickness, $\displaystyle\int_0^\delta \left(1 - \dfrac{\bar{u}_1}{U_e}\right) dx_2$

ϵ eddy viscosity (eq. (7))

ϵ_e error criteria, $1 - F_e$

$\epsilon_e{}'$ error criteria (eq. (B18))

ϵ_w convergence criteria (eq. (B24))

θ momentum thickness $\displaystyle\int_0^{\delta}\left(\frac{\bar{u}_1}{U_e} - \frac{\bar{u}_1{}^2}{U_e{}^2}\right)dx_2$

κ constant in models of turbulent terms (eqs. (12) and (13))

μ dynamic viscosity

ν kinematic viscosity, μ/ρ

ξ,η similarity coordinates (eqs. (21) and (22))

η^* constant in expression used for initial E profile (eq. (31a))

ρ density

τ local shear stress, $\mu\dfrac{\partial \bar{u}_1}{\partial x_2} - \rho\overline{u_1{}'u_2{}'}$

τ_T turbulent shear stress, $-\rho\overline{u_1{}'u_2{}'}$

ϕ turbulent scale function (eq. (8))

Subscripts:

av   average value

d   dissipation

e   edge of boundary layer, $\dfrac{\bar{u}_1}{U_e} = (1 - \epsilon_e)$

i; 1,2,3
j; 1,2,3   standard tensor notation: 1, 2, and 3 denote directions that are, respectively, parallel to the surface and in the same direction as the external velocity vector, normal to the surface, and parallel to the surface but normal to the external velocity vector

6

o initial conditions except where noted

T turbulent

t transition

w wall or surface

δ evaluated at some specified value of F

REVIEW OF PROBLEM

The following remarks are not intended as a complete or general review of the literature on turbulent boundary-layer theory. Rather, it is desired to emphasize certain aspects of previous work that are of particular significance for the present extension of the Glushko method (ref. 17).

Applications of Turbulent Kinetic Energy Equation

From physical and dimensional considerations, Prandtl (ref. 2) derived the equation for the conservation of kinetic energy of turbulent velocity fluctuations $\bar{e}$ (one of the double velocity correlations) and compared the calculated variation of $\bar{e}$ across a channel with experimental data. Nevzgljadov (ref. 3) presented a more elegant derivation of the equation for $\bar{e}$ and applied it, together with the equations for the mean motion, to the flow in a circular pipe. In these methods it was necessary to assume functional relations between $\bar{e}$ and the various other fluctuation terms which appear, such as the production and dissipation of turbulent energy; an "eddy" viscosity concept was used to formulate the Reynolds stress. (The dominant production term is usually the product of the Reynolds stress and the normal gradient of the mean velocity.) The success of the methods depends on how well the assumed functional relations represent the real situation. A characteristic length l which is interpreted as the mean scale of the turbulence enters some of the functions. In reference 3 the assumption that $l \propto \bar{e}$ was used; whereas in reference 2 it was assumed that l was related directly to the mixing length and, hence, depended on the type and geometry of the flow. In spite of these different assumptions for l, the agreement with experiment shown in both references 2 and 3 was reasonable. This agreement indicates that assumptions relating the different fluctuating properties (actually, mean values of products of fluctuating quantities) of the flow to each other may not be as critical as assumptions relating fluctuating flow properties directly to mean flow quantities.

In the method proposed by Chou (ref. 4) and applied by him to channel and flat-plate flows (refs. 5 and 20), separate equations for each of the different components of both the double and triple velocity correlations were used and the concept of an eddy viscosity was not required. If quadruple correlations are neglected, this set of equations then represents a closed system that could be used to compute any turbulent flow if sufficiently general formulations for terms that represent the diffusion and dissipation of turbulence can be determined.

Emmons (ref. 8) further developed and applied the method of Prandtl (ref. 2) to the calculation of various turbulence quantities for channel, free jet, and wake flows. By appropriate adjustment of the constants and the turbulence scale factor l, good agreement with corresponding measurements (refs. 21 to 23) was obtained. Townsend (ref. 9) assumed that the turbulent shear is directly proportional to $\bar{e}$ (and thereby abandoned the eddy viscosity concept) within the inner region of a shear layer and used the turbulent energy equation to compute mean velocity distributions for equilibrium shear flows. Levin (ref. 10) applied Rotta's method to pipe flow and obtained reasonable agreement with the experimental data of Laufer (ref. 24) for turbulent shear and the production and dissipation of turbulent energy. Spalding (ref. 11) has applied the turbulence energy equation to separated flows and used assumptions for the turbulence quantities similar to those of Prandtl (ref. 2).

As mentioned in the Introduction, numerical solutions to the complete equations are essential to determine the degree of generality of the models used for the fluctuating terms. Although numerical procedures were used in references 14 and 15, solutions were given only for simplified forms of the equations applicable to flat plate or pipe flows. In the solutions of references 17 to 19, the complete equations were retained except for the neglect of molecular shear in references 18 and 19. The equations of mean motion, continuity, and turbulence energy then become hyperbolic (ref. 18) and can therefore be solved by the method of characteristics. The numerical computing procedures are thereby considerably simplified but the wall boundary condition of zero turbulent shear cannot be satisfied directly. Nevertheless, Bradshaw, Ferriss, and Atwell (ref. 18) obtained good agreement of mean velocity, shear profiles, and the variation of thickness parameters with experimental data for both equilibrium and some nonequilibrium adverse pressure gradient cases. Bradshaw and Ferriss have applied the method of reference 18 to compressible flows (ref. 25) at low supersonic Mach numbers with only partial success. The method of Nash (ref. 19) differs from that of reference 18 only in that the computing procedure is a more conventional finite-difference method rather than the method of characteristics as applied uniquely by Bradshaw.

Integral Methods

In the conventional integral methods, the mean momentum equation is integrated across the boundary layer and solutions are then obtained by the use of assumptions for velocity profiles (or auxiliary equations for the shape factor, $H^* = \delta^*/\theta$) and skin friction as functions of θ or other mean flow parameters. Large discrepancies in predicted variations of H^*, θ, and C_f result from these methods, as shown by the recent review of Thompson (ref. 26). In another integral method that has been used extensively, the integral form of the mean kinetic energy equation is solved simultaneously with the mean flow integral momentum equation as originally done by Truckenbrodt (ref. 27). The additional requirement here is to develop a sufficiently general relation for the dissipation integral. A recent correlation scheme for this integral as described by Walz (ref. 28) has resulted in good agreement with experimental distributions of H^* in several adverse-pressure-gradient cases. The dissipation integral depends on the turbulent shear distribution across the boundary layer; however, the various integral methods provide no information on local shear or other local turbulence parameters and hence can be evaluated only in terms of mean flow properties such as H^*, θ, and C_f. Although the auxiliary relations for H^*, C_f, and the dissipation integral can be tailored to give agreement with a specific set of data, extension to other situations, particularly compressible flow, always remains doubtful.

Finite-Difference Procedures

An approach which is more basic than the integral methods is to solve the mean momentum and continuity equations directly by finite-difference procedures so that the only unknown function is the relation between the Reynolds stress and mean flow properties. The success of this approach as applied to several different types of boundary layers (refs. 29 and 30, for example) indicates that the difficulties in the integral methods (besides the basic limitations of any boundary-layer integral method) are caused mainly by deficiencies in the assumptions for the velocity profiles (or H^*), the shear stress and dissipation integrals, and the skin-friction relations. In the finite-difference methods of references 29 and 30, simple functions for the eddy viscosity ϵ in terms of local flow conditions are used. The Reynolds stress is thus assumed to depend directly on the local mean flow velocity gradient and other local mean flow properties.

On the other hand, in the finite-difference procedures of references 17 to 19, the Reynolds stress is also related to correlations of fluctuation quantities by the turbulent kinetic energy equation. Formulations for the turbulence correlation quantities in reference 17 were based primarily on the work of Prandtl and Rotta (refs. 2 and 6) where an eddy viscosity concept is used. Assumptions for the correlations in reference 18 are based on extensions of the ideas of Townsend (ref. 9); that is, all turbulence quantities

were related directly to the turbulent shear stress and the turbulence energy equation becomes an equation for the shear stress. These methods combine the advantages of a finite-difference solution of the mean momentum equation with the more general relation for the turbulent shear as supplied by the turbulence kinetic energy equation.

BOUNDARY-LAYER EQUATIONS

For conditions where a characteristic Reynolds number $U_e \delta / \nu$ is at most of the order of x_1 / δ and if $x_1 / \delta \gg 1$, the two-dimensional time-steady equations of motion for the turbulent flow of an incompressible fluid (ref. 1, pp. 453-457) reduce to:

For x_1 mean momentum:

$$\bar{u}_1 \frac{\partial \bar{u}_1}{\partial x_1} + \bar{u}_2 \frac{\partial \bar{u}_1}{\partial x_2} = -\frac{1}{\rho} \frac{dp_e}{dx_1} - \frac{\partial}{\partial x_2} \overline{u_1' u_2'} + \nu \frac{\partial^2 \bar{u}_1}{\partial x_2^2} \tag{1}$$

For turbulent kinetic energy:

$$\bar{u}_1 \frac{\partial \bar{e}}{\partial x_1} + \bar{u}_2 \frac{\partial \bar{e}}{\partial x_2} = -\overline{u_1' u_2'} \frac{\partial \bar{u}_1}{\partial x_2} - \frac{\partial}{\partial x_2} \overline{u_2' \left(\frac{p'}{\rho} + e \right)} + \nu \frac{\partial^2 \bar{e}}{\partial x_2^2} - \nu \overline{\frac{\partial u_i'}{\partial x_j} \frac{\partial u_i'}{\partial x_j}} \tag{2}$$

(In accordance with conventional notation, when a subscript i or j is repeated, summation over three directions is implied.) These equations together with the equation of continuity

$$\frac{\partial \bar{u}_1}{\partial x_1} + \frac{\partial \bar{u}_2}{\partial x_2} = 0 \tag{3}$$

and appropriate initial and boundary conditions determine the three dependent variables $\bar{u}_1$, $\bar{u}_2$, and $\bar{e}$ within the turbulent boundary layer.

Since the Reynolds shear stress

$$\tau_T = -\rho \overline{u_1' u_2'} \tag{4}$$

the diffusion of total turbulence energy by velocity fluctuations

$$\text{Diffusion} = \frac{\partial}{\partial x_2} \overline{u_2' \left(\frac{p'}{\rho} + e \right)} \tag{5}$$

and the dissipation of turbulence energy

$$\text{Dissipation} = \nu \, \overline{\frac{\partial u_i'}{\partial x_j} \frac{\partial u_i'}{\partial x_j}} \tag{6}$$

are in general unknown, these equations do not represent a closed system. Nevertheless, the dependence of the Reynolds shear stress on both the correlation terms and the mean flow properties themselves is clearly evident from equations (1) to (3).

ASSUMPTIONS FOR FLUCTUATING QUANTITIES

In order to formulate realistic expressions for the correlation of fluctuation terms in equation (2) involving Reynolds stress, diffusion of total turbulent energy, and dissipation of turbulent energy (eqs. (4) to (6)), it is desirable to rely on experimental measurements of these quantities whenever possible. Except for the diffusion of pressure energy, these terms have been measured in boundary layers with zero pressure gradient (Townsend, Klebanoff, and Corrsin and Kistler, refs. 31 to 33) and with pressure gradients for both equilibrium (Bradshaw, ref. 34) and nonequilibrium boundary layers (for example, Schubauer and Klebanoff (ref. 35) and Bradshaw and Ferriss (ref. 36)).

The expressions for correlations as developed by Glushko (ref. 17) were based on the general approach of Rotta (ref. 6) wherein the dissipation and diffusion terms are assumed to be functions of $\bar{e}$, l, and $R = \dfrac{\bar{e}l}{\nu}$. The form of these functions depends primarily on physical and dimensional reasoning. The Reynolds stress was related to the mean velocity gradient by

$$\tau_T = \epsilon \, \frac{\partial \bar{u}_1}{\partial x_2} \tag{7}$$

where the dimensionless eddy viscosity ϵ/μ is assumed to be a function only of R rather than of the local mean flow properties as in more conventional approaches, such as the methods of references 29 and 30. The mean scale of turbulence l was evaluated from flat-plate data for two-point correlation coefficients of the longitudinal velocity fluctuations in such a way that l is analogous to an integral scale (see ref. 1, p. 37) parameter. The corresponding ratio l/δ was taken as a universal function of the form

$$\frac{l}{\delta} = \phi\!\left(\frac{x_2}{\delta}\right) \tag{8}$$

As indicated by Glushko, there are few data available for the evaluation of l, even for flat-plate flows; thus, the generality of this relation remains questionable. However, in a recent experimental investigation (ref. 37) of a separating boundary layer, measurements of the two-point correlation coefficients were obtained. If these measurements are used to compute l as defined by Glushko, the resulting l/δ function is nearly identical to that of Glushko's for $\frac{x_2}{\delta} < 0.6$.

With l thus determined, Glushko (ref. 17) then evaluated the function ϵ/μ from flat-plate data of references 31 and 32 for $R > 400$ and from the wake data of Townsend (ref. 23) for $R < 100$. Although Glushko was able to obtain reasonable agreement with experimental data for $\bar{e}$, mean velocity profiles, and C_f on flat plates by adjusting constants in these formulations, no comparisons with other experimental measurements were published. Also, no calculations were reported for adverse-pressure-gradient cases which generally provide a more critical test of any theoretical method than the simpler flat-plate flows. Before proceeding to compare theoretical predictions with experimental data for both mean (including rate of boundary-layer growth) and fluctuating quantities for flat-plate and nonequilibrium, adverse-pressure-gradient flows, Glushko's formulations are considered in more detail.

Reynolds Stress

The starting point of Glushko's (ref. 17) derivation of expressions for the fluctuation quantities was a relation between the eddy viscosity ϵ/μ and the turbulent Reynolds number R. This relation had been pointed out previously by Levin (ref. 10) and was based primarily on the semiempirical results of Rotta (ref. 6) that, in turn, depend partly on the observed decay rates of homogeneous turbulence (ref. 38, pp. 101-113). From flat-plate and wake data with l determined from equation (8), as mentioned above, Glushko then obtained the simple function

$$\frac{\epsilon}{\mu} = H(R)\alpha R \tag{9a}$$

where

$$H(R) = \begin{cases} \dfrac{R}{R_0} & \left(0 < \dfrac{R}{R_0} < 0.75\right) \\[2ex] \dfrac{R}{R_0} - \left(\dfrac{R}{R_0} - 0.75\right)^2 & \left(0.75 < \dfrac{R}{R_0} < 1.25\right) \\[2ex] 1 & \left(1.25 < \dfrac{R}{R_0} < \infty\right) \end{cases} \tag{9b}$$

and α and R_O are constants. Since this result is based partly on the assumption that the dissipation rate of turbulent energy in a boundary layer is similar to that in isotropic homogeneous turbulence, it cannot be regarded as firmly established, particularly in the very near wall region (where decay of $\bar{e}$ is caused by the presence of the wall) nor in the outer portions of the boundary layer (where the decay in $\bar{e}$ is associated with the intermittent character of the flow and the edge boundary condition on $\bar{e}$). Indeed, one justification for the eddy viscosity concept itself, generally expressed as $\epsilon = l^2 \dfrac{\partial \bar{u}_1}{\partial x_2}$, is perhaps that the concept has generally given useful results. However, as shown by Townsend (ref. 9) and by Bradshaw, Ferriss, and Atwell (ref. 18), reasonable results can be obtained from simultaneous solutions of equations (1) and (2) without the use of the eddy viscosity concept.

Glushko's final expression for the Reynolds stress is then

$$\tau_T \equiv -\rho \overline{u_1' u_2'} = \mu H(R) \alpha R \frac{\partial \bar{u}_1}{\partial x_2} \tag{10}$$

For boundary-layer flows, the production of turbulent energy, which is represented by the first term on the right in equation (2), is generally large in magnitude, and therefore the formulation of τ_T is of critical importance.

Dissipation

It is known that the dissipation of energy in homogeneous turbulence is proportional to $(\bar{e})^{3/2}\big/l$ (ref. 38, p. 106) which has been used directly by Prandtl (ref. 2), Emmons (ref. 8), and Townsend (ref. 9) to compute the production of turbulent energy from equation (2) for simple shear flows. Based on Rotta's work, Glushko showed that the dissipation term in equation (2) can be written as

$$\nu \overline{\frac{\partial u_i'}{\partial x_j} \frac{\partial u_i'}{\partial x_j}} = \nu C \frac{\bar{e}}{l^2} + \kappa C \frac{(\bar{e})^{3/2}}{l} = \nu C(1 + \kappa R)\frac{\bar{e}}{l^2} \tag{11}$$

and it is seen that the second term on the right is the same as the dissipation in homogeneous turbulence. The first term on the right is important only for small R and whether this formulation is applicable to regions of the boundary layer where R is small cannot be determined except by comparison with data. Since for large R, the expression already obtained for ϵ/μ (eqs. (9)) had the desired dependence on R, Glushko assumed the final relation for the dissipation term as

$$\nu \overline{\frac{\partial u_i'}{\partial x_j} \frac{\partial u_i'}{\partial x_j}} = \nu C\left[1 + \frac{\epsilon}{\mu}(\kappa R)\right]\frac{\bar{e}}{l^2} \tag{12}$$

where $\frac{\epsilon}{\mu}(\kappa R)$ indicates the same function as given by equations (9) except that R is replaced by κR. The turbulence scale l as used by Glushko was considered as the same mean scale function given by equation (8); however, as written in equation (12), l could be considered a microscale (see ref. 1, p. 37) if C were adjusted accordingly. The possibility of introducing a microscale for l in the dissipation term is considered in the section "Results and Discussion."

The dissipation term is generally of the same order of magnitude as the production term, except very near the wall, and hence is also of critical importance. At the wall itself, equation (12) does not give the correct limiting form for the dissipation which, from equation (2), should be

$$\nu\left(\overline{\frac{\partial u_i'}{\partial x_j} \frac{\partial u_i'}{\partial x_j}}\right)_w = \nu\left(\frac{\partial^2 \bar{e}}{\partial x_2^2}\right)_w$$

An analysis similar to that of Rotta (ref. 7, p. 59) shows that $\left(\dfrac{\partial^2 \bar{e}}{\partial x_2^2}\right)_w$ is generally finite, whereas equation (12) evaluated at the wall is zero since $\bar{e}_w = 0$. The use of equation (12) thus forces $\left(\dfrac{\partial^2 \bar{e}}{\partial x_2^2}\right)_w$ to be zero, which is physically incorrect and has apparently caused some numerical difficulties in the present solutions. These difficulties have been largely avoided by rejecting negative values of $\bar{e}$ which sometimes occurred during iteration cycles in the numerical procedure.

Diffusion

Glushko reasoned that the total diffusion of turbulence energy was due to the gradient of $\bar{e}$. In addition, he specified the corresponding diffusion coefficient to be the same quantity given in brackets in equation (12). Hence, he obtained for the diffusion terms

$$\frac{\partial}{\partial x_2}\left[\nu \frac{\partial \bar{e}}{\partial x_2} - \overline{u_2'\left(\frac{p'}{\rho} + e\right)}\right] = \frac{\partial}{\partial x_2}\left\{\nu\left[1 + \frac{\epsilon}{\mu}(\kappa R)\right]\frac{\partial \bar{e}}{\partial x_2}\right\} \tag{13}$$

14

Again, it is obvious that the generality of this assumed expression for the diffusion can only be determined by comparison with data. Possible deficiencies are that the diffusion of energy by pressure fluctuations is not treated separately and that a simple gradient-type diffusion as postulated does not always occur (ref. 1, pp. 288-289). Nevertheless, for many practical cases the diffusion terms are smaller than the dissipation and production terms; thus, for these situations, the formulation of diffusion is presumably not critical.

TRANSFORMATION TO SIMILARITY COORDINATES

Profile Functions

The main reason for transforming to similarity type of coordinates is to provide scale factors that in terms of the transformed variables ξ and η, reduce or remove the rate of increase in boundary-layer thickness with distance ξ along the surface. The number of computing steps $\Delta\eta$ required across the boundary layer to obtain desired accuracy in the finite-difference procedures can thereby be reduced and kept more nearly constant. Also, in a region of approximate local similarity, the streamwise step size $\Delta\xi$ can be increased since for this situation the rate of change of the dependent variables with ξ is much reduced.

Before the boundary-layer equations (eqs. (1) to (3)) are transformed to the ξ,η coordinates, it is convenient to write them in terms of the dimensionless velocity and energy profile functions

$$\left. \begin{aligned} F &= \frac{\bar{u}_1}{U_e} \\[2mm] E &= \frac{\bar{e}}{U_e{}^2} \end{aligned} \right\} \tag{14}$$

Then with the use of equations (8) to (13) and Bernoulli's equation for the pressure gradient

$$U_e \frac{dU_e}{dx_1} = -\frac{1}{\rho}\frac{dp_e}{dx_1} \tag{15}$$

equations (1), (2), and (3) become, respectively,

for mean momentum:

$$F\frac{\partial F}{\partial x_1} + \frac{\bar{u}_2}{U_e}\frac{\partial F}{\partial x_2} = \frac{1 - F^2}{U_e}\frac{dU_e}{dx_1} + \frac{\nu}{U_e}\frac{\partial}{\partial x_2}\left(M\frac{\partial F}{\partial x_2}\right) \tag{16}$$

15

for turbulent kinetic energy:

$$F \frac{\partial E}{\partial x_1} + \frac{\bar{u}_2}{U_e} \frac{\partial E}{\partial x_2} = -2 \frac{FE}{U_e} \frac{dU_e}{dx_1} + \frac{\nu}{U_e}(M - 1)\left(\frac{\partial F}{\partial x_2}\right)^2 + \frac{\nu}{U_e} \frac{\partial}{\partial x_2}\left(D \frac{\partial E}{\partial x_2}\right) - C \frac{\nu}{U_e} \frac{DE}{l^2} \qquad (17)$$

and for continuity:

$$\frac{\partial F}{\partial x_1} + \frac{\partial}{\partial x_2} \frac{\bar{u}_2}{U_e} + \frac{F}{U_e} \frac{dU_e}{dx_1} = 0 \qquad (18)$$

where

$$\left.\begin{aligned} M &= 1 + \alpha R H(R) = 1 + \alpha H(R) \ \phi\sqrt{E}R_\delta \\ D &= 1 + \alpha\kappa R H(\kappa R) = 1 + \alpha\kappa H(\kappa R) \ \phi\sqrt{E}R_\delta \end{aligned}\right\} \qquad (19)$$

The function $H(\kappa R)$ is identical to the function $H(R)$ (eq. (9b)) except that R/R_0 is replaced by $\kappa R/R_0$. The first three terms in equation (17) account for the convection of turbulent energy and the last three terms represent, respectively, the production, diffusion, and dissipation of the turbulent energy.

The boundary conditions to be applied to this system of equations are

for $x_2 = 0$:

$$\left.\begin{aligned} F &= E = 0 \\ \bar{u}_2 &= \bar{u}_{2,w}(x_1) \end{aligned}\right\} \qquad (20a)$$

for $x_2 \to \infty$:

or

$$\left.\begin{aligned} F &\to 1.0 \\ E &\to 0 \\ E &\to E_e \end{aligned}\right\} \qquad (20b)$$

where E_e is one-half the square of the free-stream turbulence intensity.

Similarity Variables

The transformed variables are defined as

$$\xi(x_1) = \int_0^{x_1} \frac{U_e}{\nu} \, dx_1 \qquad (21)$$

16

$$\eta\left(x_1, x_2\right) = \frac{U_e}{\nu(2\xi)^{\bar{n}}} \, x_2 \tag{22}$$

where $\bar{n}$ is, in general, a variable function of ξ and is determined from the requirement that η_δ (the boundary-layer thickness in the transformed coordinates) is constant. Hence, from equation (22)

$$\bar{n} = \frac{\log_e\left[\dfrac{U_e}{U_{e,o}} \dfrac{\delta}{\delta_o} \left(2\xi_o\right)^{\bar{n}_o}\right]}{\log_e 2\xi} \tag{23}$$

In a boundary layer where the velocity profile shapes and thickness δ are changing rapidly, the value of $\bar{n}$ would also change rapidly so that a lengthy iteration procedure would be required to satisfy equation (23). An alternate procedure is to specify $\bar{n}$ as a constant; then, for U_e constant $\left(\xi = U_e x_1/\nu\right)$ and η_δ constant, $\bar{n} = \frac{1}{2}$ for laminar boundary layers, and $\bar{n} \approx 0.8$ to 1.0 for turbulent boundary layers. (Ref. 39 (p. 537) gives $\bar{n} = 0.8$ for turbulent boundary layers.)

Transformed Equations

The general transformation formulas from equations (21) and (22) may be written as

$$\left.\begin{aligned}
\frac{\partial}{\partial x_1} &= \frac{U_e}{\nu} \frac{\partial}{\partial \xi} + \frac{\partial \eta}{\partial x_1} \frac{\partial}{\partial \eta} \\[2em]
\frac{\partial}{\partial x_2} &= \frac{U_e}{\nu(2\xi)^{\bar{n}}} \frac{\partial}{\partial \eta}
\end{aligned}\right\} \tag{24}$$

The operator that appears on the left-hand side of equations (16) and (17) then becomes

$$\left(F \frac{\partial}{\partial x_1} + \frac{\bar{u}_2}{U_e} \frac{\partial}{\partial x_2}\right) = \frac{FU_e}{\nu} \frac{\partial}{\partial \xi} + \frac{U_e}{\nu(2\xi)^{2\bar{n}}} V \frac{\partial}{\partial \eta} \tag{25}$$

where V is a transformed normal velocity defined as

$$V = \frac{(2\xi)^{2\bar{n}}\nu}{U_e} F \frac{\partial \eta}{\partial x_1} + (2\xi)^{\bar{n}} \frac{\bar{u}_2}{U_e} \tag{26}$$

Equations (16), (17), and (18) can then be written for momentum:

$$(2\xi)^{2\bar{n}} F \frac{\partial F}{\partial \xi} + V \frac{\partial F}{\partial \eta} = \frac{(2\xi)^{2\bar{n}}}{U_e} \frac{dU_e}{d\xi}\left(1 - F^2\right) + \frac{\partial}{\partial \eta}\left(M \frac{\partial F}{\partial \eta}\right) \tag{27}$$

for energy:

$$(2\xi)^{2\bar{n}} F \frac{\partial E}{\partial \xi} + V \frac{\partial E}{\partial \eta} = -\frac{2(2\xi)^{2\bar{n}}}{U_e} \frac{dU_e}{d\xi} FE + (M - 1)\left(\frac{\partial F}{\partial \eta}\right)^2$$

$$+ \frac{\partial}{\partial \eta}\left(D \frac{\partial E}{\partial \eta}\right) - C \frac{(2\xi)^{2\bar{n}}}{R_\delta^2} \frac{DE}{\phi^2} \tag{28}$$

and for continuity:

$$(2\xi)^{2\bar{n}} \frac{\partial F}{\partial \xi} + \frac{\partial V}{\partial \eta} + (2\xi)^{2\bar{n}} F\left(\frac{\bar{n}}{\xi} + \frac{d\bar{n}}{d\xi} \log_e 2\xi\right) = 0 \tag{29}$$

In order to derive equation (29), it is necessary to obtain $\dfrac{\partial \bar{u}_2}{\partial \eta}$ from equation (26) and the expression (from eqs. (22) and (24))

$$\frac{\partial}{\partial \eta}\left(\frac{\partial \eta}{\partial x_1}\right) = \frac{(2\xi)^{\bar{n}}}{\nu} \frac{\partial}{\partial \xi}\left[\frac{U_e}{(2\xi)^{\bar{n}}}\right]$$

is also required.

The continuity equation is written as shown to facilitate the computational procedure of Blottner (ref. 40) which is to be used herein. For $\bar{n} = \dfrac{1}{2}$, equation (29) reduces to the form given by Blottner.

Similar Solutions

It is well-known from experimental investigations of turbulent boundary layers with $dp_e/dx = 0$ that portions of the velocity profiles are at least approximately similar in terms of law-of-the-wall and velocity defect variables (ref. 41). As the Reynolds number approaches infinity, these profile shapes should approach exact similarity across the entire boundary layer. It is therefore appropriate to inquire as to the possibility of similar solutions to equations (27) to (29), since these equations should yield approximately similar solutions if the Glushko formulations for the correlation terms are to be generally valid.

To determine whether similar solutions exist, the question is posed; what distributions of U_e and $\bar{n}$ are required for F, V, E, and ϕ to be functions only of η?

Inspection of equations (27) to (29) indicates that even with U_e constant, no such exact solutions are possible because of the R_δ factor in the M and D coefficients and in the last term (dissipation) of equation (28). This term may be written as

$$\text{Dissipation} = C \frac{(2\xi)^{2\bar{n}}}{R_\delta^2} \frac{DE}{\phi^2} = C \frac{DE}{\eta_\delta^2 \phi^2}$$

since from equation (22), $\eta_\delta = U_e \delta / \nu (2\xi)^{\bar{n}}$. Substitution for D from equation (19) with $R \gg 1$ then gives the approximation

$$\text{Dissipation} \approx C\alpha\kappa \frac{E^{3/2}}{\eta_\delta^2 \phi} \frac{U_e \delta}{\nu}$$

Thus, even if η_δ is constant, the dissipation term does not satisfy similarity requirements. However, if R_δ is large and approximately constant over some small interval of interest and U_e is constant, locally similar solutions would be possible. In general, exact similar solutions are not possible with the present variables ξ, η (eqs. (21) and (22)) and the transport coefficients M and D modeled according to equation (19). The existence of similar solutions is investigated further in appendix A where it is shown that if δ increases linearly with x_1, similar solutions in terms of the variable x_2/δ can be obtained for $R \gg 1$ and either U_e constant or

$$\frac{\delta}{U_e} \frac{dU_e}{dx_1} = \text{Constant}$$

For C_f approximately constant, this condition is equivalent to that of Clauser (ref. 42) for equilibrium flows. It is also shown in appendix A that the ratio of a dissipation microscale to an integral scale should increase as some small power of the Reynolds number in order to obtain similar solutions of the flat-plate boundary layer. Actual solutions to the equations with similarity requirements included were not obtained in this investigation because numerical procedures would still be required, and little additional information could be expected beyond that just discussed.

RESULTS AND DISCUSSION

Computation Procedure

The system of equations (27) to (29), along with auxiliary functions for M, D, and $\bar{n}(x_1)$ as defined in the previous section, is solved by a linear implicit finite-difference procedure. Complete details of the procedure including the finite-difference

expressions for the partial derivatives are given in appendix B. To increase the efficiency and accuracy of the computations, a variable grid size in the η-direction has been incorporated in the finite-difference expressions and used in some of the solutions. Details of the computer program including an operational flow diagram and program listing are given in appendix C.

General Comments

The effects of some modifications to the method of Glushko (ref. 17) on both mean and fluctuating flow properties are presented for flat-plate flow $(dp_e/dx = 0)$ and for one of Goldberg's experimental flows (ref. 43) with a large adverse pressure gradient. The principal modifications considered are to the l/δ function (eq. (8)) and to the dissipation and diffusion terms (eqs. (12) and (13)). Limited results that indicate possible advantages to be gained by the use of similarity-type variables (eqs. (21) and (22)) with $\bar{n}$ adjusted to give approximately constant boundary-layer thickness in the transformed coordinates are also mentioned.

The data from the investigation by Goldberg (ref. 43) chosen as a test case should be a particularly severe test of any method (as indicated by Bradshaw and Ferriss, ref. 44) because the boundary layer was first driven nearly to separation by a large adverse pressure gradient and then allowed to relax toward a flat-plate flow by imposing a constant pressure. Another advantage of using reference 43 as a test case is that hot-wire measurements of turbulent shear and longitudinal turbulence intensity were made. Comparisons between these data and the theoretical results assist in the evaluation of the models used for the turbulent correlation terms. Also, the turbulence intensity data can be used to provide initial E profiles which are required in order to start the calculation.

Bradshaw and Ferriss (ref. 44) and Nash (ref. 19) have applied their methods using the turbulent energy equation to this same adverse-pressure-gradient case of Goldberg and obtained reasonable agreement with experimental data for θ, H^*, and C_f. Nash also obtained reasonable agreement between the calculated profiles of mean velocity and shear stress and the experimental results of Goldberg. Bradshaw and Ferriss (ref. 44) show that the computed values of C_f in the region of its minimum were very sensitive to the initial value of θ used to start the calculation for this particular case.

In all calculations by the present method, the skin friction has been computed from the correct limiting form evaluated at the wall as

$$\tau_w = \mu \left(\frac{\partial \bar{u}_1}{\partial x_2}\right)_w$$

20

hence from equation (22),

$$\frac{C_f}{2} = \frac{\tau_w}{\rho U_e^2} = (2\xi)^{-\bar{n}} \left(\frac{\partial F}{\partial \eta}\right)_w \tag{30a}$$

and in finite-difference form

$$(C_f)_m = 2 \left[(2\xi)^{-\bar{n}}\right]_m \frac{F_{m,n=2}}{\Delta\eta_{n=1}} \tag{30b}$$

In order to obtain valid results, the value of $\Delta\eta_{n=1}$ in equation (30b) must be less than the thickness of the region where $\bar{u}_1$ varies approximately linearly with x_2.

Flat-Plate Flow

The calculation was started at $R_{x_1} = 10^4$ with input values of F and V from exact numerical solutions to the laminar Blasius flow. The input profile for the turbulent kinetic energy was taken (from ref. 17) as:

$$E(\xi_0, \eta) = E_0^* \left(\frac{\eta}{\eta^*}\right) \exp\left\{\frac{1}{2}\left[1 - \left(\frac{\eta}{\eta^*}\right)^2\right]\right\} \tag{31a}$$

where E_0^* and η^*/η_e are specified constants. Unless otherwise noted, the results shown herein were computed with $E_0^* = 2.5 \times 10^{-4}$, $\frac{\eta^*}{\eta_e} = 0.4$, $\bar{n} = 0.5$, and constant $\Delta\eta = 0.05$. Additional required inputs were

$$U_e = 100 \text{ ft/sec} \ (30.48 \text{ m/s})$$

$$\eta_{e,o} = 4.95$$

$$\nu = 1.58 \times 10^{-4} \text{ ft}^2/\text{sec} \ \left(14.68 \times 10^{-6} \text{ m}^2/\text{sec}\right)$$

$$\epsilon_e = 1 \times 10^{-4}$$

$$\epsilon_e' = 3.4 \times 10^{-4}$$

$$\epsilon_\delta = 0.01$$

The $\Delta\xi$ step size was increased with increasing ξ according to the relation:

$$\Delta\xi = f \times 10^k \qquad \left(1.0 \times 10^k \leqq \xi \leqq 10 \times 10^k\right) \qquad (31b)$$

so that the number of $\Delta\xi$ steps required to traverse one cycle (on a log scale) of ξ was the same for a given problem. Examples are shown for $f = 0.1$ and $f = 0.5$.

The l/δ function was obtained by linear interpolation from values given in table I. Three functions are given in table I: the one denoted as $\phi_{0.33}$ is based on the corresponding function as used by Glushko (ref. 17), and this $\phi_{0.33}$ function is used for the present calculation of flat-plate flow. The subscript 0.33 denotes the maximum value of l/δ.

The values of the constants in the transport functions M and D are: $\alpha = 0.2$, $\kappa = 0.4$, $C = 3.93$, $R_0 = 110$. As noted previously, these values and the ϕ function were adjusted by Glushko to give agreement with flat-plate flow. In the present report the same values, except where noted, are also applied to the adverse-pressure-gradient flow.

Form factor, skin friction, and mean-velocity profiles.- The variation of the form factor H^* with R_{x_1} is shown in figure 1. The value of H^* is at first approximately constant at the initial value of 2.592, corresponding to the Blasius solution for laminar flow, and then H^* abruptly decreases at some value of R_{x_1} depending on the step size (or f-factor), the magnitude of the input disturbance E_0^*, and modifications to the Glushko models of the correlation terms. This value of the Reynolds number where the flow properties began to change is designated $R_{x_1,t}$. Because of the behavior of H^* as well as the mean-velocity profiles and other flow properties to be presented in subsequent sections, $R_{x_1,t}$ can be considered analogous to a transition Reynolds number.[1] The two modifications used here were to the $H(R)$ function (eq. (9b)) and to the diffusion term (eq. (13)). The reasons for investigating these modifications are discussed after their effects on H^*, C_f, and the mean velocity profiles are given.

The modification to the $H(R)$ function was to disregard equation (9b) in the outer part of the boundary layer and set $H(R) = 1$ when $R/R_0 < 1.25$. This modification had no effect (within the plotting accuracy) on the values of H^*.

___

[1]It must be emphasized, however, that no claim is made regarding the possibility of computing a realistic value of transition Reynolds number from the present method in its current stage of development. The term transition Reynolds number is used herein merely as a matter of convenience. In this connection, however, Donaldson has shown in a recent paper (ref. 45) that by retaining the complete equations for each component of the correlations $\overline{u_i'u_i'}$, some of the physical characteristics of transition can be computed. Donaldson has pointed out that his preliminary models for the correlation terms are crude and that improvement of the models should ultimately result in quantitative predictions of transition.

When the step size factor was increased to 0.5 $\left(\text{with } H(R) = 1 \text{ for } x_2/\delta > 0.5\right)$, the value of R_{x_1} where H^* first began to drop was increased slightly. It is apparent that this slight increase in $R_{x_1,t}$ was a numerical effect caused by the larger $\Delta\xi$ step. Consequently, the following discussion of flat-plate results is limited to those solutions with $f = 0.1$.

Increasing the diffusion term by a factor of 3 increased the value of $R_{x_1,t}$ by a factor of about $1\frac{1}{3}$. Also when the input disturbance level E_0^* was reduced to 1×10^{-8} from 2.5×10^{-4}, $R_{x_1,t}$ was further increased to about 8×10^4. However, for all modifications shown here, the H^* curves appeared to approach a value of approximately 1.4 which is in agreement with the data of Wieghardt and Tillmann (ref. 46) considered typical of flat-plate flows.

The effects of the modification to the diffusion term and the change in E_0^* on C_f are shown in figure 2 and are of the same nature as the effects on H^*. $\left(\text{The } H(R)\right.$ modification had a negligible effect on both C_f and H^*.$\left.\right)$ That is, the "transition" Reynolds number is increased by the same factors when the larger diffusion term or the smaller E_0^* are used but the final asymptotic values of C_f are in reasonable agreement with those for fully turbulent flow as obtained from Schlichting (ref. 39, p. 540) and the data of Wieghardt and Tillmann (ref. 46). According to the variation in C_f, when the boundary layer was fully turbulent at $R_{x_1} \approx 4 \times 10^5$, the value of H^* was still decreasing at this Reynolds number as were the data of Wieghardt and Tillmann. (See fig. 1.)

The computed values of the mean velocity are plotted in conventional profile form in figure 3(a) and in law-of-the-wall and velocity defect coordinates (ref. 41) in figures 3(b) and 3(c), respectively. From figure 3(a) it is seen that the profiles develop from the laminar input profile at $R_{x_1} = 1 \times 10^4$ to turbulent type profiles for $R_{x_1} \geqq 1 \times 10^6$. At this Reynolds number the profile shapes have apparently settled out to the shape characteristic of turbulent boundary layers as indicated by the data of Wieghardt and Tillmann (ref. 46). In the transition region, that is, for $3 \times 10^4 < R_{x_1} < 2 \times 10^5$, the profile shapes appear to be in qualitative agreement with mean profiles observed in transition flow as shown, for example, in reference 47.

The effect of the $H(R)$ modification $\left(H(R) = 1 \text{ for } x_2/\delta > 0.5\right)$ is shown for the profile at $R_{x_1} = 1 \times 10^6$. This change in $H(R)$ increases the mean velocity somewhat in the outer region of the boundary layer, with the result that the profile is fuller than when the original Glushko function for $H(R)$ (eq. (9b)) is used.

When the turbulent diffusion term is increased by a factor of 3, the agreement with data is considerably improved, again in the outer part of the boundary layer. These same effects are also shown in figure 3(c) (velocity defect region). The general agreement

with the law-of-the-wall correlations (fig. 3(b)) shows that the results in the near-wall region $\left(\dfrac{u^*x_2}{\nu} < 30\right)$ and the law-of-the-wall region are in good agreement with data.

Discussion of modifications to $H(R)$ function and diffusion term.- The modification to the $H(R)$ function consists of setting $H(R) = 1$ when $R/R_0 < 1.25$ in the outer part of the boundary layer rather than using equation (9b) in this region. (The $H(\kappa R)$ function was modified in the same way, that is, $H(\kappa R) = 1$ when $\kappa R/R_0 < 1.25$ in the outer part of the boundary layer.) The main effect is then to increase the eddy viscosity (eq. (9a)) for $R < 137.5$ $(=1.25R_0)$; thus, the resulting fuller velocity profile shape as shown in figure 4 is to be expected. However, examination of the distribution of R across the boundary layer at $R_{x_1} = 1 \times 10^6$ indicates that $R > 137.5$ for $0.06 < x_2/\delta < 0.9$. Hence, there was no increase in ϵ in this range of x_2/δ and yet the mean velocity was affected in the entire midregion of the boundary layer. This result merely shows that a local change in ϵ can affect the computed mean velocities in the entire boundary layer, as it should for a nonsimilar numerical solution.

The $H(R)$ modification was thought to be more realistic than the original formulation because in the outer part of the boundary layer, any decrease in ϵ should be taken care of by the boundary condition $E_e \to 0$ which, in turn, is caused by the intermittent properties of the flow rather than by a change in the basic relations for the turbulent correlations. In any event, since this modification to $H(R)$ appeared to improve the velocity profile shapes and had little effect on skin friction and form factor, the modification has been used in most of the remaining solutions presented herein.

In regard to the modification of the diffusion term (3 times eq. (13)), a plot of the ratio of the turbulent shear stress to the turbulent velocity correlation, $\tau_T/2\rho\bar{e}$ is shown in figure 4. Results computed from the theory illustrating the effects of the $H(R)$ and diffusion-term modifications are compared with experimental data in this figure. The significance of this ratio and its tendency to be constant for widely different types of fully turbulent shear flows is discussed, for example, in references 9, 34, 48, and 49. The results obtained with terms in the turbulent kinetic energy equation identical to those of Glushko (ref. 17) were therefore considered to be unsatisfactory because of the large increase in the shear ratio in the outer part of the boundary layer[2] as shown in figure 4. The $H(R)$ modification increased τ_T in the outer part of the boundary layer so that the

---

[2]It was originally thought that the $H(R)$ modification would increase the production term $\left(-\overline{u_1'u_2'}\,\dfrac{\partial \bar{u}_1}{\partial x_2}\right)$ in equation (2) and therefore cause an increase in $\bar{e}$ in the outer part of the boundary layer. This increase in $\bar{e}$ should cause a reduction in $\tau_T/2\rho\bar{e}$. Since the modification to $H(R)$ was also applied in the same way to $H(\kappa R)$, the dissipation term was also increased. The net effect was only a slight increase in $\bar{e}$ for $\dfrac{x_2}{\delta} > 0.8$.

resulting values of $\tau_T/2\rho\bar{e}$ (fig. 4) were much too large for $\dfrac{x_2}{\delta} > 0.8$. Since $\partial F/\partial\eta$ and E both approach zero near the outer edge of the boundary layer, the production and dissipation terms (the second and fourth terms on the right-hand side in eq. (28)) both become small there, and it is therefore apparent that another possible way to correct the $\tau_T/2\rho\bar{e}$ ratio is to modify the diffusion term (the third term on the right-hand side of eq. (28)).[3] The simple expedient of increasing this term arbitrarily by a factor of three produced the desired result for the ratio $\tau_T/2\rho\bar{e}$ as shown in figure 4.

In figure 5 the computed values of $\sqrt{E}$ are shown plotted against $x_2/\delta_{F=0.995}$ for several values of R_{x_1} and with the same modification to the diffusion term as noted previously. Results from two experimental investigations at $R_{x_1} \approx 5 \times 10^6$ are shown for comparison. (The discrepancies between the data of refs. 32 and 50 are probably within the accuracy of the data.) When the terms in the turbulent kinetic energy equation are the same as those of reference 17, the changes in $\sqrt{E}$ profiles with Reynolds number duplicate those of reference 17 with some dependence on the peak turbulent intensity E_0^* at the initial station $\left(\xi_0 = 4 \times 10^4\right)$. That is, when E_0^* is decreased, the peak values of $\sqrt{E}$ at subsequent stations in the transition region are also decreased (shown in fig. 5(b) with Glushko diffusion increased three times) but the profiles for $R_{x_1} > 5 \times 10^5$ are of the same shape and magnitude regardless of the value of E_0^*. This computed behavior of the $\sqrt{E}$ profiles is qualitatively in agreement with experimental observations in the transition region. (See ref. 47, for example.) Multiplying the turbulent diffusion term by three decreased $\sqrt{E}$ in most of the boundary layer except near the outer edge where $\sqrt{E}$ was at most doubled. These latter effects would be expected because of the gradient-type model (eq. (13)) used to formulate the diffusion term.

Since the H(R) modification together with the arbitrary increase of three times the diffusion term improved the F and E profiles as well as the $\tau_T/2\rho\bar{e}$ distribution, the remaining discussion for the flat-plate case, as well as the adverse-pressure-gradient case, is limited to those results with both modifications included. It is emphasized that these simple modifications appeared to improve the agreement between the calculations and experimental data of both the fluctuating and mean characteristics of the fully turbulent boundary layer.

Boundary-layer-thickness parameters.- The momentum thickness and the boundary-layer-thickness Reynolds numbers obtained from the solutions are plotted against R_{x_1} in figure 6. The momentum thickness (fig. 6(a)) follows the laminar trend of $\sqrt{R_{x_1}}$

---

[3]Other possibilities are to restrict the H(R) modification to the turbulent shear term only or to replace C in the dissipation term by a suitable function of x_2/δ. The diffusion term is also a candidate for modification because it is the only other term in equation (28) subject to semiempirical modeling.

until somewhat downstream of the $R_{x_{1,t}}$ values noted for the H^* and C_f results. Thereafter, θ increases and appears to approach asymptotically the nominal variation of $\left(R_{x_1}\right)^{4/5}$ (ref. 39, p. 537) for turbulent boundary layers. The agreement with the data of Wieghardt and Tillmann (ref. 46) appears to be reasonable.

The variation in R_δ (fig. 6(b)), where δ was taken as the value of x_2 at which $F = 0.995$, shows the same trends as the θ variation except that $d\delta/dx_1$ appears to increase more rapidly than $d\theta/dx_1$ and reaches a well-defined peak value in the neighborhood of $R_{x_1} = 3 \times 10^5$. This same type of variation in boundary-layer thickness within a transition region has been observed in experimental investigations such as that of reference 47. These data show that the slope $d\delta/dx_1$ is larger in the transition region than in the turbulent region to which it would eventually asymptote, that is, the slope $d \log_e \delta/d \log_e x_1$ must approach the nominal value of 4/5 downstream of transition. This value of 4/5 is characteristic of fully turbulent boundary layers and appears to be an asymptotic limit for the present calculation.

Balance of turbulent kinetic energy.- The convection, production, diffusion and dissipation of turbulent kinetic energy corresponding to the first three terms, the fourth term, the fifth term, and the sixth term, respectively, in equation (28) are plotted against $x_2/\delta_{F=0.995}$ in figure 7. The scales used for the ordinate axes in this figure correspond to the dimensionless parameters used by Klebanoff (ref. 32). Computed values from the theory are shown in figures 7(a) and 7(b). The convection and diffusion terms are negligible in the region $0.1 < x_2/\delta < 0.6$. In the outer part of the boundary layer $\left(x_2/\delta > 0.85\right)$, these two terms are dominant over the other terms. In the inner part of the boundary layer for $x_2/\delta < 0.01$ (fig. 7(b)), the diffusion is of the same order as the production and dissipation terms and, as would be expected, the diffusion changes sign (proceeding outward from the wall) from a gain of energy very close to the wall to a loss of energy for $0.001 < x_2/\delta < 0.025$, back to a gain for $0.025 < x_2/\delta < 0.1$. The production and dissipation are essentially equal and opposite in sign for the region $0.1 < x_2/\delta < 0.6$, and are still the largest terms in the near-wall region. Comparison of these results with those of Klebanoff (ref. 32) replotted in figures 7(c) and 7(d) indicates, in general, qualitative agreement except for the magnitude and trends of the diffusion for $x_2/\delta < 0.5$. The computed diffusion appears to be too small for $x_2/\delta < 0.5$ and also does not duplicate all trends of the experimental results. It should be noted, however, that there may be some error in Klebanoff's diffusion (which was not measured directly) in this region, since the integral of the diffusion from his data would not be zero, as it should be. Comparison of the computed diffusion (fig. 7(a)) with the measurements of Townsend, as quoted by Hinze (ref. 1, p. 498) shows that the trends in the computed values are in agreement with Townsend's data for $0.1 < x_2/\delta < 1.0$. The agreement between the computed diffusion and the data

of Townsend could probably be further improved by multiplying the original diffusion term by a simple function of x_2 rather than by a constant.

Nonequilibrium Boundary Layer

Several investigations (refs. 36, 43, and 51, for example) have been made recently to determine the response of a turbulent boundary layer to changes in the external pressure gradient. In the investigation of Goldberg (ref. 43), detailed hot-wire measurements of turbulent shear stress and longitudinal turbulence intensities, as well as measurements of velocity profiles and wall shear stress, were made for six different pressure distributions. The test boundary layers of reference 43 were established on a 10-inch-diameter cylinder which was alined parallel to the free stream. The flow was carefully checked for axisymmetry from lateral variations of wall static pressures, wall shear stress measured with sublayer fences, and the separation line as indicated by tufts and the sublayer fences.

Since the maximum boundary-layer thickness was about 1.5 inches (0.04 m), the effects of the axisymmetric geometry on the boundary-layer characteristics must be considered. Goldberg found that the maximum difference between values of δ^* and θ from axisymmetric and two-dimensional formulas was about 10 percent whereas the maximum difference for H^* was only about 2 percent. Differences in skin friction and fluctuating properties would probably not be any larger. It is considered likely that differences of this type are smaller than three-dimensional effects in a conventional two-dimensional test channel, particularly if the boundary layer is near or at separation. The computer program described herein is at present limited to two-dimensional flows. The additional complexity of accounting for the axisymmetric geometry was not considered to be worthwhile in view of the preliminary nature of the models used for the various turbulent correlations.

It was concluded that from among the available investigations, the data by Goldberg would be the most useful as test cases and his pressure distribution number 3 (ref. 43) was selected as the most severe test case since, as mentioned previously, the boundary layer was driven almost to separation by a severe adverse pressure gradient over the first 16 inches (0.40 m) of the run and then allowed to relax toward a flat-plate boundary layer by imposing a constant pressure run for the next 24 inches (0.61 m).

The distribution of external velocity and its derivative with respect to x_1 as used to obtain the present results are shown in figure 8. There was some uncertainty in reading the small graphs published in reference 43. Also, this case appears to be unusually sensitive to initial conditions as shown by Bradshaw and Ferriss (ref. 44). Consequently, all input quantities as used in the present calculations are listed in tables II and III. Second-order interpolation was used between these tabulated values to supply sufficient detail for the calculation. Table II lists the values of F and E used at the

input station corresponding to $x_1 = 4$ inches (0.10 m) (presumably the distance from the nose of the 10-inch-diameter (0.25 m) test cylinder). Table III includes U_e, dU_e/dx_1, $dU_e/d\xi$, and ξ as functions of x_1. Two different tabulations, designated as velocity distributions a and b, are given in table III. These alternate velocity distributions are plotted in figure 8(a) and the differences between them are believed to be within the reading accuracy of the original figures in reference 43 and probably within the experimental errors of the original data. The resulting derivatives of the two velocity curves are considerably different as shown in figure 8(b) where dU_e/dx_1 used in the calculations is plotted against x_1. These differences can become important when the boundary layer approaches separation.

The initial ξ_0 (8×10^5) for the input station ($x_1 = 4$ inches (0.10 m)) was computed by assuming flat-plate flow at $U_e = 85$ ft/sec (25.9 m/s) over the upstream test cylinder length taken as 1.5 feet (0.46 m). The solutions should not be sensitive to the values of ξ_0 if all other input conditions are held fixed. This insensitivity to ξ_0 was verified by obtaining a repeat solution with $\xi_0 = 3 \times 10^6$, and all results were essentially identical to those obtained with $\xi_0 = 8 \times 10^5$. The initial velocity profile was taken directly from the data plot of reference 43 at $x_1 = 4$ inches (0.10 m) and the initial E profile was taken from the measured longitudinal intensity at the same station as

$$E = \frac{\overline{u_1'^2} + \overline{u_2'^2} + \overline{u_3'^2}}{2U_e^2} \approx \left(\frac{\overline{u_1'^2}}{U_e^2}\right)_{measured} \tag{32}$$

This expression is based on the data of reference 32 where all these components of the fluctuating velocity were measured. These data are plotted in figure 5(a) which shows that the approximate expression (32) is accurate for $0.1 < x_2/\delta < 0.8$. A constant value of $\Delta\eta$, corresponding to $K = 1$, was used for most of the solutions reported herein. Repeat solutions with variable $\Delta\eta$, corresponding to $K = 1.02$ (see appendix B) gave essentially identical results and reduced the number of $\Delta\eta$ steps to about 1/4 of the number required for $K = 1.00$.

Relation between skin friction and $\sqrt{E}$ profiles.- The calculated variation in skin friction is compared with the experimental data in figure 9. The shaded band represents the spread in the experimental skin-friction data obtained by four methods (ref. 43): (1) sublayer fence, (2) Preston tube, and from measured velocity profiles using (3) Clauser's method (ref. 42) and (4) the Ludwieg-Tillmann relation (ref. 52). Theoretical results are presented for both velocity distributions of figure 8, three values of C (dissipation constant), and three l/δ functions. The $\phi_{0.33}$ function is the same as that used for the flat-plate calculations given in table I and the other two functions as used herein are also

given in table I. Linear interpolation between the tabulated values was used in the solutions. Prandtl's mixing length relation is thereby recovered in the law-of-the-wall region (for example, $x_2/\delta < 0.2$) where production and turbulent dissipation are approximately equal. That is, by equating production and dissipation

$$\tau_T \frac{\partial \overline{u}_1}{\partial x_2} \approx \mu \overline{\frac{\partial u_i'}{\partial x_j} \frac{\partial u_i'}{\partial x_j}} \qquad (33)$$

and by eliminating $\overline{e}$ between equations (7), (9a), and (12) with $R \gg 1$ ($H(R)$ and $H(\kappa R) = 1$), there is obtained

$$\frac{\tau_T}{\rho} \approx \frac{\alpha}{\sqrt{\kappa C}} l^2 \left(\frac{\partial \overline{u}_1}{\partial x_2}\right)^2 \qquad (34a)$$

Then with $l = y$, $\alpha = 0.2$, $\kappa = 0.4$, $C = 3.93$

$$\frac{\tau_T}{\rho} \approx (0.4y)^2 \left(\frac{\partial \overline{u}_1}{\partial x_2}\right)^2 \qquad (34b)$$

which corresponds to the Prandtl mixing-length relation for turbulent boundary layers. In the following discussion, the effect of velocity distribution and C are considered first.

For velocity distribution a, $C = 3.93$, and $l/\delta = \phi_{0.33}$, the agreement with data is good (fig. 9) except in the region of the minimum C_f where the present method overpredicts C_f by as much as 100 percent. The agreement is somewhat better when the alternate velocity distribution b was used. These different values for C_f in this region indicate the sensitivity of the results to the imposed velocity distribution.

In order to determine the relative importance of the dissipation term (eq. (12)) for this particular type of flow, additional solutions with $C = 5$ and $C = 6$ for pressure distribution b and $\phi_{0.33}$ were obtained. An increase in C increases the dissipation and reduces the skin friction by an almost constant amount over the entire test region and gives improved agreement with data near the minimum C_f region, at the expense of poorer agreement elsewhere. The turbulent kinetic energy equation can be paraphrased as

$$\frac{D\overline{e}}{Dt} = \text{Production} + \text{Diffusion} - \text{Dissipation} \qquad (35)$$

where $\frac{D}{Dt}$ is the derivative following the particle. It is evident that an increase in dissipation should decrease $\overline{e}$, and this decrease, in turn, should decrease the turbulent

shear which from equation (10) is approximately

$$\tau_T \approx \alpha\rho\sqrt{\bar{e}}\,l\,\frac{\partial\bar{u}_1}{\partial x_2} \tag{36}$$

for $R > R_0$. Since the skin friction depends directly on the magnitude of τ_T in the wall region, the decrease in C_f due to the increase in C appears to be reasonable, although it is somewhat surprising to find the almost linear relation between the magnitudes of the dissipation and C_f.

In order to arrive at an explanation for the improved agreement between the computed and experimental skin friction in the minimum C_f region, as caused by larger values of C, profiles of $\sqrt{E}$ are shown in figure 10. The theoretical values in this figure were computed with the diffusion term taken as three times the Glushko diffusion ($3 \times$ eq. (13)), velocity distributions a and b, different values of C, and different l/δ functions. The first thing to note is that all these various modifications had only minor effects on the magnitude and distribution of $\sqrt{E}$ at a given x_1 station. An increase in C does reduce $\sqrt{E}\left(=\frac{\sqrt{\bar{e}}}{U_e}\right)$, as it should according to equation (35), but the best agreement with the data is generally obtained with $C = 3.93$. (The effect of the change in the l/δ function is considered in a subsequent section.) The input profile of $\sqrt{E}$ (fig. 10(a)) is similar to the flat-plate profiles of figure 5. Comparison of the $\sqrt{E}$ profiles at increasing x_1 stations as shown in figures 10(a) and 10(b) shows that as the minimum C_f region (near $x_1 = 20$ inches) is approached, the peak in both the computed and measured $\sqrt{E}$ profiles moves away from the wall and increases in magnitude. Consequently, there is a corresponding increase in the average turbulent energy $(\bar{e})_{av}$ across the entire boundary layer as x_1 increases. That this increase in $(\bar{e})_{av}$ can be associated with a decrease in a dissipation length scale l_d can be seen by noting that for large R, the dissipation (eq. (12)) can be written approximately as

$$\nu\,\overline{\frac{\partial u_i{}'}{\partial x_j}\frac{\partial u_i{}'}{\partial x_j}} \approx \nu C\left[1 + \frac{\epsilon}{\mu}(\kappa R)\right]\frac{\bar{e}}{l_d{}^2} \approx \kappa\alpha(\bar{e})^{3/2}\,l\,\frac{C}{l_d{}^2} \tag{37}$$

where l_d is defined here as a microscale of the turbulence (ref. 1, p. 37). Then if the quantity $C/l_d{}^2$ is considered as an adjustable function but with C fixed as a universal constant, the larger values of C as used for the solutions of figure 9 should be considered as equivalent to corresponding decreases in the square of the dissipation scale $l_d{}^2$. The quantity l in equation (37) is considered to be the same mean scale (analogous to an integral scale) as defined by equation (8) and as used by Glushko (ref. 17).

30

The relation between l and l_d for isotropic turbulence (ref. 1, p. 185) may be written as

$$\left(\frac{l_d}{l}\right)^2 \approx \frac{C'}{\left(\frac{\sqrt{\bar{e}}\,l}{\nu}\right)_{av}}$$ (38)

where C' is a constant. This relation is seen to be in agreement with the results of figure 9 as related to the change in $\sqrt{E}$ profiles with x_1 (fig. 10) since as $(\bar{e})_{av}$ increased, l_d should decrease which, according to the preceding reasoning, accounts for an increase in dissipation and the reduction in C_f, as computed. The reduction in C_f follows from the approximate equivalence of production and dissipation (eq. (33)) but with the dissipation given by relation (37). Relation (34a) then becomes

$$\frac{\tau_T}{\rho} \approx \frac{\alpha}{\sqrt{\kappa}} l \left(\frac{\partial \bar{u}_1}{\partial x_2}\right)^2 \frac{l_d}{\sqrt{C}}$$

and substitution of the expression (38) into this relation gives

$$\frac{\tau_T}{\rho} \approx \frac{\alpha}{\sqrt{\kappa}} \frac{l^2}{U_e} \left(\frac{\partial \bar{u}_1}{\partial x_2}\right)^2 \sqrt{\frac{C'}{C}} \frac{1}{\left(\frac{\sqrt{E}\,l}{\nu}\right)_{av}}$$

which indicates that a functional relation for l_d of the type given by equation (38) would improve the agreement between theory and data over the entire test length for this case because of the way $\left(\sqrt{E}\right)_{av}$ varies with x_1. This explanation depends on the assumption that the mean scale l is not affected by $(\bar{e})_{av}$; that is, l/δ is assumed to be a fixed function of x_2/δ.

Boundary-layer thickness parameters and mean velocity profiles.- The computed values of θ and δ are compared in figure 11 with the experimental data. In figure 11 and all remaining figures, the theoretical values of δ are taken at the point where $F = 0.995$, and the experimental values of δ were taken directly from figure 20 of reference 43. The differences between the theoretical and experimental values of θ are small. However, these small differences can lead to large effects on C_f since the momentum integral equation

$$\frac{d\theta}{dx_1} + \frac{\theta}{U_e} \frac{dU_e}{dx_1}(H + 2) = \frac{C_f}{2}$$ (39)

shows that when C_f approaches zero in a large adverse pressure gradient (negative dU_e/dx_1), the skin friction equals the difference between two large terms, and any small changes in either of these terms can lead to large changes in C_f.[4] The difference between the theoretical and experimental values of δ are also small, as shown in figure 11(b). The use of velocity distribution a, $C = 3.93$, and $l/\delta = \phi_{0.25}$ generally gives the best agreement with the data except for the θ distributions when $x_1 \geqq 20$ inches (0.51 m) where the $\phi_{0.33}$ solution (with $C = 3.93$ and velocity distribution a) gives the best agreement. However, it is obvious that a comparison of θ and δ alone are not sufficient to judge the accuracy of a method when C_f approaches 0.

The shape parameter H^* is a more sensitive indicator of the accuracy of a method as shown by figure 12 where the effects of the two velocity distributions, the values of C, and the l/δ functions are shown. The velocity distribution b and the largest value of C give the best agreement with the experimental data for $l/\delta = \phi_{0.33}$. However, the use of the other two l/δ functions gives the best overall agreement with the data, and the results bracket the data in the vicinity of the peak H^*.

The reason for the better agreement of H^* with data for $l/\delta = \phi_{0.20}$ and $\phi_{0.25}$ is apparent from figure 13 where the computed velocity profiles at three x_1 stations are compared with the data. (Here again the subscripts denote the maximum values of the l/δ functions; these functions are given in table I.) The agreement between theoretical and experimental velocity profiles for all ϕ functions is fair at $x_1 = 12$ inches (0.30 m) (fig. 13(a)) where dU_e/dx_1, according to figure 8(b), is near its peak value. However, at $x_1 = 20$ inches (0.51 m) (fig. 13(b)) where dU_e/dx_1 is approaching zero, the agreement is poor for $l/\delta = \phi_{0.33}$ for both velocity distributions a and b and for all values of C. When $\phi_{0.20}$ and $\phi_{0.25}$ are used, the theoretical results bracket the data for this station of $x_1 = 20$ inches (0.51 m), which is apparently a critical region where the calculation is very sensitive to the l/δ function. Near the end of the constant pressure run at $x_1 = 36$ inches (0.91 m) (fig. 13(c)), the good agreement between the theory (with $l/\delta = \phi_{0.33}$) and data may be fortuitous.

Discussion of turbulence scale functions.- It has already been noted from figure 10 that $\sqrt{E}$ is relatively insensitive to changes in free-stream velocity distribution, C, and the l/δ function. Figure 13 shows that the mean velocity profiles at a given x_1 station are insensitive to the two velocity distributions and the values of C considered, but can be affected considerably by a change in l/δ. Since the turbulent shear, production, and dissipation are the dominant terms in the equations, it is apparent from the preceding discussion and from the form of these terms (see eqs. (36) and (37)) that the only way to

---

[4]Note that in the present method C_f was not computed from equation (39), but from equation (30) which probably requires more stringent accuracy criteria in the calculation than equation (39) would.

change the mean velocity profiles, and hence the H^* values to any appreciable extent is to modify the turbulence scale function l/δ. In the previous section, a change in C was related to a change in a dissipation microscale l_d, but from equation (34), a change in C is equivalent to a change in the mixing length constant of Prandtl. Since the mixing length relation of Prandtl is known to apply even in an adverse pressure gradient in the law-of-the-wall region, the l/δ function was not changed for $x_2/\delta < 0.2$. Goldberg's experimental values of mixing length (ref. 43) indicate that l/δ should be decreased in the region of $x_2/\delta > 0.2$. Since this decrease would reduce the turbulent shear and thereby result in a more linear velocity profile, the l/δ functions were changed in the manner shown in figure 14(a). (See also table I.)

The corresponding values of the eddy viscosity function ϵ/μ at $x_1 = 20$ inches (0.51 m) are shown in figure 14(b). As would be expected, the ϵ/μ function does not depend on the two free-stream velocity distributions or the values of C used, since $\sqrt{E}$ was independent of these parameters. However, the distribution and magnitude of ϵ/μ are directly dependent on l/δ and the theoretical curve for $l/\delta = \phi_{0.20}$ is closer to the experimental values of reference 43. This direct dependence of ϵ/μ on l/δ is, of course, the reason for the marked effect of the l/δ function on both C_f (fig. 9) and $\bar{u}_1/U_e$ (fig. 13).

The success of these modifications to l/δ indicates that further minor adjustments to these functions should give further improvement in agreement with experimental data. In particular, the trends in $\sqrt{E}$ (fig. 10) for this problem indicate the magnitude of the change in l/δ should probably depend on the level of $(\bar{e})_{av}$. Spalding (ref. 53) has applied to free shear flows a differential equation for the mean scale of turbulence. This equation was based on Rotta's hypothesis (ref. 6, part II) and relates the scale of turbulence to $(\bar{e})_{av}$ and τ_T. It is possible that the use of a similar relation may improve the predictions of the present method.

Comparisons with empirical correlations of mean velocity.- Comparisons between calculated and experimental values of mean velocity are also shown in figure 15 in law-of-the-wall coordinates. At $x_1 = 12$ inches (0.30 m) (fig. 15(a)) both the data and theory deviate from the logarithmic law of the wall for large values of $u^* x_2/\nu$ as is characteristic of boundary layers with adverse pressure gradients. In the minimum C_f region ($x_1 = 20$ inches (0.51 m), fig. 15(b)), the data and the theory for $\phi_{0.25}$ still follow the law of the wall up to $\dfrac{u^* x_2}{\nu} \approx 70$. At the downstream station of $x_1 = 36$ inches (0.91 m) (fig. 15(c)), after a constant pressure run of about 12 inches (0.30 m), the logarithmic variation is followed by both data and theory (with $\phi_{0.25}$) for $25 < \dfrac{u^* x_2}{\nu} < 400$. It can

be concluded, therefore, that the mean velocity profiles have completely adjusted to the zero-pressure-gradient condition.

Fluctuating flow quantities.- The total turbulent intensity profiles in the form of $\sqrt{\bar{E}}$ are shown in figure 10 and have been discussed previously. Experimental values were obtained from the measured longitudinal intensities by the use of expression (32). The agreement in both trends and magnitude is generally good over the portion of the boundary layer where the approximate relation (32) is applicable.

The variation in the ratio of turbulent shear to twice the turbulent kinetic energy across the boundary layer at three stations is shown in figure 16. As mentioned previously, this ratio $\tau_T/2\rho\bar{e}$ tends to have an approximately universally constant value in the intermediate region of the boundary layer. By the use of equation (32), the ratio $\tau_T/2\rho\bar{e}$ was obtained from the data of Goldberg (ref. 43) and Bradshaw and Ferriss for a relaxing boundary layer (ref. 36). These values are plotted for comparison with the theoretical results in figure 16. The stations of x_1 = 47, 59, and 95 inches (1.09, 1.5, and 2.41 m) should be comparable to Goldberg's stations x_1 = 14, 20, and 36 inches (0.35, 0.51, and 0.91 m) (figs. 16(a), 16(b), and 16(c)), respectively, in terms of the relative distributions of external velocity and velocity gradient in the two investigations. The theoretical results are generally in reasonable agreement with the data. (Note that the best agreement with Goldberg's data was generally obtained with $(l/\delta) = \phi_{0.20}$ or $\phi_{0.25}$.) It is seen that the ratio $\tau_T/2\rho\bar{e}$ is roughly the same at all stations and for the two sets of data shown except at the critical station of x_1 = 20 inches (0.51 m) (fig. 16(b)). Note that at x_1 = 36 inches (0.91 m) (fig. 16(c)), where the mean velocity profile and H^* have relaxed to flat-plate values (figs. 15(c) and 12), the experimental and theoretical values of $\tau_T/2\rho\bar{e}$ are still somewhat below that typical of flat-plate flow.

The distributions across the boundary layer of the four terms in the turbulent kinetic energy equation at four x_1 stations are shown in figure 17 for velocity distribution a, C = 3.93, and $l/\delta = \phi_{0.25}$. The scales used in the figure correspond to the dimensionless parameters used in equation (28). At x_1 = 8 and 12 inches (0.20 and 0.30 m) (figs. 17(a) and 17(b)), the distributions are similar to those of the equilibrium boundary layer of Bradshaw for a = -0.15 (fig. 14(c) of ref. 34). At x_1 = 17.4 inches (0.44 m) (fig. 17(c)) the trends are more nearly like those of Bradshaw for a = -0.255 (fig. 14(d) of ref. 34) in that the relative magnitude of the diffusion is increased in the central part of the boundary layer. The distribution of production and convection terms at x_1 = 20 inches (0.51 m) and 36 inches (0.91 m) (figs. 17(c) and 17(d)) are qualitatively similar to the corresponding results for the relaxing boundary layer of Bradshaw and Ferriss at x_1 = 53 (1.35 m) and 83 inches (2.11 m) (ref. 36).

Comparison of the results shown in figure 17 with corresponding results for velocity distribution b and other values of C indicates that the trends and magnitudes of the various terms are not greatly affected by these changes in external velocity distribution

34

and C except near the wall. The location and magnitude of the peak values (nearest the wall) of the terms are shown in the following table:

Velocity distribution	l/δ	C	x_2/δ	Production	x_2/δ	Dissipation	x_2/δ	Diffusion	x_2/δ	Convection
				$x_1 = 8$ inches	(0.20 m)					
a	$\phi_{0.33}$	3.93	0.021	1.37	0.005	-2.55	0.005	2.05	0.005	-0.445
b	$\phi_{0.33}$	3.93	.021	1.4	.005	-3.86	.005	2.85	.005	.919
b	$\phi_{0.33}$	5	.026	1.25	.016	-.833	.0106	1.0	.0106	-.597
b	$\dot{\phi}_{0.33}$	6	.026	1.139	.0107	-.785	.0107	.764	.016	-.224
				$x_1 = 20$ inches	(0.51 m)					
a	$\phi_{0.33}$	3.93	0.014	0.533	0.0028	-1.08	0.0028	0.919	0.0028	0.154
b	$\phi_{0.33}$	3.93	.014	.483	.008	-.376	.0054	.534	.0054	-.352
b	$\phi_{0.33}$	5	.017	.384	.0028	-1.44	.0028	1.18	.0055	.258
b	$\phi_{0.33}$	6	.017	.315	.0028	-1.0	.0028	.76	.0028	.244
				$x_1 = 20$ inches	(0.51 m)					
a	$\phi_{0.20}$	3.93	0.019	0.139	0.0028	-0.778	0.0028	0.654	0.0058	0.137
a	$\phi_{0.25}$	3.93	.017	.293	.0028	-1.27	.0028	1.07	.0058	.246

Comparison of these peak values shows that the dissipation is not always increased when C is increased. This result is presumably an indication of the nonlinear nature of the problem. It is also of interest to note that the location of the peaks in all terms is usually closer to the wall (in terms of x_2/δ) at $x_1 = 20$ inches (0.51 m) than at $x_1 = 8$ inches (0.20 m). Another item worth noting from the table is that when the velocity distribution and C are the same but l/δ is different, the magnitude (except for the dissipation and diffusion) and location of the peaks are appreciably different, in spite of the fact that the l/δ function was not changed in the wall region. (See fig. 14(a).) This result is, of course, an important confirmation of the experimental fact that the upstream history of the flow in this kind of a boundary layer has a large effect on local conditions.

Other adverse-pressure-gradient cases.- Any method for predicting the development of turbulent boundary layers cannot be considered satisfactory until the results for several different types of flows with a variety of initial and boundary conditions are compared with experimental data. Some comparisons of this type for the modified Glushko method have been reported by the present authors in reference 54. The method was applied to several cases and reasonable agreement in H^*, C_f, and R_θ was generally obtained.

CONCLUDING REMARKS

The equations for the incompressible turbulent boundary layer with constant fluid properties have been solved by a numerical procedure in similarity type coordinates. A parameter in the definition of these coordinates could be adjusted to keep the turbulent boundary-layer thickness in the transformed coordinate system approximately constant; this procedure gives a nearly constant number of computing steps across the boundary layer. The conservation equations for mass, mean momentum, and turbulent kinetic energy are solved simultaneously by a linearized, implicit, finite-difference procedure wherein all boundary conditions at the surface and outside edge of the boundary layer are satisfied directly.

Mathematical models of the turbulent production, dissipation, and diffusion terms developed by Glushko (Bull. Acad. Sci. USSR, Mech. Ser., no. 4, 1965) for flat-plate turbulent flow have been modified and applied also to a nonequilibrium turbulent boundary layer subjected initially to a large adverse pressure gradient which is followed by a constant-pressure region. Comparisons of calculated values for both mean and fluctuating flow properties with experimental measurements in this nonequilibrium boundary layer as well as the flat-plate boundary layer have indicated generally good agreement.

For the flat-plate calculation, the laminar Blasius velocity profile and arbitrary small disturbance-type profiles for the turbulent kinetic energy were used as initial conditions at a Reynolds number of 10^4. As the calculation proceeded, little change in the mean profiles of velocity and turbulent kinetic energy were noted until at some downstream station, depending on the level of the input disturbance and a modification to the turbulence diffusion term, rather abrupt changes began. The subsequent mean velocity profiles, turbulent kinetic energy profiles, and skin friction were qualitatively similar to those observed experimentally in the transition region between laminar and fully turbulent flow. The dependence on the level of the input turbulent kinetic energy of the Reynolds number at which these changes in the mean profiles were first obtained in the calculation was shown by Glushko. It is shown herein that modifications to the models of the turbulent terms also affected this Reynolds number. The value of this Reynolds number was an order of magnitude lower than minimum experimental transition Reynolds numbers and cannot yet be related to the physical phenomenon of transition. Nevertheless, the indications are that further development of the method may ultimately yield a useful technique for the numerical investigation of transition.

It was found that when the turbulent diffusion term of Glushko was multiplied by an arbitrary factor of three, the agreement with experimental values of mean velocity and the ratio of turbulent shear to turbulent energy was improved in the outer portion of the fully turbulent boundary layer for both the flat-plate and nonequilibrium flows. It was also

36

found that when the dissipation term was changed, the skin friction was reduced by almost constant increments that depended directly on reductions in the square of the dissipation scale. Analysis of these results indicated that the microscale (dissipation scale) may be related to the integral scale of turbulence in about the same way as that for isotropic turbulence. The best overall agreement with measured values of skin friction, form factor, mean velocity profiles, and fluctuating properties was obtained by reducing the value of the turbulence scale from a peak of 0.33 to 0.20 or 0.25 of the boundary-layer thickness in the midregion of the boundary layer. The linear relation of turbulence scale with distance from the wall, in accordance with Prandtl's mixing length theory and as used by Glushko, was retained in the law-of-the-wall region. It is concluded that simple modifications to the turbulence scale function and to the turbulent correlation terms as modeled by Glushko result in accurate calculations of mean and fluctuating characteristics of turbulent boundary layers with arbitrary boundary conditions.

The existence of similar solutions to the equations with the turbulence correlation terms modeled according to Glushko was investigated briefly. It is shown that exact similar solutions are not possible in the coordinates used in the numerical calculation. However, approximate similar solutions exist for other coordinate systems. In one of these systems, the normal coordinate is simply the physical distance from the surface divided by the local boundary-layer thickness which is then required to increase linearly with distance along the surface in order to obtain similar solutions.

Langley Research Center,
    National Aeronautics and Space Administration,
        Langley Station, Hampton, Va., August 1, 1968,
            124-07-01-32-23.

APPENDIX A

REQUIREMENTS FOR SIMILAR SOLUTIONS

Analyses of results from many experimental investigations have shown that the mean velocity profiles in the incompressible turbulent boundary layer, with $dp_e/dx_1 = 0$, are similar in terms of $\dfrac{\bar{u}_1}{u^*}$, $\dfrac{x_2 u^*}{\nu}$ and $\dfrac{\bar{u}_1 - U_e}{u^*}$, $\dfrac{x_2}{\delta}$ in the inner and outer parts of the boundary layer, respectively (ref. 41). For $dp_e/dx_1 \neq 0$, Clauser (ref. 42) has shown that velocity profiles are self-preserving or approximately similar if the parameter $\left(\dfrac{\delta^*}{\tau_w}\right)\dfrac{dp_e}{dx_1}$ is a constant. As the Reynolds number approaches infinity, all velocity and length scales except δ and U_e should become independent of x_1; therefore, even with an imposed pressure gradient, the entire mean velocity profile would presumably depend only on x_2/δ. For a limited range of conditions or within certain regions of the boundary layer, similar solutions to the turbulent boundary-layer equations are therefore possible as shown, for example, in references 9, 14, 20, 55, and 56. The purpose of this appendix is to discuss briefly the conditions required for the existence of similar solutions to the equations of mean momentum, turbulent kinetic energy, and mass continuity in the form of equations (16) to (18). It is hoped that the discussion will assist in the evaluation of the models proposed by Glushko for the shear, dissipation, and diffusion of turbulence.

For this purpose, it is convenient to introduce general coordinates defined as

$$\left.\begin{aligned} X(x_1) &= \int_0^{x_1} P \, dx_1 \\[2mm] Y(x_1, x_2) &= PQx_2 \end{aligned}\right\} \tag{A1}$$

where P and Q are as yet unspecified functions of x_1. It is necessary at the outset to exclude the viscous sublayer region in order to obtain similarity. Hence, the restriction $R \gg 1$ is imposed and the coefficient functions M and D (eq. (19)) become

$$\left.\begin{aligned} M &\approx \alpha \, \frac{U_e \delta}{\nu} \sqrt{E} \, \frac{l}{\delta} \\[2mm] D &\approx \alpha \kappa \, \frac{U_e \delta}{\nu} \sqrt{E} \, \frac{l}{\delta} \end{aligned}\right\} \tag{A2}$$

The transformation of equations (16), (17), and (18) to the variables X and Y then gives for momentum:

$$\frac{F}{Q} \frac{\partial F}{\partial X} + V \frac{\partial F}{\partial Y} = \frac{1 - F^2}{QU_e} \frac{dU_e}{dX} + \alpha PQ\delta \frac{\partial}{\partial Y}\left(\frac{l}{\delta} \sqrt{E} \, \frac{\partial F}{\partial Y}\right) \tag{A3}$$

for energy:

$$\frac{F}{Q}\frac{\partial E}{\partial X} + V\frac{\partial E}{\partial Y} = -2\frac{FE}{QU_e}\frac{dU_e}{dX} + \alpha PQ\delta\left[\frac{l}{\delta}\sqrt{E}\left(\frac{\partial F}{\partial Y}\right)^2 + \kappa\frac{\partial}{\partial Y}\left(\frac{l}{\delta}\sqrt{E}\frac{\partial E}{\partial Y}\right)\right] - C\alpha\kappa\frac{E^{3/2}}{PQl_d} \quad (A4)$$

and for continuity:

$$\frac{1}{Q}\frac{\partial F}{\partial X} + \frac{\partial V}{\partial Y} + \frac{F}{Q}\frac{d}{dX}\left(\log_e\frac{U_e}{PQ}\right) = 0 \quad (A5)$$

where

$$V = \frac{F}{PQ}\frac{\partial Y}{\partial x_1} + \frac{\bar{u}_2}{U_e} \quad (A6)$$

From equations (A3), (A4), and (A5), it can be seen that the profile functions F, E, and V may be functions only of Y if the following conditions are satisfied:

$$\frac{1}{QU_e}\frac{dU_e}{dX} = \frac{1}{PQU_e}\frac{dU_e}{dx_1} = C_1 \quad (A7)$$

$$\frac{1}{Q}\frac{d}{dX}\left(\log_e\frac{U_e}{PQ}\right) = \frac{1}{PQ}\frac{d}{dx_1}\left(\log_e\frac{U_e}{PQ}\right) = C_2 \quad (A8)$$

$$PQ = \frac{C_3}{\delta} \quad (A9)$$

$$\frac{l}{\delta} = \frac{l_d}{\delta} = \phi(Y) \quad (A10)$$

where the C values are constants. The transformed variable Y then becomes simply

$$Y = C_3\frac{x_2}{\delta} \quad (A11)$$

and equation (A10) is the function ϕ as assumed by Glushko. The requirements on U_e and δ are obtained by combining equations (A7), (A8), and (A9) to give

$$\frac{\delta}{U_e}\frac{dU_e}{dx_1} = C_1 \quad (A12)$$

$$\frac{d\delta}{dx_1} = C_2 - C_1 \quad (A13)$$

Hence, δ must vary linearly with x_1 in agreement with the results of reference 56 (pp. 81-83). (See also ref. 7, pp. 105-109.) By means of Bernoulli's equation, condition (A12) may be written as

$$\frac{\delta}{\rho U_e{}^2} \frac{dp}{dx_1} = -C_1$$

which is essentially the same as Clauser's condition for equilibrium boundary layers (ref. 42, pp. 49-50)

$$\frac{\delta^*}{\rho U_e{}^2 C_f} \frac{dp}{dx} = \text{Constant}$$

provided that $\delta^*/\delta C_f$ is approximately constant as would be the case for equilibrium layers. Consequently, the requirement of equation (A12) would be approximately satisfied by equilibrium boundary layers (including the zero-pressure-gradient case) but the requirement of a linear variation of δ with x_1 would not be satisfied in general.

Another class of similar solutions without this restriction on δ can be derived by dividing equations (A3) to (A5) by P. (Note that in the previous class of solutions where Y varies as x_2/δ, P is arbitrary.) The transformed normal velocity is then defined by

$$V(Y) = \frac{F}{P^2 Q} \frac{\partial Y}{\partial x_1} + \frac{\bar{u}_2}{P U_e}$$

and the remaining requirements for similar solution are

$$\frac{1}{P^2 Q U_e} \frac{dU_e}{dx_1} = C_1{}' \tag{A14}$$

$$\frac{1}{P^2 Q} \frac{d}{dx_1}\left(\log_e \frac{U_e}{PQ}\right) = C_2{}' \tag{A15}$$

$$Q = \frac{C_3{}'}{\delta} \tag{A16}$$

where all C quantities are constants. The function l/δ in equations (A3) and (A4) is again required to be a function only of Y

$$\frac{l}{\delta} = \phi(Y) \tag{A17}$$

However, the dissipation scale l_d in the last term of equation (A4) must now satisfy the relation

40

$$\frac{l_d}{l} = \frac{C_4}{P^2} \tag{A18}$$

where equations (A16) and (A17) have been used.

To find the P function, equations (A14) to (A16) are combined to give

$$\frac{\delta}{P} \frac{d}{dx_1} \frac{\delta}{P} = C_5 \delta$$

where $C_5 = \left(C_2' - C_1'\right)C_3'$. Integration of this expression yields

$$\left(\frac{\delta}{P}\right)^2 = 2C_5 \int_0^{x_1} \delta \, dx_1 \tag{A19}$$

and the ratio of the dissipation scale to the transport scale (eq. (A18)) becomes

$$\frac{l_d}{l} = \frac{C_6}{\delta^2} \int_0^{x_1} \delta \, dx_1 \tag{A20}$$

where $x_1 = 0$ represents the effective origin of the turbulent boundary layer. The conditions given by equations (A16), (A19), and (A20) are more general than those of equations (A12) and (A13) since no restriction on δ is required.

The P and l_d functions given by equations (A19) and (A20) could presumably be determined by numerical iteration techniques for any boundary layer; however, equations (A14), (A16), and (A19) give the additional requirement that

$$d\left(\log_e U_e\right) = \frac{C' \delta \, dx_1}{\displaystyle\int_0^{x_1} \delta \, dx_1}$$

For $\dfrac{dU_e}{dx_1} = 0$ and over a limited range of x_1, the boundary-layer thickness varies as

$$\frac{U_e \delta}{\nu} \propto \left(\frac{U_e x_1}{\nu}\right)^n \tag{A21}$$

Substitution of this expression into equation (A20) yields

$$\frac{l_d}{l} = C_6' \left(\frac{U_e x_1}{\nu}\right)^{1-n} \tag{A22}$$

Thus, if $n = 0.8$, which is a realistic value, the dissipation length scale would increase as the 0.2 power of the Reynolds number in order to obtain similar solutions for a

flat-plate boundary layer with δ increasing according to relation (A21). It is of interest to compare the ratio l_d/l (ratio of dissipation microscale to the transport, or integral, scale) from equation (A22) to the corresponding ratio for isotropic turbulence as given by Hinze (ref. 1, p. 185, and eq. (57)). This result for isotropic turbulence may be written as

$$\frac{l_d}{l} \propto \frac{1}{\left(\dfrac{l}{\delta} \dfrac{\sqrt{E}}{U_e} \dfrac{U_e \delta}{\nu}\right)^{1/2}} \tag{A23}$$

or by the use of relation (A21)

$$\frac{l_d}{l} \propto \frac{1}{\left[\dfrac{l}{\delta} \sqrt{E} \left(\dfrac{U_e x_1}{\nu}\right)^n\right]^{1/2}} \tag{A24}$$

Equation (A24) indicates that if l/δ and E are similar profiles, and if the flat-plate dissipation varied in the same way as isotropic dissipation, l_d/l would decrease with increasing Reynolds number. The isotropic expression (A23) appears to be in qualitative agreement with requirements for l_d in nonequilibrium boundary layers (see discussion concerning eq. (38)); however, by comparison with equation (A22), it can be concluded that the isotropic expression would not be applicable to a flat-plate equilibrium boundary layer.

Other forms for P and Q that would yield similar solutions can be derived by multiplying equations (A3) to (A5) by $P^m Q^i$ where m and i are constants. Since these other forms appear to give results of limited interest or applicability, they are not discussed.

APPENDIX B

NUMERICAL COMPUTATION PROCEDURE

The system of equations (27) to (29), along with auxiliary functions for M, D, and $\bar{n}(x_1)$ as defined in the section "Transformation to Similarity Coordinates" is solved by a linear implicit finite-difference procedure. This procedure combines certain aspects of the methods given in references 17 and 40.

Grid Notation

The boundary-layer region is divided into finite grids of $\Delta\xi$ width and $\Delta\eta$ height as shown in the sketch, where the grid or nodal-point notation is also illustrated. To increase the efficiency and accuracy of the finite-difference procedure, a variable grid size in the η-direction is included. The grid size in the ξ-direction may also vary.
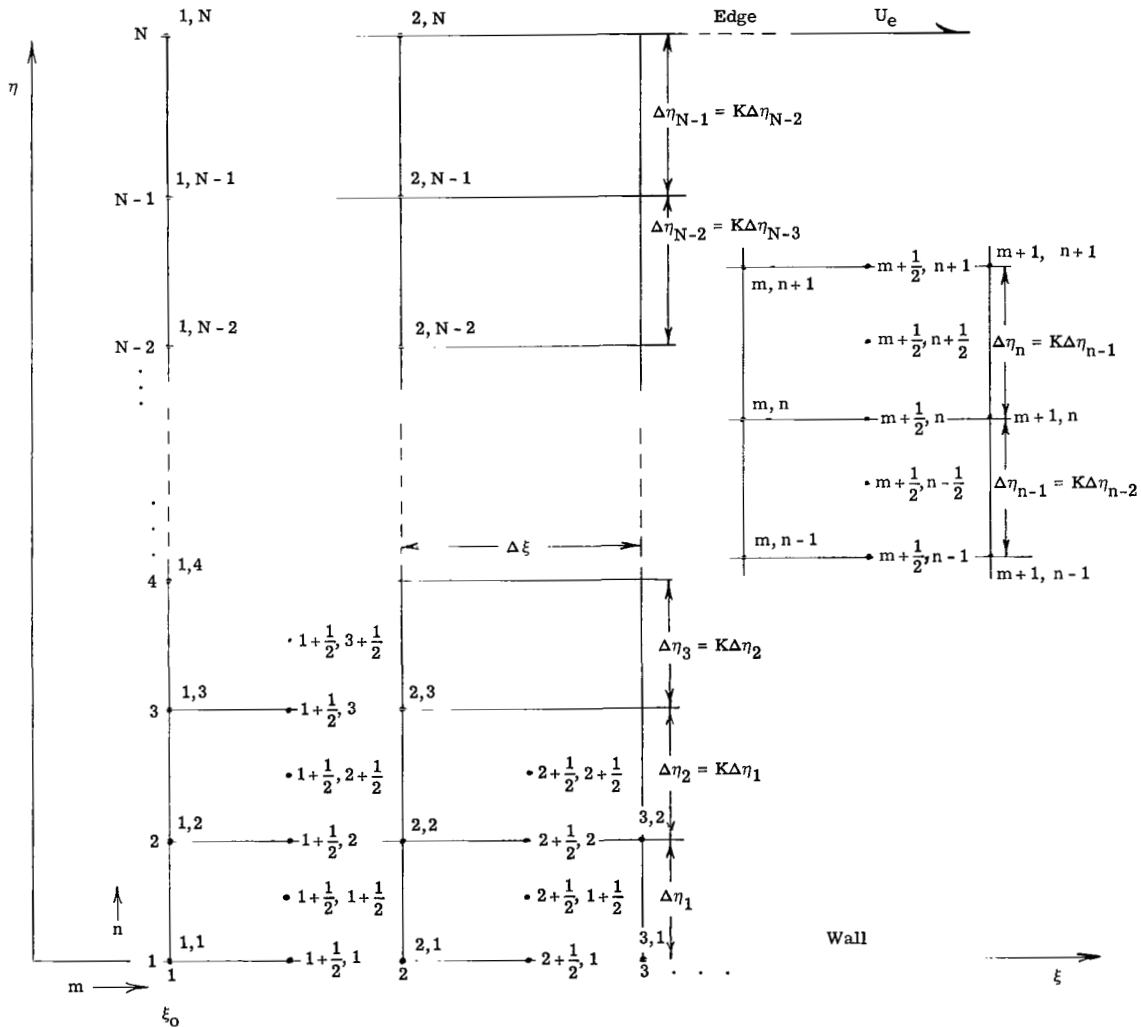
APPENDIX B

The variation in the $\Delta\eta$ grid size is controlled by the parameter K where, as illustrated,

$$K = \frac{\Delta\eta_n}{\Delta\eta_{n-1}} \tag{B1}$$

When K is a constant, the successive $\Delta\eta_n$ values form a geometric progression; hence,

$$\Delta\eta_n = K^{n-1}\,\Delta\eta_1 \tag{B2}$$

The total number of steps across the boundary layer is $N-1$; thus, the size of the last step is

$$\Delta\eta_{N-1} = K^{N-2}\,\Delta\eta_1 \tag{B3}$$

The maximum thickness of the boundary layer η_e is given by

$$\eta_e = \frac{K^{N-1}-1}{K-1}\,\Delta\eta_1 \tag{B4}$$

Thus if η_e, $\Delta\eta_1$, and the number of steps $N-1$ are specified, K and $\Delta\eta_{N-1}$ can be determined from equations (B3) and (B4). Generally, K will be a constant slightly greater than 1.0 in order to give smaller steps near the surface. The smaller steps near the surface increase the accuracy and efficiency of the computation for a typical turbulent boundary layer because the changes in mean velocity near the surface are usually much greater than those in the outer part of the boundary layer. Other parameters such as E and τ may also change rapidly near the outer edge where, with $K > 1.0$, the step size could be considerably larger than that near the surface. Check solutions, however, with $K = 1.00$ and 1.02 have given essentially identical results for all quantities including E and τ_T. Apparently, with $K = 1.02$, enough detail can be retained near the outer edge to avoid any loss of accuracy.

Boundary and Initial Conditions

The external velocity U_e and its derivative dU_e/dx_1 must be specified functions of ξ. The nominal boundary-layer thickness δ, as used in equation (8), is taken as the point where $1 - F = \epsilon_\delta$ which is a specified small constant ($\epsilon_\delta = 0.01$, for example, in the computation of ref. 17). In order to insure an asymptotic boundary condition at the outer edge of the boundary layer, another boundary-layer thickness δ_e, defined as the point where $1 - F = \epsilon_e$, has been used with $\epsilon_e \ll \epsilon_\delta$. (For further discussion of edge boundary conditions, see section "Determination of Number of $\Delta\eta$ Steps.") For the

44

conventional boundary layers to be treated herein, both ϵ_e and ϵ_δ would be small positive numbers. The corresponding values of η from equation (22) are

$$\left. \begin{array}{l} \eta_\delta = \dfrac{U_e}{\nu(2\xi)^{\bar{n}}} \delta \\[4ex] \eta_e = \dfrac{U_e}{\nu(2\xi)^{\bar{n}}} \delta_e \end{array} \right\} \tag{B5}$$

The initial conditions in the form of F, E, and V profiles are specified at $\xi_0 (m = 1)$ from $n = 1$ to $n = N$, from which values of all variables are to be computed at the next station $\xi_0 + \Delta\xi$ or $m = 2$. If it is assumed that the initial profiles for E and V are locally similar (that is, $\partial V/\partial\xi$ and $\partial E/\partial\xi$ are neglected), these profiles may be computed from equations (27) and (29) and the input F_0 profile. In this procedure, equation (29) is solved first for V and then equation (27) can be solved directly for E since M is a function of E from equation (19).

Linear Finite-Difference Expressions

The various types of derivatives in equations (27), (28), and (29) are replaced by linear difference quotients and equations (27) and (28) are evaluated at the intermediate grid points represented generally by the subscript $m + \frac{1}{2}, n$. The values at the intermediate points are computed to a satisfactory approximation as appropriate numerical averages illustrated by the expressions:

$$\left. \begin{array}{l} f_{m+\frac{1}{2},n,i} = \dfrac{1}{2}\left(f_{m,n} + f_{m+1,n,i-1}\right) \\[4ex] f_{m+\frac{1}{2},\, n+\frac{1}{2},\, i} = \dfrac{1}{4}\left(f_{m,n+1} + f_{m,n} + f_{m+1,\, n+1,\, i-1} + f_{m+1,n,i-1}\right) \end{array} \right\} \tag{B6}$$

where f represents any desired quantity or function, and where the subscript i denotes the current step in the iteration cycle and the subscript i - 1 denotes the value obtained in the previous iteration. The partial and total derivatives in equations (27) and (28) are then written with first-order accuracy as illustrated by the following examples:

$$\left(\frac{\partial F}{\partial \xi}\right)_{m+\frac{1}{2},n} = \frac{F_{m+1,n} - F_{m,n}}{\Delta\xi} \tag{B7}$$

$$\left(\frac{\partial F}{\partial \eta}\right)_{m+\frac{1}{2},n} = \frac{1}{2}\left(\frac{F_{m+1,\, n+1} - F_{m+1,\, n-1}}{\Delta\eta_n + \Delta\eta_{n-1}} + \frac{F_{m,n+1} - F_{m,n-1}}{\Delta\eta_n + \Delta\eta_{n-1}}\right) \tag{B8}$$

45

$$
\left[\frac{\partial}{\partial \eta}\left(M \frac{\partial F}{\partial \eta}\right)\right]_{m+\frac{1}{2}, n} = \frac{1}{\Delta\eta_n + \Delta\eta_{n-1}}\left[\frac{M_{m+\frac{1}{2}, n+\frac{1}{2}}\left(F_{m+1,n+1} - F_{m+1,n}\right)}{\Delta\eta_n}\right.
$$

$$
- \frac{M_{m+\frac{1}{2}, n-\frac{1}{2}}\left(F_{m+1,n} - F_{m+1,n-1}\right)}{\Delta\eta_{n-1}} + \frac{M_{m+\frac{1}{2}, n+\frac{1}{2}}\left(F_{m,n+1} - F_{m,n}\right)}{\Delta\eta_n}
$$

$$
\left. - \frac{M_{m+\frac{1}{2}, n-\frac{1}{2}}\left(F_{m,n} - F_{m,n-1}\right)}{\Delta\eta_{n-1}}\right] \tag{B9}
$$

All other terms and coefficients of derivatives appearing in the equations are linearized by evaluating them at the intermediate points $m + \frac{1}{2}$ according to equations (B6). Furthermore, the $(M - 1)\left(\frac{\partial F}{\partial \eta}\right)^2$ term in equation (28) (which is treated as a linear equation for E) is evaluated as

$$
\left[(M - 1)\left(\frac{\partial F}{\partial \eta}\right)^2\right]_{m+\frac{1}{2},n,i} = \left(M_{m+\frac{1}{2},n,i} - 1\right)\frac{4\left(F_{m+\frac{1}{2}, n+\frac{1}{2}, i} - F_{m+\frac{1}{2}, n-\frac{1}{2}, i}\right)^2}{\left(\Delta\eta_n + \Delta\eta_{n-1}\right)^2} \tag{B10}
$$

An alternate expression, which is equivalent to the same accuracy as equations (B7) to (B9), is

$$
\left[(M - 1)\left(\frac{\partial F}{\partial \eta}\right)^2\right]_{m+\frac{1}{2},n,i} = \left(M_{m+\frac{1}{2},n,i} - 1\right)\left(\frac{F_{m+1,n+1,i-1} - F_{m+1,n-1,i-1}}{\Delta\eta_n + \Delta\eta_{n-1}}\right)\left(\frac{F_{m,n+1} - F_{m,n-1}}{\Delta\eta_n + \Delta\eta_{n-1}}\right) \tag{B11}
$$

In this manner the direct coupling between equations (27) and (28) is removed during any one iteration; however, the coupling is actually retained in the complete iteration procedure wherein the intermediate $m + \frac{1}{2}$ values are continually improved, as indicated by equations (B6), until convergence to the desired degree of accuracy is attained.

Computational Equations

<u>Mean momentum</u>.- Substitution of the linear-difference quotients given by equations (B7) to (B9) into equation (27) and collecting terms gives

$$A_n F_{m+1,n+1} + B_n F_{m+1,n} + C_n F_{m+1,n-1} = D_n \tag{B12}$$

where

$$A_n = \frac{V_{m+\frac{1}{2},n}}{2\left(\Delta\eta_n + \Delta\eta_{n-1}\right)} - \frac{M_{m+\frac{1}{2},n+\frac{1}{2}}}{2\,\Delta\eta_n\,\Delta\eta_{n-1}}$$

$$B_n = \left[\frac{(2\xi)^{2\bar{n}}}{\Delta\xi}\right]_{m+\frac{1}{2}} F_{m+\frac{1}{2},n} + \frac{\bar{K}M_{m+\frac{1}{2},n+\frac{1}{2}} + K^*M_{m+\frac{1}{2},n-\frac{1}{2}}}{2\,\Delta\eta_n\,\Delta\eta_{n-1}}$$

$$C_n = -\frac{V_{m+\frac{1}{2},n}}{2\left(\Delta\eta_n + \Delta\eta_{n-1}\right)} - \frac{K^*M_{m+\frac{1}{2},n-\frac{1}{2}}}{2\,\Delta\eta_n\,\Delta\eta_{n-1}} \qquad\qquad\left.\right\} \tag{B13}$$

$$D_n = -A_n F_{m,n+1} + \left\{\left[\frac{(2\xi)^{2\bar{n}}}{\Delta\xi}\right]_{m+\frac{1}{2}} - \frac{\bar{K}M_{m+\frac{1}{2},n+\frac{1}{2}} + K^*M_{m+\frac{1}{2},n-\frac{1}{2}}}{2\,\Delta\eta_n\,\Delta\eta_{n-1}}\right\}F_{m,n}$$

$$-C_n F_{m,n-1} + \left[\frac{(2\xi)^{2\bar{n}}}{\Delta\xi\,U_e}\right]_{m+\frac{1}{2}}\left(\frac{dU_e}{d\xi}\,\Delta\xi\right)_{m+\frac{1}{2}}\left(1 - F^2_{m+\frac{1}{2},n}\right)$$

where

$$\left.\begin{aligned}\bar{K} &= \frac{2}{1+K}\\[2mm]K^* &= \frac{2K}{1+K}\end{aligned}\right\} \tag{B14}$$

Since all quantities appearing in the A, B, C, and D coefficients are known from the completed calculation at the previous step m, or for the intermediate values at $m + \frac{1}{2}$ from the previous iteration, equations (B12) represent a system of N - 2 equations with N - 2 unknowns which are the values of F_{m+1} from n = 2 to n = N - 1. (The boundary conditions require $F_{m+1,1} = 0$ and $F_{m+1,N} = F_e = 1 - \epsilon_e$). The matrix of the linear system (B12) is tri-diagonal; thus, the unknown F_{m+1} values are easily obtained by successive elimination of the unknowns (refs. 40 and 57) with the formulas

$$F_{m+1,n} = G_n F_{m+1,n+1} + g_n \tag{B15}$$

which are applied by starting the calculation at the outer edge of the boundary layer where $F_{m+1,N} = F_e$ and successively obtaining all other values of F_{m+1} down to the wall where F = 0 (eq. (20)). The functions G_n and g_n are computed from the recursion formulas

$$\left.\begin{aligned} G_n &= \frac{-A_n}{B_n + C_n G_{n-1}} \\[2mm] g_n &= \frac{D_n - C_n g_{n-1}}{B_n + C_n G_{n-1}} \end{aligned}\right\} \tag{B16}$$

which are applied by starting at the wall (n = 1) and working out successively to n = N - 1. This procedure can be started by noting that with the wall boundary conditions, $F_{m+1,1} = 0$, $G_1 = g_1 = 0$ from equation (B15). (See ref. 57.) Then, from equation (B16),

$$\left.\begin{aligned} G_2 &= - \frac{A_2}{B_2} \\[2mm] g_2 &= \frac{D_2}{B_2} \end{aligned}\right\} \tag{B17}$$

Determination of number of $\Delta\eta$ steps (N).- Before the complete set of unknown values F_{m+1} can be obtained, it is necessary to determine the number of steps in η required to satisfy the outer asymptotic boundary condition of $F_e = 1 - \epsilon_e$. The number of steps at any ξ location is determined from the physical requirement that

$$\left(\frac{\partial F}{\partial \eta}\right)_{\eta = \eta_e} \leqq \epsilon_e' \tag{B18}$$

where ϵ_e' is a small specified error criteria (generally a positive number for conventional boundary layers). The finite-difference form of inequality (B18) is written

$$F_{m+1,N} - F_{m+1,N-1} \leqq \Delta\eta_{N-1}\, \epsilon_e'$$ (B19)

Then from equation (B15) $\left(\text{with } F_{m+1,N} = F_e\right)$,

$$F_{m+1,N-1} = G_{N-1}F_e + g_{N-1}$$

which upon substitution into inequality (B19) gives the requirement

$$F_e\left(1 - G_{N-1}\right) - g_{N-1} \leqq \Delta\eta_{N-1}\, \epsilon_e'$$ (B20)

The computer program (appendix C) is written so that $F_e = F_{m=1,N} = 1 - \epsilon_e$; that is, the value of ϵ_e is the same as that for the initial input profile. Thus with the error criteria ϵ_e and ϵ_e' specified, successive values of G_n and g_n are used in inequality (B20), and when the outer edge of the boundary layer is approached, the point at which the inequality is first satisfied determines the value of $N - 1$ and hence the number of $\Delta\eta$ steps required.

If the value of η_e increases with ξ (with $\bar{n}$ constant), the computer program as described in appendix C is set up so that the required values of $F_{m,n>N_o}$ are obtained from the initial input profile of F as a function of η. Partly for this reason and partly because of the computing procedure used, it is necessary to specify $F_{m=1,N}$ as a number very close to unity $\left(\text{that is, } \epsilon_e \approx 1 \times 10^{-4}\right)$ in order to obtain $\left(\dfrac{\partial F}{\partial \eta}\right)_{\eta=\eta_e} \leqq \epsilon_e'$ as required by equations (B18) to (B20).

<u>Continuity.</u>- The values of $V_{m+\frac{1}{2},n}$ required in the A_n and C_n functions are obtained from the continuity equation (29) which, evaluated in finite-difference form at point $m + \frac{1}{2}$, $n - \frac{1}{2}$ gives

$$V_{m+\frac{1}{2},n} = V_{m+\frac{1}{2},n-1} - \frac{\Delta\eta_{n-1}}{2}\left[\frac{(2\xi)2\bar{n}}{\Delta\xi}\right]_{m+\frac{1}{2}}\left(F_{m+1,n} - F_{m,n} + F_{m+1,n-1} - F_{m,n-1}\right)$$

$$- \Delta\eta_{n-1}\left[(2\xi)2\bar{n}\right]_{m+\frac{1}{2}}F_{m+\frac{1}{2},n-\frac{1}{2}}\left[\left(\frac{\bar{n}}{\xi}\right)_{m+\frac{1}{2}} + \left(\frac{\log_e 2\xi}{\Delta\xi}\right)_{m+\frac{1}{2}}\left(\bar{n}_{m+1} - \bar{n}_m\right)\right]$$ (B21)

After a set of $F_{m+1,n}$ values are obtained, equation (B21) is used to compute an updated set of $V_{m+\frac{1}{2},n}$ values where from the wall boundary conditions (eq. (20)) and the definition of V (eq. 26)),

$$V_{m+\frac{1}{2},1} = \left(V_w\right)_{m+\frac{1}{2}} = \left[(2\,\xi)^{2\bar{n}}\right]_{m+\frac{1}{2}} \frac{\bar{u}_{2,w}}{U_e} \tag{B22}$$

For zero mass transfer at the wall, $\bar{u}_{2,w} = 0$; otherwise, this normal velocity at the wall may be a specified function of x_1. Successive application of equation (B21) from $n = 1$ to $n = N$ then gives the new values of $V_{m+\frac{1}{2},n}$ which may be utilized during the iteration cycle for obtaining convergence of the $F_{m+1,n}$ values from equation (B12). In the present method, this convergence criteria is based on the shear stress from the expression

$$\left| \frac{\left(\frac{\partial F}{\partial \eta}\right)_{w,i} - \left(\frac{\partial F}{\partial \eta}\right)_{w,i-1}}{\left(\frac{\partial F}{\partial \eta}\right)_{w,i-1}} \right| \leqq \epsilon_w \tag{B23}$$

where ϵ_w was generally specified as 0.01 unless otherwise stated. Since $F_w = 0$, this inequality may be written in finite-difference form as

$$\left| F_{m+1,2,i} - 1 \right| \leqq F_{m+1,2,i-1}\left(\epsilon_w\right) \tag{B24}$$

The convergence criteria ϵ_w is not an input quantity but appears in the program listing (appendix C) in the first statement in the section "Test for Iteration on FP."

Since input values of $\bar{u}_2$ at $\xi_0(m = 1)$ are not generally available $\bigl($for the computation of $V_{1,n}$ directly from eq. (26)$\bigr)$, it is necessary to compute the $V_{1+\frac{1}{2},n,i=1}$ values from equation (29) by dropping the ξ derivatives. The resulting equation is written as

$$V_{1+\frac{1}{2},n,i=1} \approx V_{1,n} = V_{1,n-1} - \frac{\Delta\eta_{n-1}}{2}\left[(2\,\xi)^{2\bar{n}}\frac{\bar{n}}{\xi}\right]_{m=1}\left(F_{1,n} + F_{1,n-1}\right) \tag{B25}$$

For all the calculations presented, the value of $\bar{n}$ was retained as a constant. It was found that appreciable savings in computer time could be obtained by the use of a value of $\bar{n}$ appropriate to the type of flow being computed. For example, for the flat-plate problem, if the value of $\bar{n}$ at $\xi = 5 \times 10^4$ was changed from 0.5 to 0.8, the number of $\Delta\eta$ steps required at $\xi = 10^6$ was reduced from 290 to 125. Actually, the problem had to be reinitialized at $\xi = 5 \times 10^4$ to accommodate the new value of $\bar{n}$, but the computer time from that point on was reduced by approximately one-half.

Energy.- The finite-difference form of equation (28) is derived in the same way as equation (B12) and, with the use of equation (B11), is written in the same form as equation (B12)

$$\hat{A}_n E_{m+1,n+1} + \hat{B}_n E_{m+1,n} + \hat{C}_n E_{m+1,n-1} = \hat{D}_n \tag{B26}$$

The $\hat{A}_n$, $\hat{B}_n$, $\hat{C}_n$, and $\hat{D}_n$ coefficients are obtained as

$$\hat{A}_n = \frac{V_{m+\frac{1}{2},n}}{2\left(\Delta\eta_n + \Delta\eta_{n-1}\right)} - \frac{\bar{K}D_{m+\frac{1}{2},n+\frac{1}{2}}}{2\,\Delta\eta_n\,\Delta\eta_{n-1}}$$

$$\hat{B}_n = \left[\frac{(2\xi)2\bar{n}}{\Delta\xi}\right]_{m+\frac{1}{2}} F_{m+\frac{1}{2},n} + \frac{\bar{K}D_{m+\frac{1}{2},n+\frac{1}{2}} + K^{*}D_{m+\frac{1}{2},n-\frac{1}{2}}}{2\,\Delta\eta_n\,\Delta\eta_{n-1}}$$

$$\hat{C}_n = -\frac{V_{m+\frac{1}{2},n}}{2\left(\Delta\eta_n + \Delta\eta_{n-1}\right)} - \frac{K^{*}D_{m+\frac{1}{2},n-\frac{1}{2}}}{2\,\Delta\eta_n\,\Delta\eta_{n-1}}$$

$$\hat{D}_n = -\hat{A}_n E_{m,n+1} + \left\{\left[\frac{(2\xi)2\bar{n}}{\Delta\xi}\right]_{m+\frac{1}{2}} F_{m+\frac{1}{2},n} - \frac{\bar{K}D_{m+\frac{1}{2},n+\frac{1}{2}} + K^{*}D_{m+\frac{1}{2},n-\frac{1}{2}}}{2\,\Delta\eta_n\,\Delta\eta_{n-1}}\right\} E_{m,n}$$

$$- \hat{C}_n E_{m,n-1} - 2\left[\frac{(2\xi)\bar{n}}{U_e\,\Delta\xi}\right]_{m+\frac{1}{2}} \left(\frac{dU_e}{d\xi}\Delta\xi\right)_{m+\frac{1}{2}} E_{m+\frac{1}{2},n} F_{m+\frac{1}{2},n}$$

$$+ \frac{M_{m+\frac{1}{2},n} - 1}{\left(\Delta\eta_n + \Delta\eta_{n-1}\right)^2}\left(F_{m,n+1} - F_{m,n-1}\right)\left(F_{m+1,n+1} - F_{m+1,n-1}\right)_{i-1} - C\,\frac{D_{m+\frac{1}{2},n}E_{m+\frac{1}{2},n}}{\eta_{\delta,m+\frac{1}{2}}^{2}\phi_n^{2}}$$

$$\tag{B27}$$

It should be noted that in these computations,

$$\phi\left(\frac{x_2}{\delta}\right) = \phi\left(\frac{\eta}{\eta_\delta}\right)$$

because of the definition of η (eq. (22)). The procedure for solving the system of equation (B26) is identical to that outlined, except that the number of $\Delta\eta$ steps required is not recomputed separately to satisfy directly the edge physical requirement that $\left(\frac{\partial E}{\partial \eta}\right)_e$ approach 0. Instead, the value of N already determined from equation (B20) is used also for the solution of the energy equation, and at this value of N, the edge boundary condition of $E_N = E_e$ is imposed where E_e is generally specified as a small finite number. It has been found that in all cases computed, this procedure gives $\left(\frac{\partial E}{\partial \eta}\right)_e$ approaching 0 to the desired degree of accuracy.

APPENDIX C

DIGITAL COMPUTER PROGRAM DESCRIPTION

By Carolyn C. Thomas
Langley Research Center

This program computes the nonsimilar development of an incompressible turbulent or laminar boundary layer by the finite-difference procedure described in appendix B.

Minimum machine requirements on the Control Data 6400/6600 computer system are 67000 octal locations of core storage. The program is written in FORTRAN 2.0 which is compatible with FORTRAN IV in most instances. The time required to calculate a grid point is approximately 0.0014 second per iteration. The total computing time required for a typical Goldberg case was 122.5 seconds where the pertinent inputs were: $K = 1.02$, $\Delta \eta_1 = 0.005$, $\bar{n} = 0.5$, $\epsilon_w = 0.01$, $\epsilon_e' = 1 \times 10^{-5}$, and $\Delta \xi = 1 \times 10^3$. The average number of $\Delta \eta$ steps across the boundary layer was about 95 and there were a total of 910 $\Delta \xi$ steps for this particular case. With the iteration criteria of $\epsilon_w = 0.01$, the solution was iterated only 34 times over 910 ξ-stations (or columns) computed. Several of these iterations were required in the first 3 or 4 $\Delta \xi$ steps where the initial input profiles for F and E are being adjusted to achieve consistency with the equations of motion.

Input

One card of case identification using all 80 columns. The remaining input is loaded by using the FORTRAN version 2.0 NAMELIST. The input symbols are as follows:

Symbol (see section "SYMBOLS")	Machine name	Comments
	FPTAB	Input table of up to 600 values
$F = F(\eta)$	NUMFP	Number of values in FPTAB table (Integer value)
	ETATABF	ETA table that corresponds to FPTAB
$E_0{}^*$	EO	
ρ	RHO	
ν	NU	

α	ALPHA	
K	KN	Ratio of $\Delta\eta$ at $n+1$ to $\Delta\eta$ at n.
R_O	RO	
C	C	
κ	K	
ξ_O	XIO	
$\bar{n}$	NBAR	
N_O	NMAX	Initial number of steps in boundary layer (Integer value)
$\Delta\xi$	DELXI	
$\Delta\eta$	DELETA	Initial value of $\Delta\eta$
η^*/η_e	ETAMOE	
x_2/δ	TX2ODEL ⎫	
l/δ	TLODEL ⎬	Table of up to 8 values
$\epsilon_e{}'$	EPSLON	
	NUMETA	Total number of values expected at end of case (can be 1 to 600) (Integer value)
	MPRINT	Table of values at which complete print out is desired — up to 40 values
	FINLPRT	Final value from MPRINT table

54

ξ	XITAB	Table of values used to obtain U_e value from UETAB and $dU_e/d\xi$ value from DUETAB (50 values)
U_e	UETAB	Table of up to 50 values. If U_e is constant, all values in table should be set to this value.
$dU_e/d\xi$	DUETAB	Table of $dU_e/d\xi$ values (up to 50 values)
	ETAB	Input table of up to 600 values
$E = E(\eta)$	NUME	Number of values in ETAB (Integer value)
	ETATABE	ETA table that corresponds to ETAB input
	IEREAD	$=0$ (E table read), $\neq 0$ (E table computed) (Integer value)

The program will interpolate between input values of F and E to fill a table having NUMETA values with a spacing of $\Delta\eta$. As mentioned in appendix B, it is necessary to specify N_0 at a point on the input profile where $1 - F_n < 1 \times 10^{-4}$ in order to obtain the desired slope $\left(\dfrac{\partial F}{\partial \eta}\right)_{\eta=\eta_e} = \epsilon_e{}'$ at subsequent profiles. Furthermore, because of the interpolation procedure used to fill the F table, the last value of F in the input table must be slightly greater than F at $n = N$.

Output

Identifications of case and input data are printed at beginning of output.

Symbol	Machine name	Comments
	MCOL (designates m column)	These are printed at every m column
$\xi_{m+\frac{1}{2}}$	XIA	

ξ	XI	
C_f	CF	
θ	THETA (ft)	
δ^*	DELSTAR (ft)	These are printed at every m column
H^*	H	
R_θ	RTHETA	
η	ETA	
F	FP (computed column)	
E	E (computed column)	
$V_{m+\frac{1}{2},n}$	VA	
$\bar{u}_1/u^*$	UUSTAR	Group I
u^*y/ν	USYNU	
$\dfrac{U_e - \bar{u}_1}{u^*}$	UUEUS	
n	KCH	
$(M - 1)\left(\dfrac{\partial F}{\partial \eta}\right)^2$	PROD	
$CDE\big/\eta\delta^2\phi^2$	DISIP	
$(2\xi)^{2\bar{n}}F\,\dfrac{\partial E}{\partial \xi} + V\,\dfrac{\partial E}{\partial \eta}$	CONVEC	Group II
$\dfrac{\partial}{\partial \eta}\left(D\,\dfrac{\partial E}{\partial \eta}\right)$	DIFUS	

$$2(2\xi)^{2\bar{n}} \frac{dU_e}{d\xi} \frac{FE}{U_e} \qquad \text{DUETRM}$$

$$\tau_T / 2\rho\bar{e} \qquad \text{TORHOE}$$

Group II

Print out is controlled by MPRINT table. Groups I and II are printed only when ξ corresponds to a value in MPRINT table. XI table must be filled with values in ascending order.

APPENDIX C

NASA-LANGLEY RESEARCH CENTER

01 4	01 7 PROGRAM NO		01 14 DATE
LAR	D2170	COMPUTER PROGRAM ABSTRACT	072268

01 20 TITLE OF PROGRAM (61 CHARACTERS MAXIMUM)			PARENT PROGRAM		
Calculation of Turbulent and/or Laminar Boundary Layers	02 14 CATEGORY	02 15 SITE	02 18 PROGRAM NO

02 26 CATEGORY	02 27 LANGUAGE NO 1	02 32 LANGUAGE NO 2	02 37 KEY WORDS 8 MAXIMUM SEPARATED BY COMMAS
R	FØR6M		Boundary Layer, Turbulent, Laminar, Finite Difference Procedure, Implicit

WHO TO CONTACT ABOUT THE PROGRAM

05 14 CONTACT	05 28 SITE	05 31 ORGN CODE	05 39 PROJECT NO	05 45 NASA CENTER	05 48 STATUS	05 49
C. C. Thomas	LAR	11.160	RGL 151		☐ A UNDER DEVELOPMENT ☒ B OPERATIONAL ☐ C COMPLETED	☐ A THIS PROGRAM IS NOT FOR SHARING

DATES

05 50 INITIATED	05 54 COMPLETED	05 56 REVISION CODE	TIME AND COST FOR DEVELOPMENT			
			05 59 MANMONTHS	05 64 MACHINE HOURS	05 69 COMPUTER TYPE	05 74 TOTAL COST (DOLLARS)
0966		☐ A REVISION ☐ B CANCELLATION	59 60 61 62 63	64 65 66 67 68	6000	74 75 76 77 78 79 80

ELITE MARGIN | PICA MARGIN

CARD NUMBER | COLUMN 14 | ABSTRACT

06   An implicit finite-difference scheme is used to compute
07 incompressible boundary layers with arbitrary pressure
08 gradient and wall blowing. To compute a turbulent boundary
09 layer, an eddy viscosity concept is used wherein the eddy
10 viscosity is assumed to be a certain function of the kinetic
11 energy of turbulent fluctuations and the scale of the turbu-
12 lence. The differential equation for this turbulent energy is
13 then solved simultaneously with the conventional momentum
14 equation to obtain the distribution of the mean velocity and the
15 distribution of the turbulent energy. Auxiliary functions are
16 supplied for the eddy viscosity and the turbulence scale. The
17 objectives of the present investigation are to develop the com-
18 puting procedure and to determine the range of applicability of
19 the auxiliary functions.
20
21
22
23
24
25
26
27
28
29
30
31
32
33
34
35
36
37
38
39
40
41
42

APPENDIX C

Flow Diagram

Flowchart:

- (71) → **Compute G constants for momentum equation** → **Compute new boundary height** → **Compute new FP and VA tables** — **Compute CF, THETA, DELSTAR, H, and RTHETA**

- → **Print** $\xi_{m+\frac{1}{2}}$, ξ, C_f, θ, δ^*, H, and R_θ

- → **New FP tables acceptable** — no → **ITER < 10** — no → **Halve DELXI** — **Recompute column using initial values for this column** → (39)

- **ITER < 10** — yes → **Compute average values for turbulent energy equation**

- **New FP tables acceptable** — yes → **Print tables** — no → **Compute average values for turbulent energy equation**

- **Print tables** — yes → **Compute UUSTAR, USYNU, and UUEUS** → **Print** η, F'(2), E(2), VA, UUSTAR, USYNU, and UUEUS → **Compute PROD, DISIP, CONVEC, DIFUS, DUETRM, and TORHOE** → **Print PROD, DISIP, CONVEC, DIFUS, DUETRM, and TORHOE**

- **Compute average values for turbulent energy equation** → **Compute G constants for turbulent energy equation** → **Compute new E table** → (1922)

60

APPENDIX C

Program Listing


```
JOB,01,2000,67000.          D2170,31366,1,CAROLYN C THOMAS,          ,1192-C R16,
LINECNT(40000)
RUN(S)
SETINDF.
LGO.
EXIT.
DMP(FL)
-
      PROGRAM D2170 (INPUT,OUTPUT,TAPE5=INPUT,TAPE6=OUTPUT)
C               **********
C     PROGRAM TO COMPUTE THE NON-SIMILAR DEVELOPMENT OF AN INCOMPRESSIBLE
C         TURBULENT OR LAMINAR BOUNDARY LAYER
C               **********
C     *****CAROLYN C. THOMAS*****ANALYSIS AND COMPUTATION DIVISION*****1967
C
      DIMENSION ID(8),FP(600,2),FP1(600),FP2(600),FPTAB(600),FPA(600),
     1 FPA1(600),E(600,2),EA(600),ETAB(600),ETA(600),ETATABF(600),
     2 ETATABE(600),M(600,2),MA1(600),MA2(600),MA(600),D(600,2),DA(600),
     3 DA1(600),DA2(600),A(600),B(600),T(600),S(600),Q(600),U(600),
     4 W(600),Z(600),VA(600),VAINT(600),X2(600),TX2ODEL(8),TLODEL(8),
     5 LODEL(600,2),LODELA(600),DELTA(2),CAPG(600),SMLG(600),UETAB(50),
     6 DUETAB(50),XITAB(50),MPRINT(40),DELETA(600)
      EQUIVALENCE (MA2(1),MA1(2)),(DA2(1),DA1(2))
      EQUIVALENCE (FP1(1),FP(1,1)),(FP2(1),FP(1,2))
      EQUIVALENCE (A(1),Q(1)),(B(1),U(1)),(T(1),W(1)),(S(1),Z(1))
      EQUIVALENCE (FPTAB(1),FP(1,2)),(ETAB(1),E(1,2)),
     1 (ETATABF(1),VAINT(1)),(ETATABE(1),M(1,2))
      REAL L,LODEL,M,K,MA1,MA2,NU,NBAR,MA,LODELA,MPRINT,IFPT,KN
      LOGICAL KFIRST
      NAMELIST /DATA/FPTAB,ETAB,ETATABF,ETATABE,EO,RHO,NU,ALPHA,RO,C,K,
     1 XIO,NBAR,NMAX,DELXI,DELETA,ETAMOE,EE,TX2ODEL,TLODEL,EPSLON,
     2 NUMETA,MPRINT,FINLPRT,XITAB,UETAB,DUETAB,IEREAD,NUMFP,NUME,KN
C
C                 INPUT AND INITIALIZATION
      NUME=0
    1 READ (5,2) ID
    2 FORMAT (8A10)
      READ (5,DATA)
      IFPT=MPRINT(1)+DELXI
      IP=1
      WRITE (6,DATA)
      PRINT 3,ID
    3 FORMAT (1H1//8A10///)
      UEPRES=UETAB(1)
      DELUEPS=DUETAB(1)*DELXI
```

```
      MCOL=1
      ITER=0
      XI=XIO
      XIA=(XIO+DELXI+XIO)/2.0
      J=1
      KFIRST=.TRUE.
      XMULT1=2.0*KN/(1.0+KN)
      XMULT2=2.0/(1.0+KN)
      NEM1=NUMETA-1
      TWONBAR=2.0*NBAR
      NMAX20=NMAX+20
      NMAX40=NMAX+40
      MORDF=2
      MORDE=2
      ETA(1)=0.0
      IF (IEREAD .NE. 0) GO TO 200
      NECK=.90*FLOAT(NUME)
      ETANECK=ETATABE(NECK)
  200 DO 300 ITAB=1,NUMETA
      CALL FTLUP (ETA(ITAB),FP(ITAB,1),MORDF,NUMFP,ETATABF(1),FPTAB(1))
      IF (FP(ITAB,1) .GE. .9) MORDF=1
      IF (IEREAD .NE. 0) GO TO 250
       CALL FTLUP (ETA(ITAB),E(ITAB,1),MORDE,NUME,ETATABE(1),ETAB(1))
      IF (ETA(ITAB) .GE. ETANECK) MORDE=1
  250 DELETA(ITAB+1)=KN*DELETA(ITAB)
      ETA(ITAB+1)=ETA(ITAB)+DELETA(ITAB)
  300 CONTINUE
      IF (IEREAD .EQ. 0) GO TO 400
C
C     COMPUTE  E(N,1) FOR N=1,NUMETA     (INITIAL VALUES)
      ETAE=ETA(NMAX)
      ETAM=ETAMOE*ETAE
      DO 4 N=1,NUMETA
      ETAQ=ETA(N)/ETAM
    4 E(N,1)=EO*ETAQ**2*(EXP(.5*(1.0-ETAQ**2)))**2
  400 CONTINUE
      VA(1)=0.0
      DO 126 NA=1,NEM1
      VAO=VA(NA)
      VA(NA+1)=VAO-DELETA(NA)*TWONBAR*(2.*XIA)**(TWONBAR-1.0)*FP(NA+1,1)
  126 CONTINUE
C
      FPTEST=FP(NMAX,1)
C
C         COMPUTATION OF DELTA AND DELTA(E)
```

```
C
   39 XFP=.990
  393 NEWE=0
      IF (J .NE. 1) GO TO 391
      CALL FTLUP (XFP,XETA,1,NMAX,FP1(1),ETA(1))
      GO TO 392
  391 CALL FTLUP (XFP,XETA,1,NMAX,FP2(1),ETA(1))
  392 DELTA(J)=(NU*(2.0*XI)**NBAR)/UEPRES*XETA
C     FREQUENTLY USED EXPRESSIONS.
      NMAX20=NMAX+20
      IF (NMAX20 .GT. NEM1) NMAX20=NEM1
      NMAX40=NMAX+40
      IF (NMAX40 .GT. NEM1) NMAX40=NEM1
      TWOXIA=2.0*XIA
      TXIANBR=TWOXIA**NBAR
      TXIA2NB=TWOXIA**TWONBAR
C
C     COMPUTATION OF AUXILIARY FUNCTIONS R,H(R),M,D,L
C
      HR=HKR=0.0
      NMAX71=NMAX40+31
      IF (NMAX71 .GT.NUMETA) NMAX71=NUMETA
   40 DO 6 NROW=1,NMAX71
      X2(NROW)=(NU*TXIANBR)/UEPRES*ETA(NROW)
      X2ODEL=X2(NROW)/DELTA(J)
      IF (X2ODEL .LE. 1.4) GO TO 46
      LODEL(NROW,J)=0.01
      GO TO 47
   46 CALL FTLUP (X2ODEL,LODEL(NROW,J),1,8,TX2ODEL(1),TLODEL(1))
   47 L=LODEL(NROW,J)*DELTA(J)
      IF (E(NROW,J) .LT. 0.0) E(NROW,J)=0.0
      R=SQRT(E(NROW,J))*UEPRES*L/NU
      RRO=R/RO
      IF(HR.EQ.1.)GO TO 45
      IF(RRO .LT. 1.25) GO TO 41
      HR=1.0
      GO TO 45
   41 IF (RRO .LT. 0.75) GO TO 42
      HR=RRO-(RRO-0.75)**2
      GO TO 45
   42 IF (RRO .GE. 0.0) GO TO 44
      PRINT 43,R,RO,NROW
   43 FORMAT (//32H M=1,R/RO NEGATIVE,WHAT HAPPENED/3H R=E16.8,5X,
     13HRO=E16.8,5X,2HN=I5/)
   44 HR=RRO
```

```
   45 EPSLONR=ALPHA*R*HR
      M(NROW,J)=1.0+EPSLONR
      RK=R*K
      RKRO=RK/RO
      IF(HKR.EQ.1.)GO TO 50
      IF (RKRO .LT. 1.25) GO TO 451
      HKR=1.0
      GO TO 50
  451 IF (RKRO .LT. 0.75) GO TO 452
      HKR=RKRO-(RKRO-0.75)**2
      GO TO 50
  452 IF (RKRO .GE. 0.0) GO TO 49
      PRINT 48,RK,RO,NROW
   48 FORMAT (//33H M=1,RK/RO NEGATIVE,WHAT HAPPENED/4H RK=E16.8,5X,
     13HRO=E16.8,5X,2HN=I5/)
   49 HKR=RKRO
   50 EPSLNKR=ALPHA*R*K*HKR
      D(NROW,J)=1.0+EPSLNKR
    6 CONTINUE
C
      XIBAR=TXIA2NB/DELXI
C
      IF (KFIRST) 61,51
C     SET INITIAL VALUES OF VARIABLES IN COLUMN 2 EQUAL TO VALUES IN COLUMN 1
C
   61 DELTA(2)=DELTA(1)
      DO 5 N=1,NMAX71
      LODEL(N,2)=LODEL(N,1)
      M(N,2)=M(N,1)
    5 D(N,2)=D(N,1)
      DO 53 N=1,NUMETA
      FP(N,2)=FP(N,1)
      E(N,2)=E(N,1)
      VAINT(N)=VA(N)
   53 CONTINUE
C
C         INITIALIZE XI,UE,AND DELUE FOR EACH COLUMN
      SLOPE=FP(2,2)/DELETA(1)
      J=2
      XI=XI+DELXI
      TWOXI=2.0*XI
      TXINBAR=TWOXI**NBAR
      UEPREV=UEPRES
      DELUEPV=DELUEPS
      CALL FTLUP (XI,UEPRES,1,50,XITAB(1),UETAB(1))
```

```
      CALL FTLUP (XI,DELUEPS,1,50,XITAB(1),DUETAB(1))
      DELUEPS=DELUEPS*DELXI
C
C     COMPUTATION OF AVERAGE VALUES OF M,FP,UE,AND DELUE FOR MOMENTUM EQUATION
C
   51 FPA1=0.0
      MA1(1)=1.0
      FPA(1)=(FP(1,1)+FP(1,2))/2.0
      DO 7 NA=1,NMAX40
      FPA(NA+1)=(FP(NA+1,1)+FP(NA+1,2))/2.0
      FPA1(NA+1)=(FP(NA,1)+FP(NA,2)+FP(NA+1,1)+FP(NA+1,2))/4.0
      MA1(NA+1)=(M(NA,1)+M(NA,2)+M(NA+1,1)+M(NA+1,2))/4.0
    7 CONTINUE
      UEA=(UEPRES+UEPREV)/2.0
      DELUEA=(DELUEPS+DELUEPV)/2.0
      UEA1=UEA
      DELUEA1=DELUEA
C
      KFIRST=.FALSE.
C
C       COMPUTATIONS TO OBTAIN G CONSTANTS FOR MOMENTUM EQUATION
C
      NMAX39=NMAX40-1
   76 DO 8 KG=2,NMAX39
      CON7=2.0*DELETA(KG)*DELETA(KG-1)
      CON1=VA(KG)/(2.0*(DELETA(KG)+DELETA(KG-1)))
      CON2=(MA1(KG)*XMULT1+MA2(KG)*XMULT2)/CON7
      CON3=XIBAR*FPA(KG)
      A(KG)=CON1-MA2(KG)*XMULT2/CON7
      B(KG)=CON3+CON2
      T(KG)=-(CON1+MA1(KG)*XMULT1/CON7)
      CON4=CON3-CON2
      CON5=XIBAR*DELUEA/UEA*(1.0-FPA(KG)**2)
      S(KG)=-A(KG)*FP(KG+1,1)+CON4*FP(KG,1)-T(KG)*FP(KG-1,1)+CON5
    8 CONTINUE
      CAPG(2)=-A(2)/B(2)
      SMLG(2)=(S(2)-T(2)*FP(1,2))/B(2)
      DO 9 KG=3,NMAX39
      CAPG(KG)=-A(KG)/(B(KG)+T(KG)*CAPG(KG-1))
    9 SMLG(KG)=(S(KG)-T(KG)*SMLG(KG-1))/(B(KG)+T(KG)*CAPG(KG-1))
C
C               COMPUTE NEW BOUNDARY HEIGHT
      KMAX=NMAX-10
      DO 90 JJ=KMAX,NMAX20
      TSTVAL=EPSLON*DELETA(JJ)
```

```
      CKVAL=FPTEST*(1.0-CAPG(JJ))-SMLG(JJ)
      NMAX=JJ+2
      IF (CKVAL .LE. TSTVAL) GO TO 91
   90 CONTINUE
C
C               COMPUTE NEW FP AND VA VALUES
C
   91 NBACK=-(NMAX-1)
      FPPREV=FP(2,2)
      DO 10 NF=NBACK,-2
      KF=IABS(NF)
      FP(KF,2)=CAPG(KF)*FP(KF+1,2)+SMLG(KF)
   10 CONTINUE
C
      VA(1)=0.0
      DO 18 NA=1,NMAX40
   52 VAO=VA(NA)
   18 VA(NA+1)=VAO-DELETA(NA)/2.0*XIBAR*(FP(NA+1,2)-FP(NA+1,1)+FP(NA,2)-
     1 FP(NA,1))-DELETA(NA)*TWONBAR*TWOXIA**(TWONBAR-1.0)*FPA1(NA+1)
C
C               COMPUTE CF AND THETA
 1003 SLOPREV=SLOPE
      SLOPE=FP(2,2)/DELETA(1)
      CF=2.0/TXINBAR*SLOPE
      PRINT 1012,SLOPREV,SLOPE
 1012 FORMAT (/9H SLOPREV=E16.8,5X,6HSLOPE=E16.8/)
      DFLSTAR=0.0
      THETA=0.0
      DO 1020 KGT=1,NMAX
      DELSTAR=DELSTAR+(1.0-FP(KGT,2))*DELETA(KGT)
 1020 THETA=THETA+FP(KGT,2)*(1.0-FP(KGT,2))*DELETA(KGT)
      DELSTAR=TXINBAR*NU/UEA*DELSTAR
      THETA=NU*TXINBAR/UEA*THETA
      RTHETA=UEA*THETA/NU
      H=DELSTAR/THETA
      PRINT 1050,MCOL,XIA,XI,CF,THETA,DELSTAR,H,RTHETA
 1050 FORMAT (19H  READY FOR COLUMN I5/5H XIA=E16.8,5X,3HXI=E16.8,5X,
     1 3HCF=E16.8,5X,6HTHETA=E16.8/10X,11HDELTA STAR=E16.8,5X,
     2 2HH=E16.8,5X,7HRTHETA=E16.8/)
C
C               TEST FOR ITERATION ON FP
      IF(ABS((FP(2,2)-FPPREV)/FPPREV)-.005 .GT. 0.0) GO TO 1005
C
      IF (ABS(XI-IFPT) .GE. DELXI) GO TO 800
      IP=IP+1
```

```
        IFPT=MPRINT(IP)
     92 WRITE (6,999)
    999 FORMAT (9X,8HETA(KCH),8X,9HFP(KCH,2),9X,8HE(KCH,2),10X,
       1 7HVA(KCH),6X,11HUUSTAR(KCH),7X,10HUSYNU(KCH),7X,10HUUEUS(KCH),
       2 5X,3HKCH)
        SQRTCF2=SQRT(CF/2.0)
        DO 1002 KCH=1,NMAX
        UUSTAR=FP(KCH,2)/SQRTCF2
        USYNU=ETA(KCH)*TXINBAR*SQRTCF2
        UUEUS=(1.0-FP(KCH,2))/SQRTCF2
        PRINT 1001,ETA(KCH),FP(KCH,2),E(KCH,2),VA(KCH),UUSTAR,USYNU,
       1 UUEUS,KCH
   1001 FORMAT (7E17.6,I8)
   1002 CONTINUE
C
C       COMPUTE AND PRINT PROD,DISIP,CONVEC,DIFUS,DUETERM,AND TORHOE
        DO 16 KGE=2,NMAX
        CON7=2.0*DELETA(KGE)*DELETA(KGE-1)
        FORDETA=2.0*(DELETA(KGE)+DELETA(KGE-1))
        CON12=EA(KGE)/LODELA(KGE)**2
        PROD=(MA(KGE)-1.)/(DELETA(KGE)+DELETA(KGE-1))**2*(FP(KGE+1,1)-
       1FP(KGE-1,1))*(FP(KGE+1,2)-FP(KGE-1,2))
        DISIP=TXIA2NB*C*(NU/(UEA*DELTAA))**2*DA(KGE)*CON12
        CONVEC=VA(KGE)/FORDETA*(E(KGE+1,2)+E(KGE+1,1))-VA(KGE)/FORDETA*
       1(E(KGE-1,2)+E(KGE-1,1))+TXIA2NB/DELXI*FPA(KGE)*(E(KGE,2)-E(KGE,1))
        DIFUS=DA2(KGE)*XMULT2/CON7*(E(KGE+1,2)-E(KGE,2)-E(KGE,1)+
       1 E(KGE+1,1))+DA1(KGE)*XMULT1/CON7*(E(KGE-1,2)-E(KGE,2)-E(KGE,1)+
       2 E(KGE-1,1))
        DUETRM=2.0*TXIA2NB/UEA*DELUEPS/DELXI*EA(KGE)*FPA(KGE)
        IF (EA(KGE) .NE. 0.0) GO TO 1008
        TORHOE=0.0
        GO TO 1009
   1008 TORHOE=(MA(KGE)-1.0)/(EA(KGE)*2.*TXIANBR)*1./FORDETA*
       1((FP(KGE+1,2)+FP(KGE+1,1))-(FP(KGE-1,2)+FP(KGE-1,1)))
   1009 IF (KGE .NE. 2) GO TO 705
        PRINT 706
    706 FORMAT (/10X,10HPRODUCTION,9X,11HDISSIPATION,10X,10HCONVECTION,
       1 11X,9HDIFUSION,12X,8HDUE TERM,12X,8HTAUORHOE)
    705 PRINT 707,PROD,DISIP,CONVEC,DIFUS,DUETRM,TORHOE,KGE
    707 FORMAT (6E20.8,I8)
     16 CONTINUE
    800 MCOL=MCOL+1
        NFWE=1
        GO TO 105
C
```

```
C                 INITIALIZATION FOR NEXT COLUMN
  103 DO 102 KS=1,NMAX20
      FP(KS,1)=FP(KS,2)
  102 E(KS,1)=E(KS,2)
  106 XIA=XIA+DELXI
      KFIRST=.TRUE.
      J=1
      ITER=0
      IF (XI .GE. FINL.RT) GO TO 1
      GO TO 39
C
C                 CHECK TO SEE IF MAXIMUM ITERATIONS HAVE TAKEN PLACE
 1005 ITER=ITER+1
      IF (ITER .LT. 10) GO TO 105
C
C         HALVE THE INTERVAL DELXI AND RE-INITIALIZE AND TRY AGAIN
      ITER=0
      J=1
      XI=XI-DELXI
      DELXI=DELXI/2.0
      XIA=(XI+XI+DELXI)/2.0
      KFIRST=.TRUE.
      UFPRES=UFPREV
      DELUEPS=DELUEPV
      DO 104 NVA=1,NMAX40
  104 VA(NVA)=VAINT(NVA)
      GO TO 39
C
C         COMPUTATION OF AVERAGE VALUES OF E,M,AND D FOR ENERGY EQUATION
C
  105 DELTAA=(DELTA(1)+DELTA(2))/2.0
      DA1(1)=1.0
      DO 11 NA=1,NMAX40
      DA(NA)=(D(NA,1)+D(NA,2))/2.0
      DA1(NA+1)=(D(NA,1)+D(NA,2)+D(NA+1,1)+D(NA+1,2))/4.0
      DA1(NA+1)=DA1(NA+1)*3.0
      LODELA(NA)=(LODEL(NA,1)+LODEL(NA,2))/2.0
      EA(NA)=(E(NA,1)+E(NA,2))/2.0
   11 MA(NA)=(M(NA,1)+M(NA,2))/2.0
C
C     COMPUTATIONS TO OBTAIN G CONSTANTS FOR ENERGY EQUATION
C
      DO 12 KGE=2,NMAX
      CON7=2.0*DELETA(KGE)*DELETA(KGE-1)
      CON6=VA(KGE)/(2.0*(DELETA(KGE)+DELETA(KGE-1)))
```

```
      Q(KGF)=CON6-DA2(KGE)*XMULT2/CON7
      CON8=XIBAR*FPA(KGE)
      CON9=(DA1(KGE)*XMULT1+DA2(KGE)*XMULT2)/CON7
      U(KGE)=CON8+CON9
      W(KGE)=-(CON6+DA1(KGE)*XMULT1/CON7)
      IF (LODELA(KGE) .NE. 0.0) GO TO 113
      CON12=0.0
      GO TO 12
  113 CON12=EA(KGE)/LODELA(KGE)**2
      Z(KGE)=-Q(KGE)*E(KGE+1,1)+(CON8-CON9)*E(KGE,1)-W(KGE)*E(KGE-1,1)-
     12.0*XIBAR*DELUEA/UEA*EA(KGE)*FPA(KGE)-XIBAR*DELXI*C*(NU/(UEA*
     2DELTAA))**2*DA(KGE)*CON12+((MA(KGE)-1.0)/(DELETA(KGE)+
     3LELETA(KGE-1))**2
     3     *(FP(KGE+1,1)-FP(KGE-1,1))*(FP(KGE+1,2)-FP(KGE-1,2)))
   12 CONTINUE
      CAPG(2)=-Q(2)/U(2)
      SMLG(2)=(Z(2)-W(2)*E(1,2))/U(2)
      DO 13 KGE=3,NMAX
      CAPG(KGE)=-Q(KGE)/(U(KGE)+W(KGE)*CAPG(KGE-1))
   13 SMLG(KGE)=(Z(KGE)-W(KGE)*SMLG(KGE-1))/(U(KGE)+W(KGE)*CAPG(KGE-1))
C
C         COMPUTATION OF NEW E VALUES
C
      DO 14 NE=NBACK,-2
      KE=IABS(NE)
   14 E(KE,2)=CAPG(KE)*E(KE+1,2)+SMLG(KE)
C
C     CHECK TO SEE IF ITERATING OR IF YOU HAVE ACCEPTABLE ANSWERS
C           IF ITERATING GO TO 39 *** IF ACCEPTABLE ANSWERS GO TO 103
 1922 IF (NEWE .EQ. 1) GO TO 103
      GO TO 39
      END
```

REFERENCES

1. Hinze, J. O.: Turbulence. McGraw-Hill Book Co., Inc., 1959.

2. Prandtl, L. (Suppl. by K. Wieghardt): On a New Representation of Fully Developed Turbulence. Publ. No. 13, Jet Propulsion Lab., California Inst. Technol., Aug. 1952. (Translation of "Über ein neues Formelsystem für die ausgebildete -Turbulenz." Nachrichten der Akademie der Wissenschaften, Göttingen, Mathematisch-Physikalische Klasse, 1945.)

3. Nevzgljadov, V.: A Phenomenological Theory of Turbulence. J. Phys. (USSR), vol. IX, no. 3, 1945, pp. 235-243.

4. Chou, P. Y.: On Velocity Correlations and the Solutions of the Equations of Turbulent Fluctuation. Quart. Appl. Math., vol. III, no. I. Apr. 1945, pp. 38-54.

5. Chou, P. Y.: Pressure Flow of a Turbulent Fluid Between Two Infinite Parallel Planes. Quart. Appl. Math., vol. III, no. 3, Oct. 1945, pp. 198-209.

6. Rotta, J.: Statistical Theory of Nonhomogeneous Turbulence. Part I: Z. Physik, Bd. 129, 1951, pp. 547-572. Part II: Z. Physik, Bd. 131, 1951, pp. 51-77.

7. Rotta, J. C.: Turbulent Boundary Layers in Incompressible Flow. Boundary Layer Problems. Vol. 2 of Progress in Aeronautical Sciences, Antonio Ferri, D. Küchemann, and L. H. G. Sterne, eds., Macmillan Co., c.1962, pp. 1-219.

8. Emmons, Howard W.: Shear Flow Turbulence. Proceedings of the Second U.S. National Congress of Applied Mechanics, Paul M. Naghdi, ed., Amer. Soc. Mech. Eng., c.1955, pp. 1-12.

9. Townsend, A. A.: Equilibrium Layers and Wall Turbulence. J. Fluid Mech., vol. 11, pt. 1, Aug. 1961, pp. 97-120.

10. Levin, V. B.: The Calculation of the Fundamental Properties of Turbulent Flow With Transverse Shear. High Temp. (USSR), vol. 2, no. 4, July-Aug. 1964, pp. 531-540.

11. Spalding, D. B.: Heat Transfer From Separated Flows. J. Fluid Mech., vol. 27, pt. 1, Jan. 11, 1967, pp. 97-109.

12. McDonald, H.: On Incompressible Two-Dimensional Turbulent Boundary Layers. Rep. E110339-2, Res. Lab., United Aircraft Corp., Nov. 1966.

13. Kovasznay, Leslie S. G.: Structure of the Turbulent Boundary Layer. Phys. Fluids (Suppl.), vol. 10, no. 9, Sept. 1967, pp. S25-S30.

14. Nee, Victor W.; and Kovasznay, Leslie S. G.: A Phenomenological Theory of Quasi-Parallel Turbulent Shear Flows. Rep. No. 1 (Contract DA-31-124-ARO-D-313), Dep. Mech., Johns Hopkins Univ., July 1967. (Available from DDC as AD 657602.)

15. Harlow, Francis H.; and Nakayama, Paul I.: Turbulence Transport Equations. Phys. Fluids, vol. 10, no. 11, Nov. 1967, pp. 2323-2332.

16. Harlow, Francis H.; and Nakayama, Paul I.: Transport of Turbulence Energy Decay Rate. LA-3854 (Contract W-7405-ENG. 36), Los Alamos Sci. Lab., Univ. of California, Feb. 20, 1968.

17. Glushko, G. S.: Turbulent Boundary Layer on a Flat Plate in an Incompressible Fluid. Bull. Acad. Sci. USSR, Mech. Ser., no. 4, 1965, pp. 13-23.

18. Bradshaw, P.; Ferriss, D. H.; and Atwell, N. P.: Calculation of Boundary-Layer Development Using the Turbulent Energy Equation. J. Fluid Mech., vol. 28, pt. 3, May 26, 1967, pp. 593-616.

19. Nash, John F.: A Finite-Difference Method for the Calculation of Incompressible Turbulent Boundary Layers in Two Dimensions. ER-9655, Lockheed-Georgia Co., Feb. 1968.

20. Chou, P. Y.: The Turbulent Flow Along a Semi-Infinite Plate. Quart. Appl. Math., vol. V, no. 3, Oct. 1947, pp. 346-353.

21. Laufer, John: Investigation of Turbulent Flow in a Two-Dimensional Channel. NACA Rep. 1053, 1951. (Supersedes NACA TN 2123.)

22. Liepmann, Hans Wolfgang; and Laufer, John: Investigations of Free Turbulent Mixing. NACA TN 1257, 1947.

23. Townsend, A. A.: Momentum and Energy Diffusion in the Turbulent Wake of a Cylinder. Proc. Roy. Soc. (London), ser. A, vol. 197, no. 1048, May 11, 1949, pp. 124-140.

24. Laufer, John: The Structure of Turbulence in Fully Developed Pipe Flow. NACA Rep. 1174, 1954. (Supersedes NACA TN 2954.)

25. Bradshaw, P.; and Ferriss, D. H.: Calculation of Boundary-Layer Development Using the Turbulent Energy Equation. II — Compressible Flow on Adiabatic Walls. NPL Aero Rep. 1217, Brit. A.R.C., Nov. 24, 1966.

26. Thompson, B. G. J.: A Critical Review of Existing Methods of Calculating the Turbulent Boundary Layer. Brit. A.R.C. 26 109, Aug. 7, 1964.

27. Truckenbrodt, E.: A Method of Quadrature for Calculation of the Laminar and Turbulent Boundary Layer in Case of Plane and Rotationally Symmetrical Flow. NACA TM 1379, 1955.

28. Walz, Alfred: New General Law for the Turbulent Dissipation Integral. Phys. Fluids (Suppl.), vol. 10, no. 9, Sept. 1967, pp. S161-S164.

29. Mellor, George L.: Incompressible, Turbulent Boundary Layers With Arbitrary Pressure Gradients and Divergent or Convergent Cross Flows. AIAA J., vol. 5, no. 9, Sept. 1967, pp. 1570-1579.

30. Smith, A. M. O.; and Cebeci, T.: Numerical Solution of the Turbulent-Boundary-Layer Equations. Rep. No. DAC 33735 (Contract NOw 66-0324-C), Douglas Aircraft Co., Inc., May 29, 1967.

31. Townsend, A. A.: The Structure of the Turbulent Boundary Layer. Proc. Cambridge Phil. Soc., vol. 47, pt. 2, Apr. 1951, pp. 375-395.

32. Klebanoff, P. S.: Characteristics of Turbulence in a Boundary Layer With Zero Pressure Gradient. NACA Rep. 1247, 1955. (Supersedes NACA TN 3178.)

33. Corrsin, Stanley; and Kistler, Alan L.: Free-Stream Boundaries of Turbulent Flows. NACA Rep. 1244, 1955. (Supersedes NACA TN 3133.)

34. Bradshaw, P.: The Turbulence Structure of Equilibrium Boundary Layers. J. Fluid Mech., vol. 29, pt. 4, Sept. 1967, pp. 625-645.

35. Schubauer, G. B.; and Klebanoff, P. S.: Investigation of Separation of the Turbulent Boundary Layer. NACA Rep. 1030, 1951. (Supersedes NACA TN 2133.)

36. Bradshaw, P.; and Ferriss, D. H.: The Response of a Retarded Equilibrium Turbulent Boundary Layer to the Sudden Removal of Pressure Gradient. NPL Aero Rep. 1145, Brit. A.R.C., Mar. 16, 1965.

37. Spangenburg, W. G.; Rowland, W. R.; and Mease, N. E.: Measurements in a Turbulent Boundary Layer Maintained in a Nearly Separating Condition. Fluid Mechanics of Internal Flow, Gino Sovran, ed., Elsevier Publ. Co., 1967, pp. 110-151.

38. Batchelor, G. K.: The Theory of Homogeneous Turbulence. Cambridge Univ. Press, 1959.

39. Schlichting, Hermann (J. Kestin, transl.): Boundary Layer Theory. Fourth ed., McGraw-Hill Book Co., Inc., 1960.

40. Blottner, F. G.: Nonequilibrium Laminar Boundary-Layer Flow of Ionized Air. AIAA J., vol. 2, no. 11, Nov. 1964, pp. 1921-1927.

41. Coles, D. E.: The Turbulent Boundary Layer in a Compressible Fluid. U.S. Air Force Proj. RAND Rep. R-403-PR, The RAND Corp., Sept. 1962.

42. Clauser, Francis H.: The Turbulent Boundary Layer. Vol. IV of Advan. Appl. Mech., H. L. Dryden and Th. von Kármán, eds., Acad. Press, Inc., 1956, pp. 1-51.

43. Goldberg, Perry: Upstream History and Apparent Stress in Turbulent Boundary Layers. Rep. No. 85 (Contract Nonr 1841(91)), Gas Turbine Lab., Massachusetts Inst. Technol., May 1966. (Available from DDC as AD 636323.)

44. Bradshaw, P.; and Ferriss, D. H.: The Effect of Initial Conditions on the Development of Turbulent Boundary Layers. NPL Aero Rep. 1223, Brit. A.R.C., Feb. 3, 1967.

45. Donaldson, Coleman duP.: A Computer Study of An Analytical Model of Boundary Layer Transition. AIAA Paper No. 68-38, Jan. 1968.

46. Wieghardt, K.; and Tillmann, W.: On the Turbulent Friction Layer for Rising Pressure. NACA TM 1314, 1951.

47. Schubauer, G. B.; and Klebanoff, P. S.: Contributions on the Mechanics of Boundary-Layer Transition. NACA Rep. 1289, 1956. (Supersedes NACA TN 3489.)

48. Bradbury, L. J. S.: The Structure of a Self-Preserving Turbulent Plane Jet. J. Fluid Mech., vol. 23, pt. 1, Sept. 1965, pp. 31-64.

49. Eschenroeder, Alan Q.: A Turbulence Spectrum for Shear Flows. BSD-TR-65-279, U.S. Air Force, May 1965. (Available from DDC as AD 469580.)

50. Sandborn, Virgil A.; and Braun, Willis H.: Turbulent Shear Spectra and Local Isotropy in the Low-Speed Boundary Layer. NACA TN 3761, 1956.

51. Moses, Hal L.: The Behavior of Turbulent Boundary Layers in Adverse Pressure Gradients. Rep. No. 73 (Contract Nonr 1841(91)), Gas Turbine Lab., Massachusetts Inst. Technol., Jan. 1964. (Available from DDC as AD 438000.)

52. Ludwieg, H.; and Tillmann, W.: Investigation of the Wall-Shearing Stress in Turbulent Boundary Layers. NACA TM 1285, 1950.

53. Spalding, D. B.: The Calculation of the Length Scale of Turbulence in Some Turbulent Boundary Layers Remote From Walls. TWF/TN/31, Dep. Mech. Eng., Imp. Coll. Sci. Technol., Sept. 1967.

54. Beckwith, Ivan E.; and Bushnell, Dennis M.: Calculation of Mean and Fluctuating Properties of the Incompressible Turbulent Boundary Layer. NASA Paper Presented at AFOSR-IFP-Stanford 1968 Conference on Turbulent Boundary Layer Prediction (Stanford Univ.), Aug. 1968.

55. Rotta, J.: On the Theory of the Turbulent Boundary Layer. NACA TM 1344, 1953.

56. Pai, Shih-I: Viscous Flow Theory. II – Turbulent Flow. D. Van Nostrand Co., Inc., c.1957.

57. Richtmyer, Robert D.: Difference Methods for Initial-Value Problems. Interscience Publ. Inc., 1957.

TABLE I.- FUNCTIONS FOR MEAN SCALES
OF TURBULENCE

x_2/δ	l/δ		
	$\phi_{0.33}$	$\phi_{0.20}$	$\phi_{0.25}$
0	0	0	0
.2	.20	.20	.20
.4	.30	.20	.25
.5	.33	.20	.25
.6	.32	.20	.25
.7	.30	.20	.25
.8	.26	.20	.20
$\gtrsim 1.4$	.01	.01	.01

TABLE II.- INITIAL VELOCITY AND ENERGY PROFILES AND OTHER INPUT DATA FOR ADVERSE PRESSURE GRADIENT CASE

[Values based on Goldberg's data (ref. 43): $\xi_o = 8 \times 10^5$;
$\nu = 1.8 \times 10^{-4}$ ft²/sec (16.7 × 10⁻⁶ m²/s); $\rho = 0.0765$ lb/ft³
(1.23 kg/m³); $U_{e,o} = 77.8$ ft/sec (23.7 m/s); $\Delta\xi = 625$;
$\Delta\eta_1 = 0.025$; $\bar{n} = 0.5$; $\epsilon_{e,o} = 9 \times 10^{-4}$; $\epsilon_e' = 1 \times 10^{-5}$;
$\epsilon_w = 0.01$; $\sqrt{E_e} = 1 \times 10^{-2}$]

η	F_{ξ_o}	E_{ξ_o}
0	0	0
.1	.215	$.22 \times 10^{-2}$
.2	.415	.54
.3	.540	1.05
.4	.580	1.04
.5	.608	.92
.6	.626	.86
.8	.644	.78
1.0	.662	.72
1.2	.681	.675
1.4	.700	.64
1.8	.731	.615
2.2	.760	.579
2.6	.790	.530
3.0	.818	.474
4.0	.880	.321
5.0	.924	.203
6.0	.956	.108
6.5	.968	.069
7.0	.975	.039
7.5	.982	.010
8.0	.991	.01
8.5	.996	.01
9.0	.999	.01

TABLE III.- FREE-STREAM DISTRIBUTIONS OF VELOCITY AND VELOCITY DERIVATIVES FOR ADVERSE PRESSURE GRADIENT CASE

[Values based on Goldberg's data (ref. 43)]

(a) Velocity distribution a.

x_1		U_e		$-\dfrac{dU_e}{dx_1}$,	ξ	$-\dfrac{dU_e}{d\xi}$	
in.	m	ft/sec	m/s	sec^{-1}		ft/sec	m/s
4.0	0.10	77.8	23.7	20.7	8×10^5	4.8×10^{-5}	1.46×10^{-5}
4.55	.11	76.8	23.4	23.7	8.2	5.55	1.69
5.1	.13	75.7	23.0	25.0	8.4	5.95	1.81
5.7	.14	74.5	22.7	26.3	8.6	6.35	1.93
6.3	.16	73.2	22.3	27.2	8.8	6.7	2.04
6.9	.17	71.8	21.8	27.9	9.0	7.0	2.13
7.55	.19	70.36	21.4	28.1	9.2	7.2	2.19
8.2	.21	68.9	21.0	28.1	9.4	7.35	2.24
8.8	.22	67.42	20.5	27.7	9.6	7.41	2.26
9.45	.24	65.98	20.1	27.4	9.8	7.49	2.28
10.1	.26	64.52	19.6	27.0	10.0	7.52	2.29
10.8	.27	63.06	19.2	26.4	10.2	7.54	2.29
11.5	.29	61.60	18.8	25.8	10.4	7.55	2.30
12.2	.31	60.14	18.3	25.1	10.6	7.52	2.29
12.85	.32	58.68	17.9	23.9	10.8	7.34	2.24
13.5	.34	57.28	17.4	22.3	11.0	7.0	2.13
14.25	.36	56.04	17.1	20.3	11.2	6.47	1.97
15.0	.38	54.92	16.7	16.9	11.4	5.55	1.69
15.7	.40	53.92	16.4	14.37	11.6	4.8	1.46
16.5	.42	53.0	16.1	12.37	11.8	4.2	1.28
17.4	.44	52.2	15.9	10.5	12.0	3.61	1.10
18.25	.46	51.8	15.8	9.12	12.2	3.17	.97
19.2	.49	50.9	15.5	7.6	12.4	2.68	.82
20.0	.51	50.4	15.3	6.16	12.6	2.20	.67
20.85	.53	50.0	15.2	4.92	12.8	1.77	.54
21.7	.55	49.7	15.1	3.65	13.0	1.32	.40
22.6	.57	49.5	15.1	2.50	13.2	.91	.28
23.45	.59	49.35	15.0	1.43	13.4	.52	.16
24.35	.62	49.25	15.0	0	13.6	0	0
32.3	.82	49.25	15.0	0	15.4	0	0
40.0	1.0	49.25	15.0	0	17.1	0	0

TABLE III.- FREE-STREAM DISTRIBUTIONS OF VELOCITY AND VELOCITY DERIVATIVES FOR ADVERSE PRESSURE GRADIENT CASE – Concluded

[Values based on Goldberg's data (ref. 43)]

(b) Velocity distribution b.

x_1		U_e		$-\dfrac{dU_e}{dx_1}$,	ξ	$-\dfrac{dU_e}{d\xi}$	
in.	m	ft/sec	m/s	sec^{-1}		ft/sec	m/s
4.0	0.10	77.8	23.7	23.8	8 $\times 10^5$	5.55 $\times 10^{-5}$	1.68 $\times 10^{-5}$
4.55	.11	76.7	23.4	23.9	8.2	5.62	1.71
5.1	.13	75.58	23.0	24.4	8.4	5.8	1.77
5.7	.14	74.42	22.7	24.8	8.6	6.0	1.83
6.3	.16	73.22	22.3	25.3	8.8	6.2	1.89
6.9	.17	71.98	21.9	25.5	9.0	6.4	1.95
7.55	.19	70.70	21.5	26.0	9.2	6.62	2.02
8.2	.21	69.38	21.1	26.6	9.4	6.9	2.10
8.8	.22	68.0	20.7	27.2	9.6	7.21	2.20
9.45	.24	66.56	20.3	28.4	9.8	7.67	2.34
10.1	.26	65.03	19.8	28.9	10.0	8.0	2.44
10.8	.27	63.43	19.3	31.0	10.2	8.8	2.68
11.5	.29	61.67	18.8	32.9	10.4	9.6	2.93
12.2	.31	60.75	18.5	32.7	10.6	9.7	2.96
12.85	.32	58.81	17.9	31.5	10.8	9.65	2.94
13.5	.34	56.88	17.3	25.5	11.0	8.1	2.47
14.25	.36	55.26	16.8	18.9	11.2	6.15	1.87
15.0	.38	54.03	16.4	16.0	11.4	5.3	1.62
15.7	.40	52.97	16.1	13.5	11.6	4.6	1.40
16.5	.42	52.05	15.8	11.1	11.8	3.85	1.17
17.4	.44	51.28	15.6	9.0	12.0	3.15	.96
18.25	.46	50.65	15.4	7.18	12.2	2.55	.78
19.2	.49	50.14	15.3	5.76	12.4	2.07	.63
20.0	.51	49.74	15.16	4.55	12.6	1.65	.50
20.85	.53	49.42	15.06	3.6	12.8	1.3	.40
21.7	.55	49.16	14.98	2.54	13.0	.93	.28
22.6	.57	49.0	14.94	1.635	13.2	.6	.18
23.45	.59	48.9	14.9	.543	13.4	.2	.06
24.35	.618	48.9	14.9	0	13.6	0	0
32.3	.820	48.9	14.9	0	15.4	0	0
40.0	1.02	48.9	14.9	0	17.1	0	0
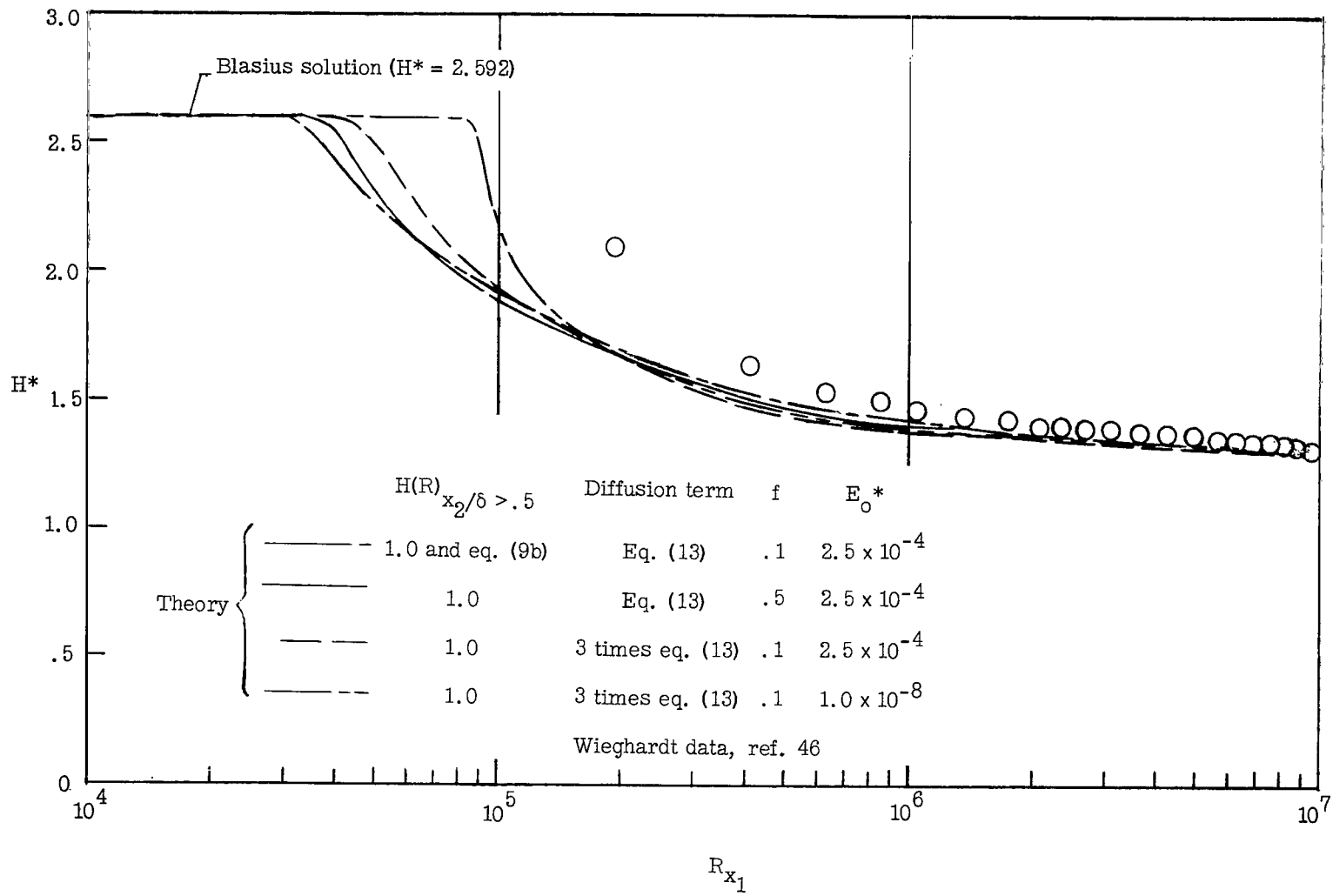
Figure 1.- Effect of modifications to the H(R) function, the $\Delta\xi$ step size, the diffusion term, and E_0^* value on form factor H^* for flat-plate flow.
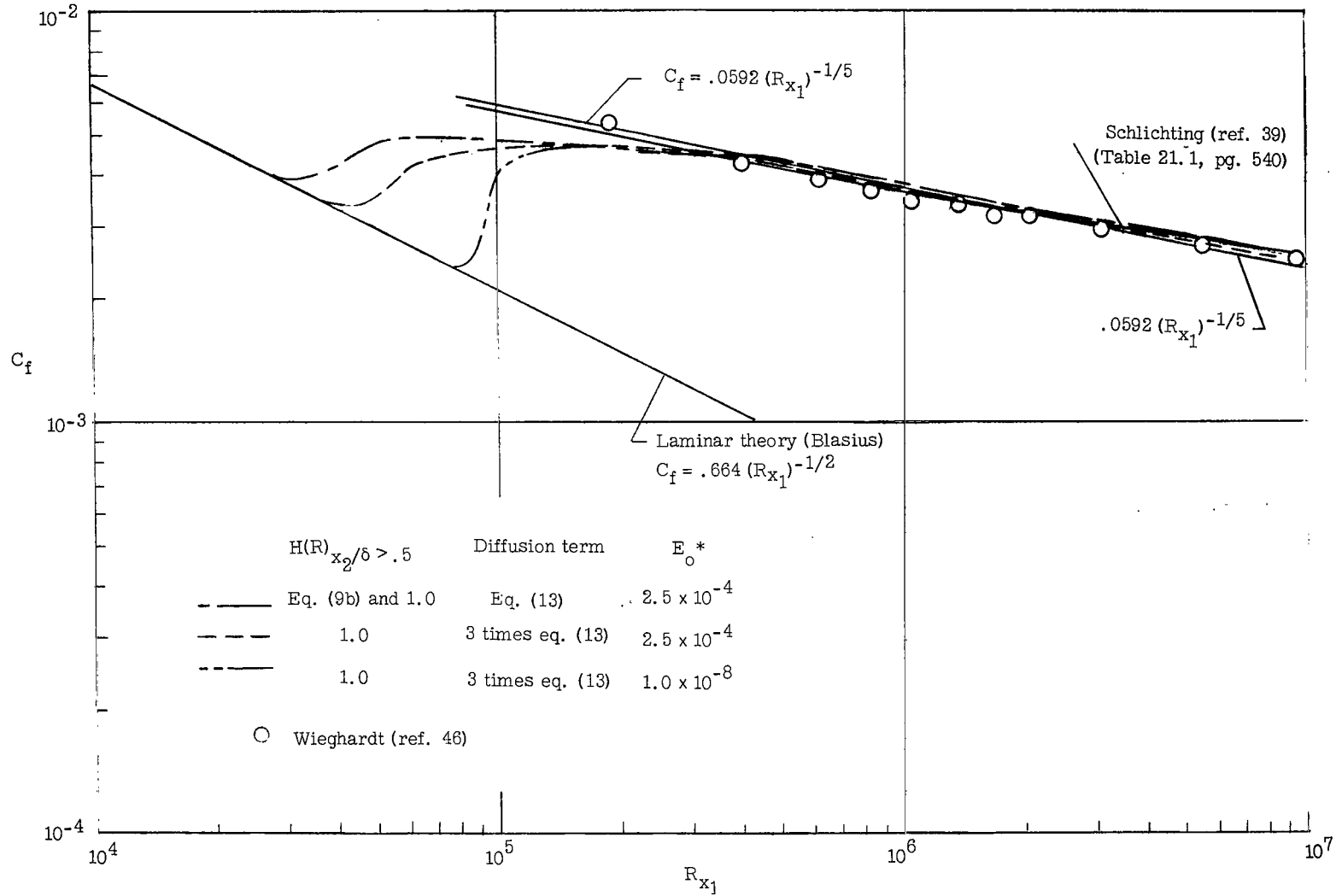
Figure 2.- Effects of modification to diffusion term and of different values of E_0^* on C_f distribution for flat-plate flow.

$H(R)_{x_2/\delta > .5}$ Diffusion term

	Eq. (9b)	Eq. (13)
	1.0	Eq. (13)
	1.0	3 times eq. (13)

R_{x_1}

6.3×10^5 ○ } Data of
1.1×10^6 □ } Wieghardt (ref. 46)

$\dfrac{x_2}{\delta}_{F=.995}$

R_{x_1}

0.01×10^6
$.06 \times 10^6$
$.2 \times 10^6$
1.0×10^6
5.0×10^6

R_{x_1}

0.2×10^6
1.0×10^6
5.0×10^6

1.0×10^6

$F = \bar{u}_1/U_e$
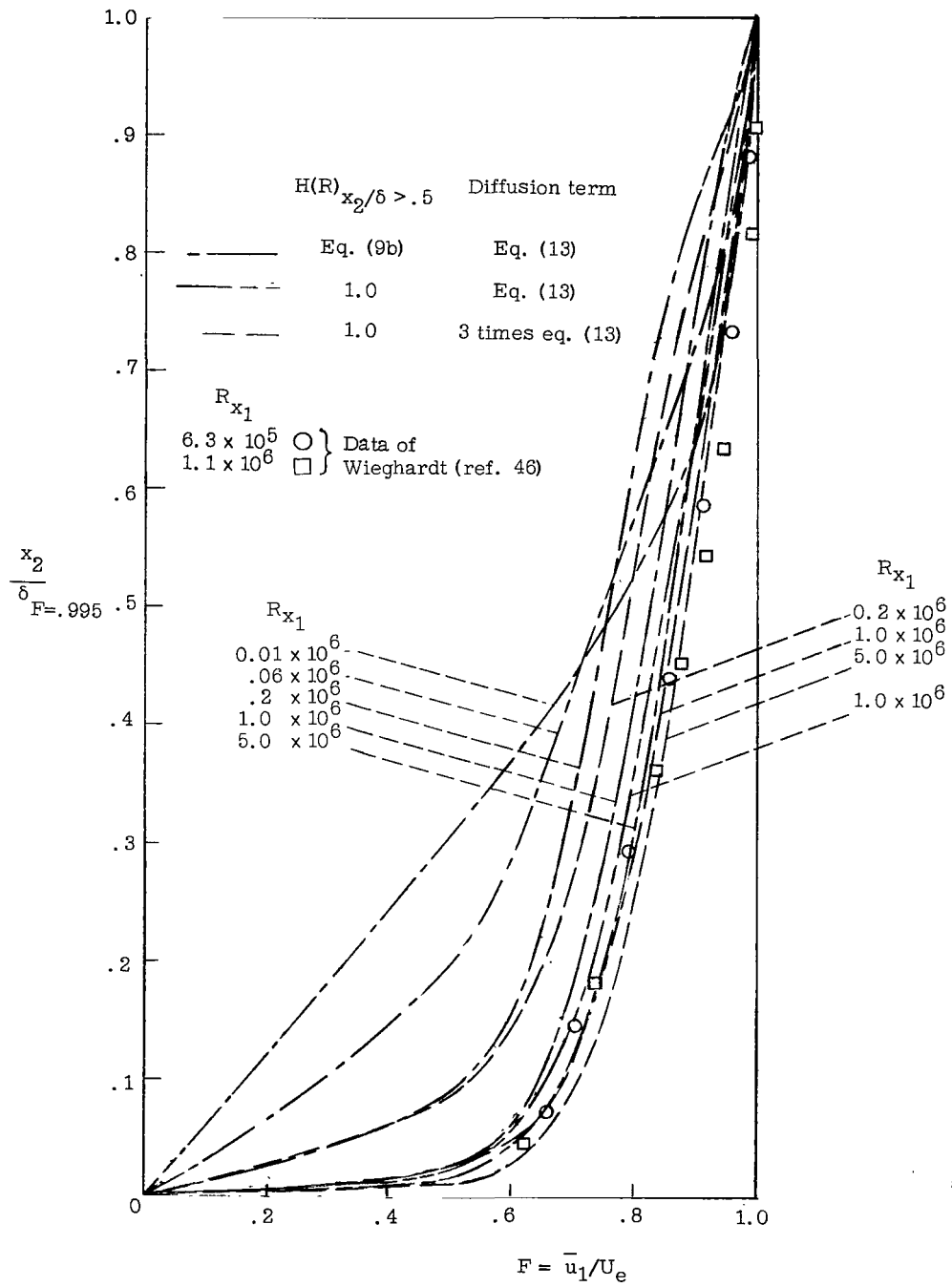
(a) Development of velocity profiles from laminar input at $R_{x_1} = 1 \times 10^4$ to turbulent at $R_{x_1} \geqq 1 \times 10^6$ for dp/dx = 0.

Figure 3.- Mean velocity distributions.

81
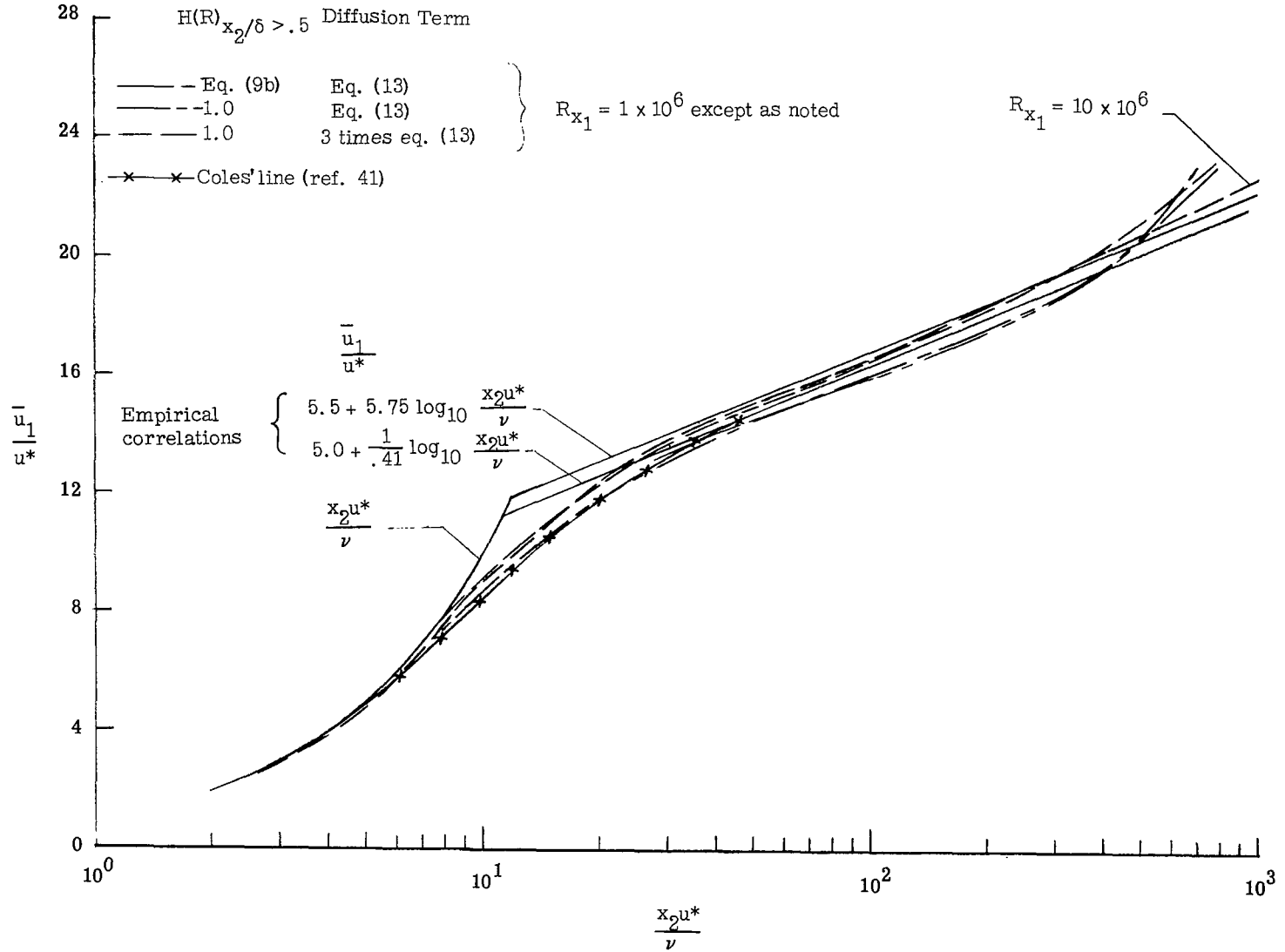
(b) Law-of-the-wall parameters.

Figure 3.- Continued.
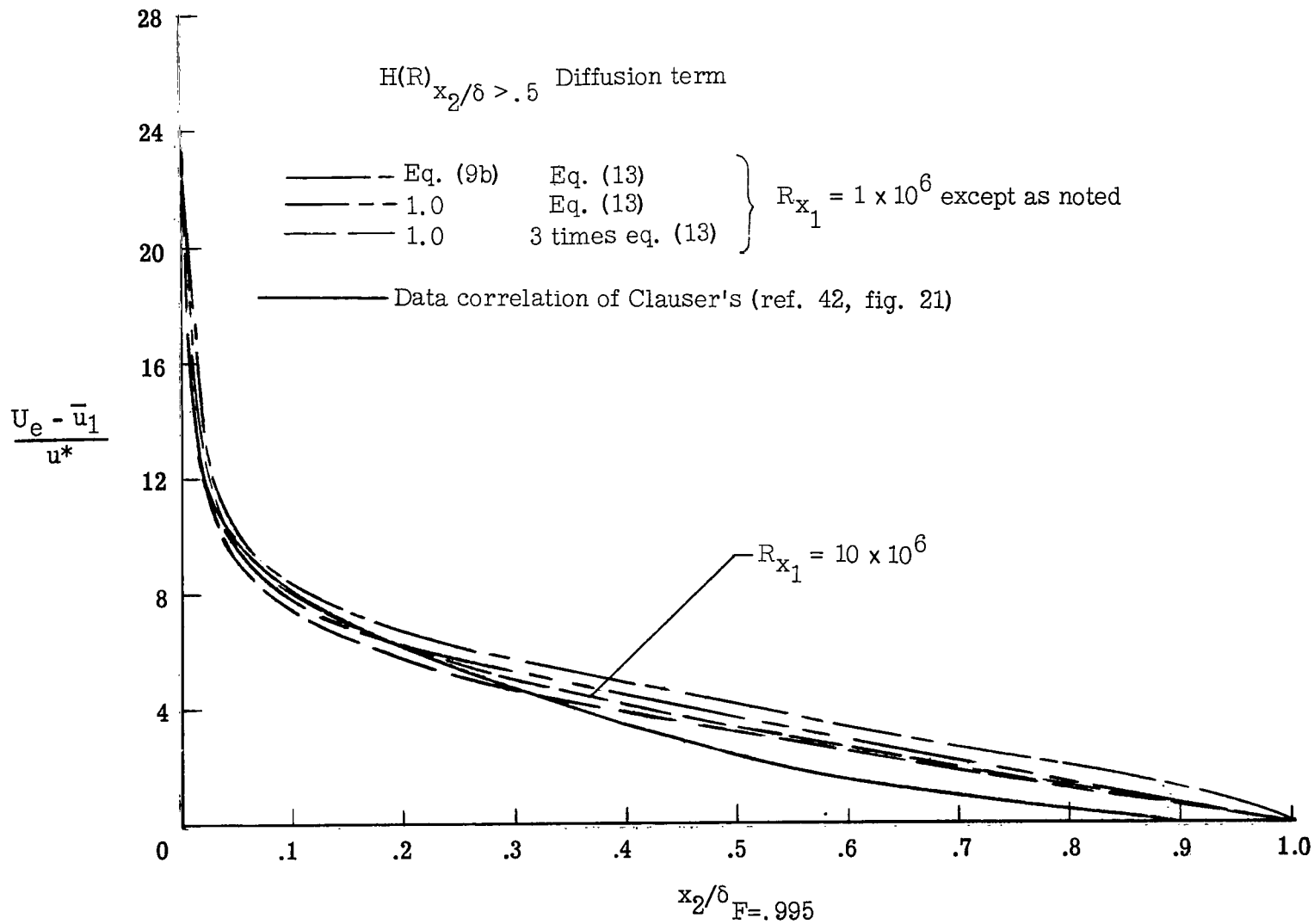
(c) Velocity defect parameters.

Figure 3.- Concluded.

$H(R)_{x_2/\delta > .5}$ Diffusion term

— ·· — — Eq. (9b)   Eq. (13)

Theory — — — — 1.0   Eq. (13)

—— —— 1.0   3 times eq. (13)

———— Limits from measurements in
equilibrium boundary layers (refs. 32 and 34)

.28

.24

.20

— Constant value used in theory
of Bradshaw (ref. 18)

.16

$\dfrac{dp}{dx_1} = 0$

$\dfrac{\tau_T}{2\rho\bar{e}} = \dfrac{-\overline{u_1' u_2'}}{2\bar{e}}$

.12

— Positive $\dfrac{dp}{dx_1}$

.08

.04

0   .1   .2   .3   .4   .5   .6   .7   .8   .9   1.0

$x_2/\delta_{F=.995}$
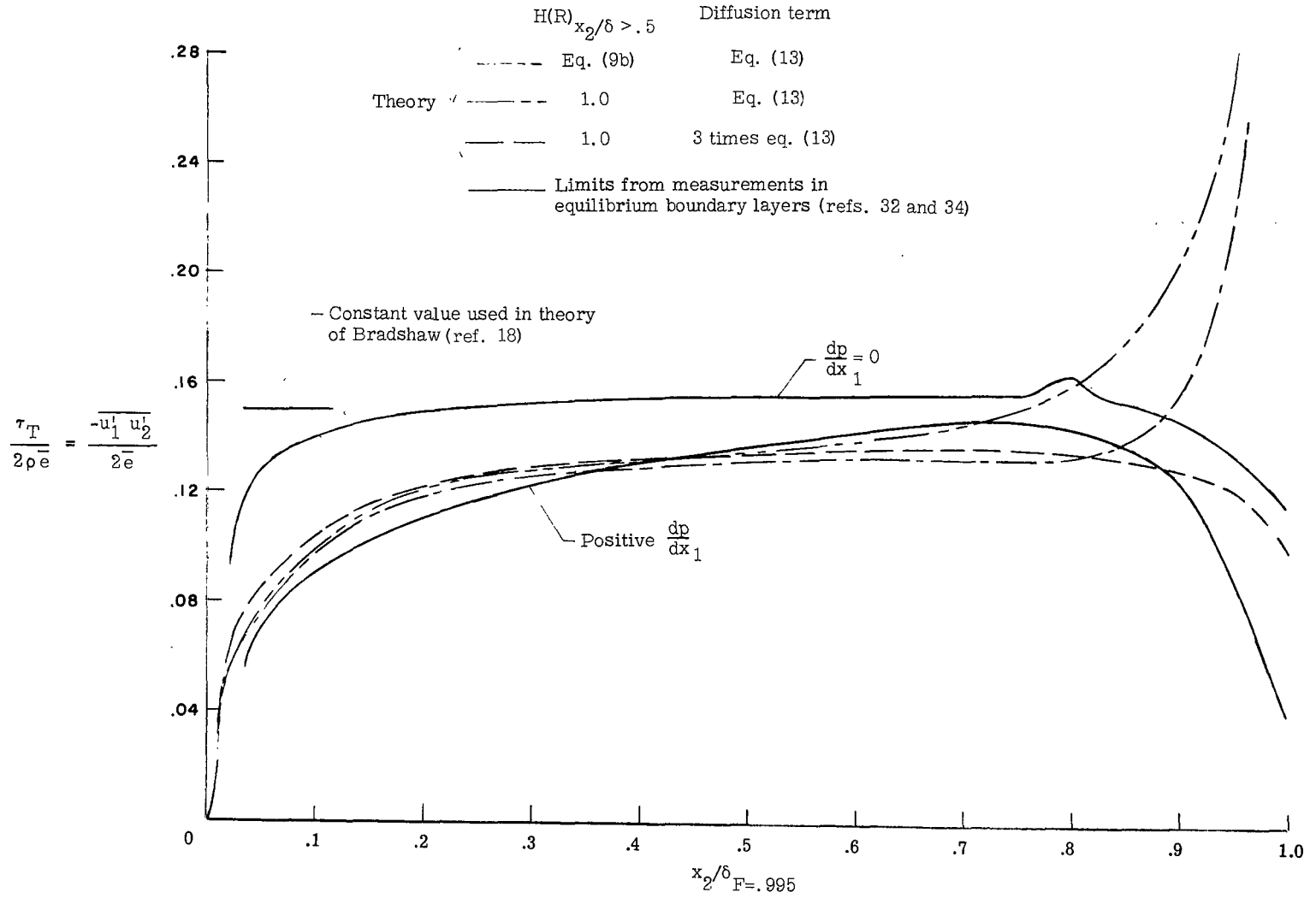
Figure 4.- Variation across boundary layer of ratio of turbulent shear stress to twice turbulent kinetic energy for flat-plate flow at $R_{x_1} = 1 \times 10^6$. $E_0^* = 2.5 \times 10^{-4}$.
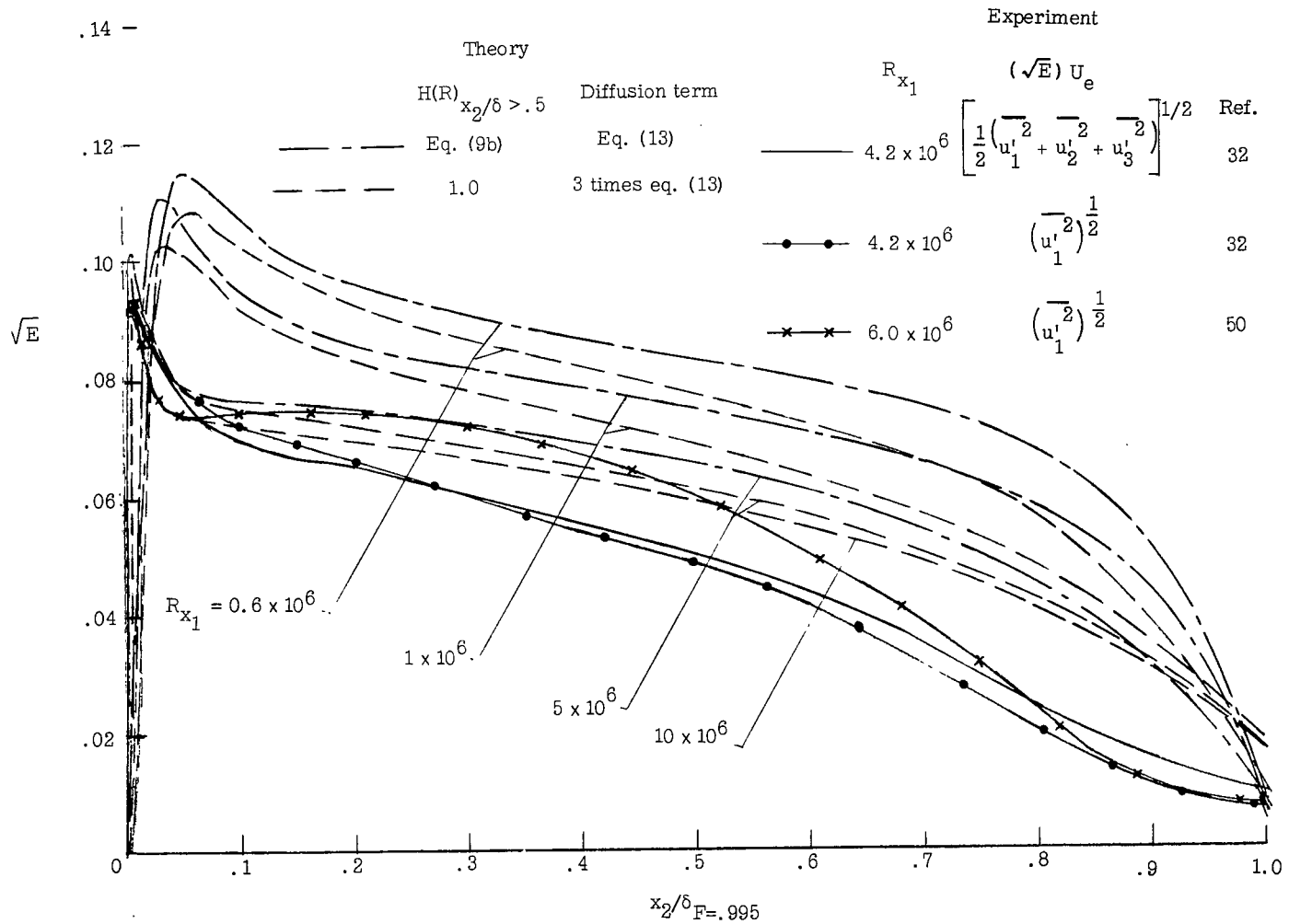
(a) Curves shown are for $E_0^* = 2.5 \times 10^{-4}$, but for $R_{x_1} \geqq 5 \times 10^5$, the use of $E_0^* = 1 \times 10^{-8}$ gives same curves.

Figure 5.- The variation in $\sqrt{E} = \left(\overline{u_1'^2} + \overline{u_2'^2} + \overline{u_3'^2}\right)^{1/2} \Big/ 2U_e$ across the flat-plate boundary layer as computed for various values of R_{x_1} with different assumptions for diffusion, and as measured by Klebanoff (ref. 32).
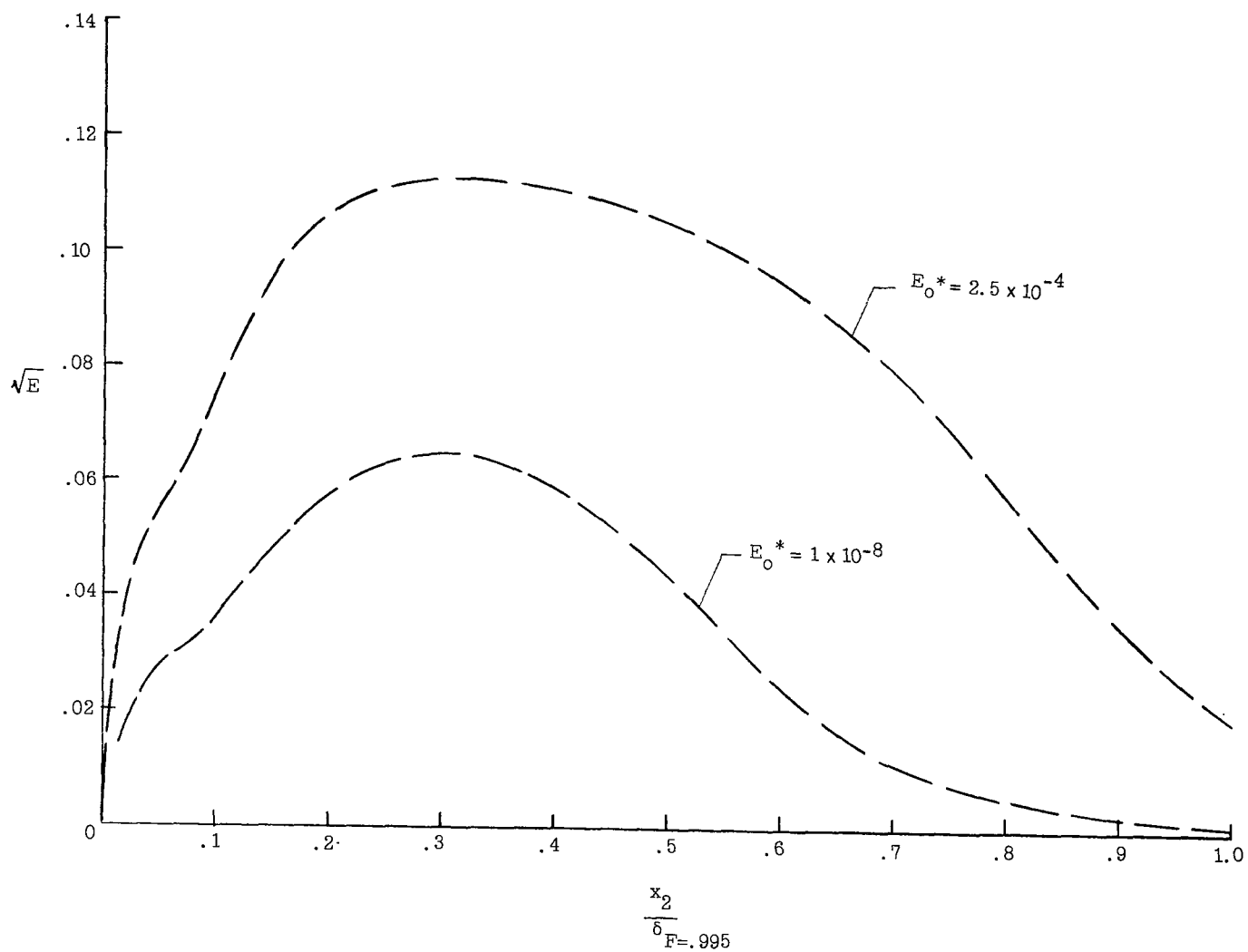
(b) Effect of E_0^* in transition region $\left(R_{x_1} = 9 \times 10^4\right)$. Diffusion is three times Glushko diffusion. $H(R) = 1$ for $\frac{x_2}{\delta} > 0.5$.

Figure 5.- Concluded.
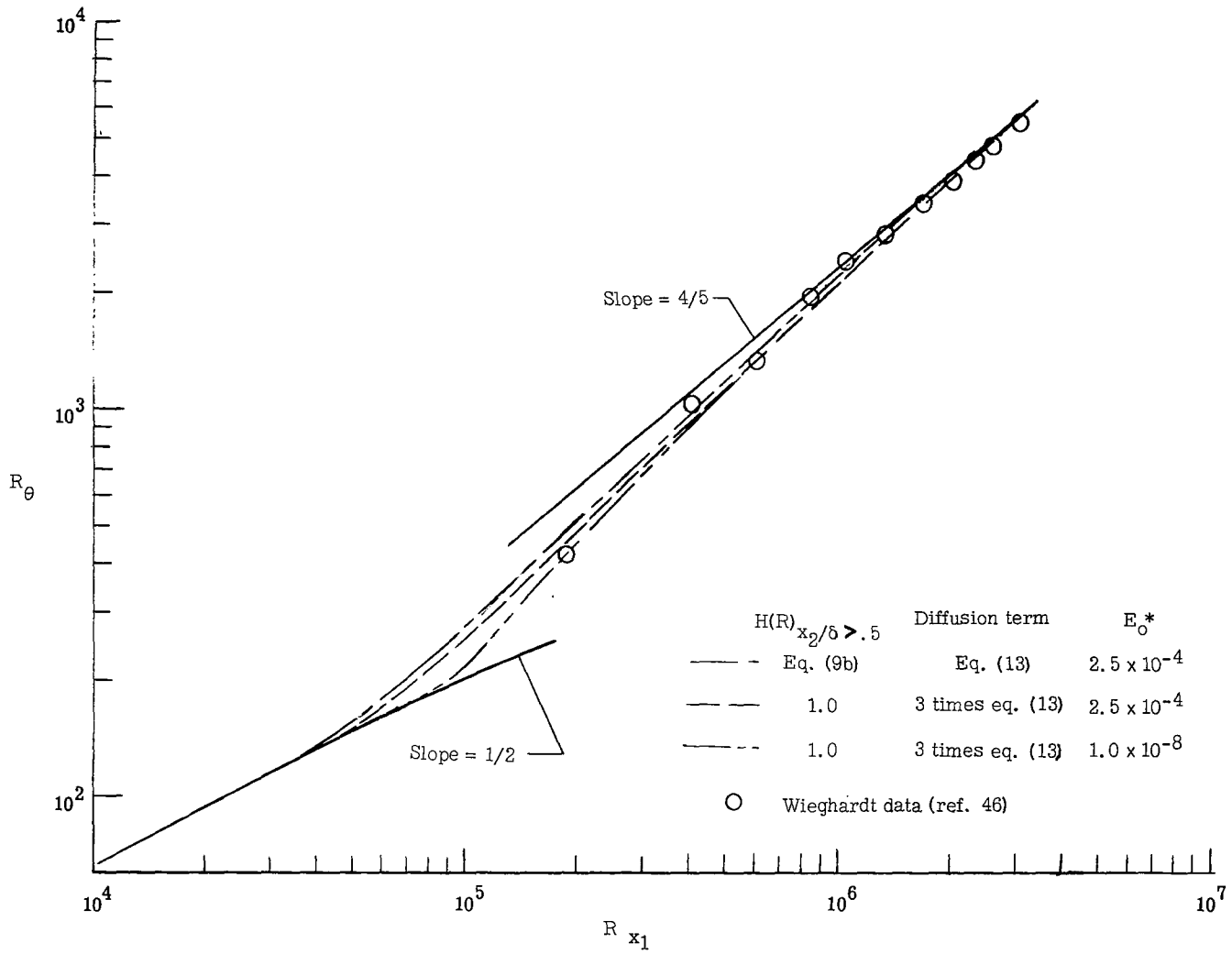
(a) Momentum thickness, θ.

Figure 6.- Effect on boundary-layer thickness parameters for flat-plate flow of increasing Glushko's (ref. 17) turbulent diffusion term three times and of changing E_0^*.
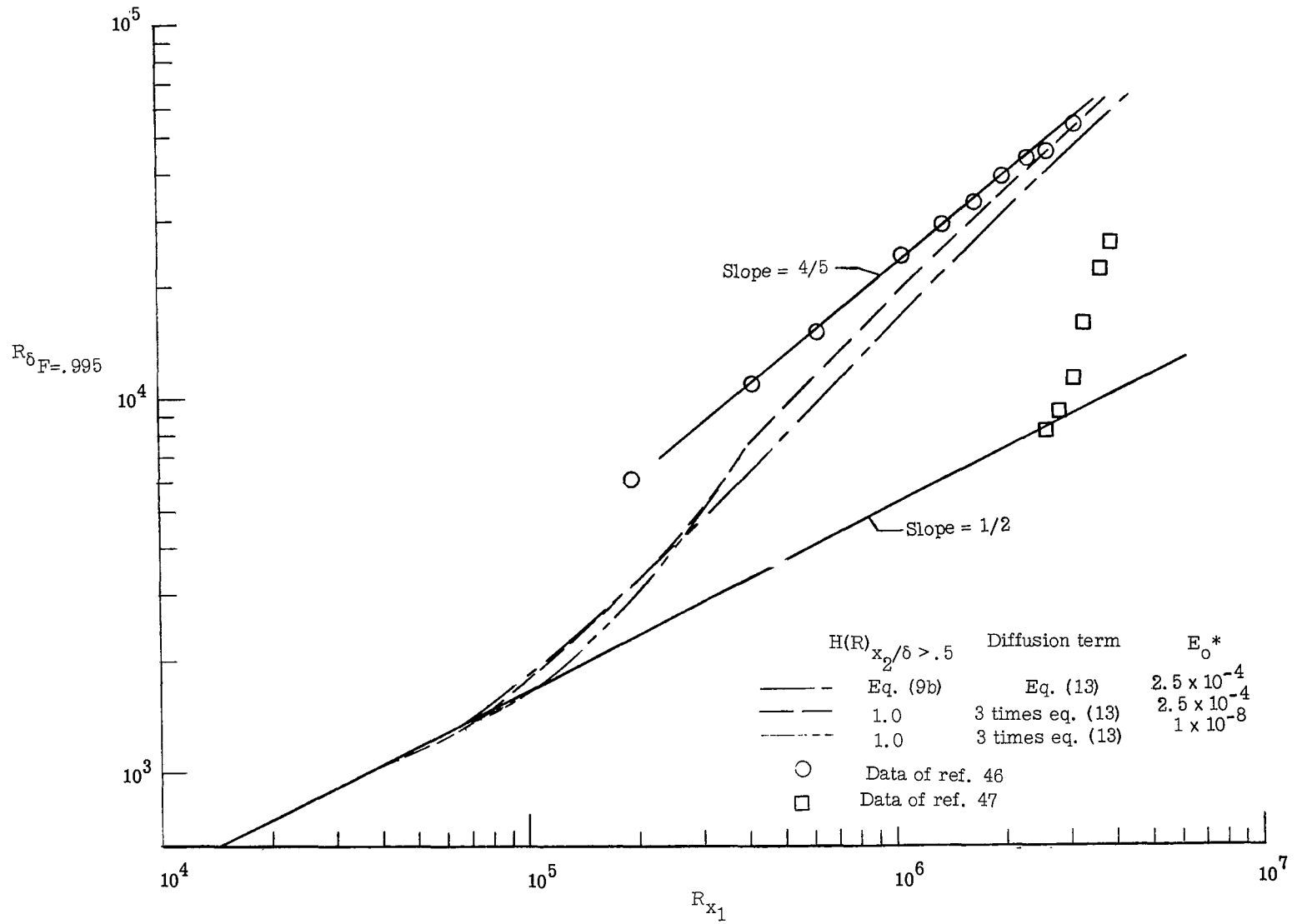
(b) Boundary-layer thickness at F = 0.995.

Figure 6.- Concluded.

Figure 7.- Turbulent kinetic energy balance for flat-plate flow at $R_{x_1} = 5 \times 10^6$. Calculations used are three times Glushko diffusion. $E_0{}^* = 2.5 \times 10^{-4}$.
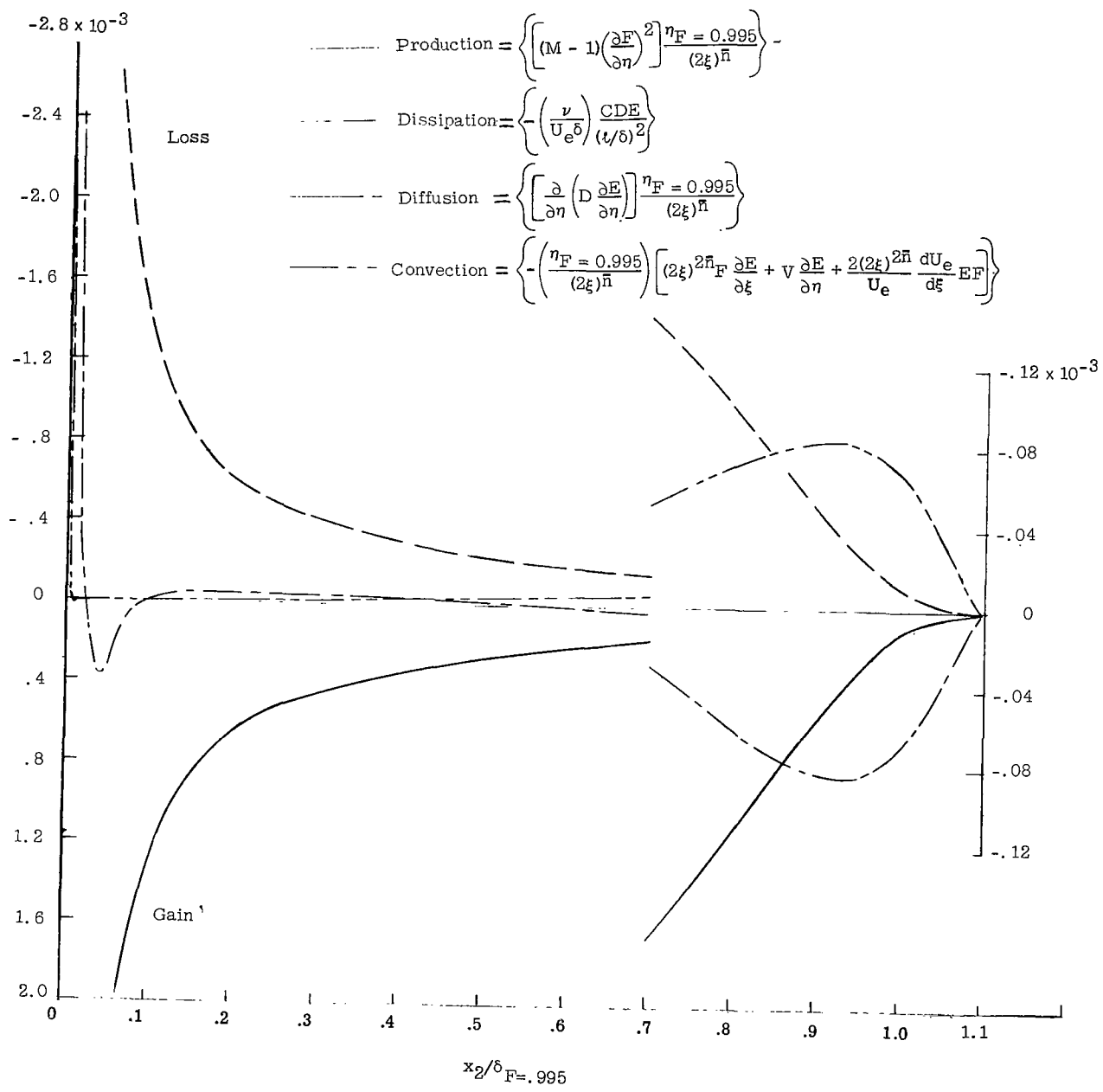
(a) Computed results for $\dfrac{x_2}{\delta_{F=0.995}}$ from 0 to 1.1.
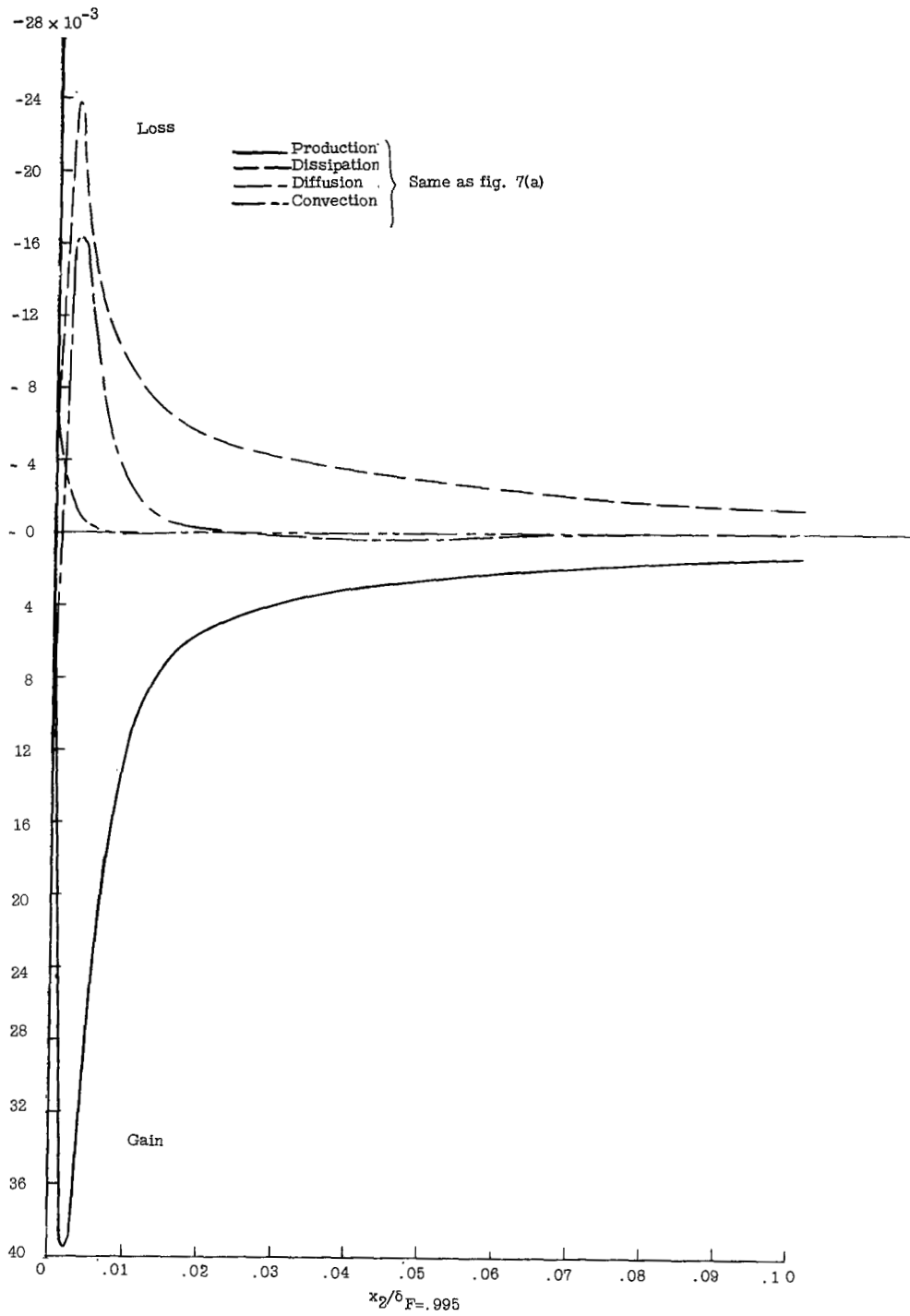
(b) Computed results for $\frac{x_2}{\delta}$ from 0 to 0.1.

Figure 7.- Continued.
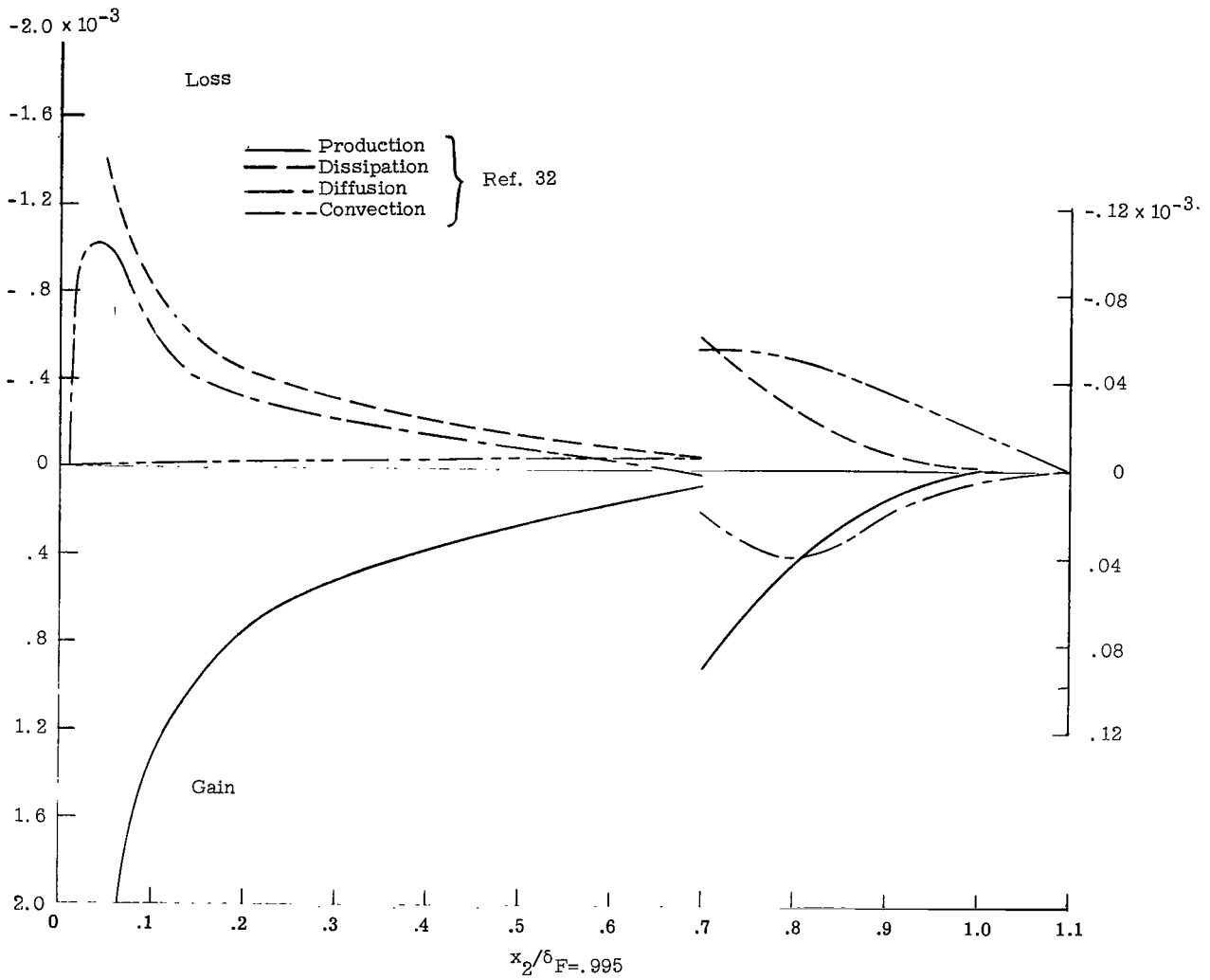
(c) Experimental results from reference 32 as found in the reference for $\dfrac{x_2}{\delta_{F=0.995}}$ from 0 to 1.1. $R_{x_1} = 4.3 \times 10^6$.

Figure 7.- Continued.
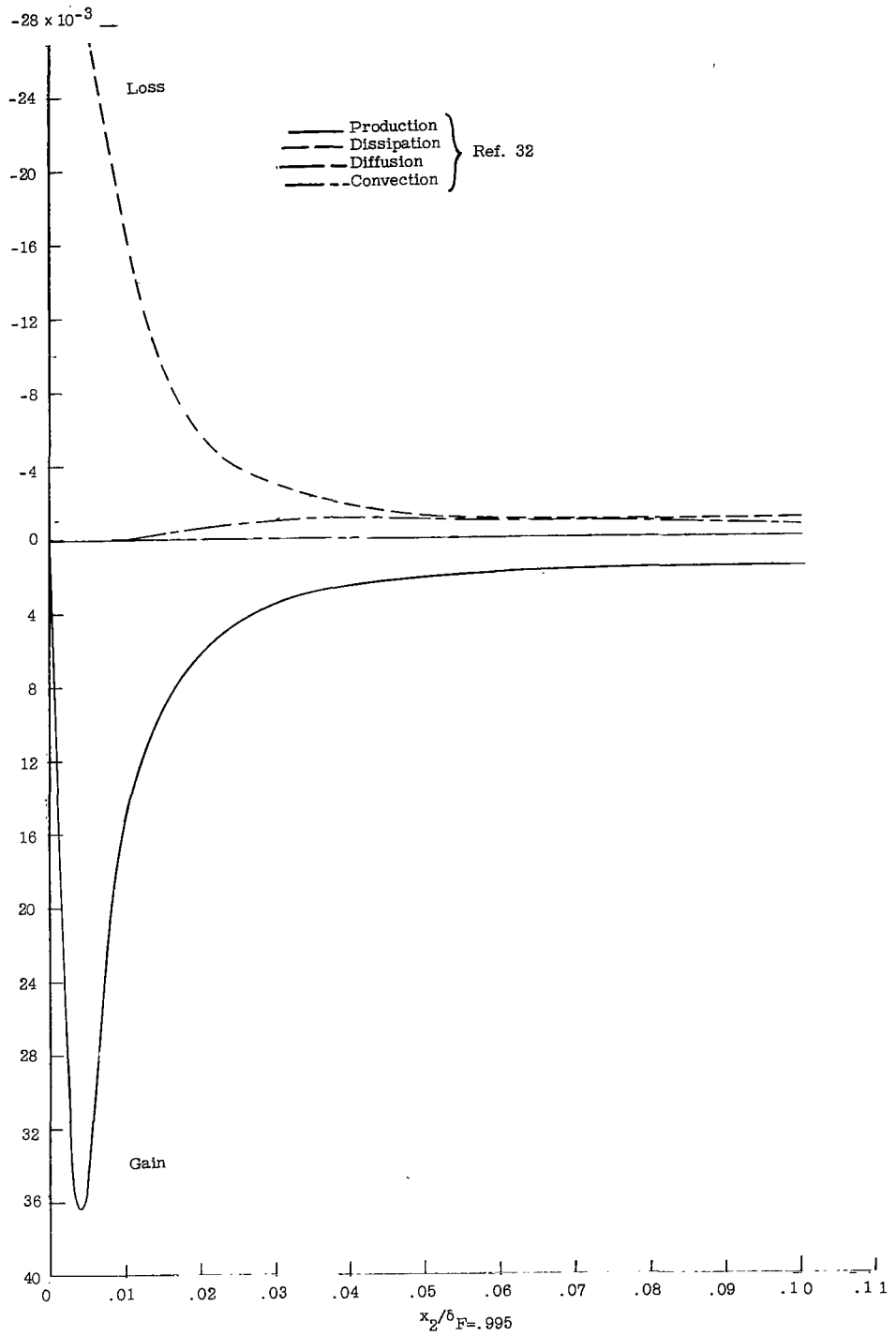
(d) Experimental results from reference 32 for $\dfrac{x_2}{\delta_{F=0.995}}$ from 0 to 0.1. $R_{x_1} = 4.3 \times 10^6$.

Figure 7.- Concluded.
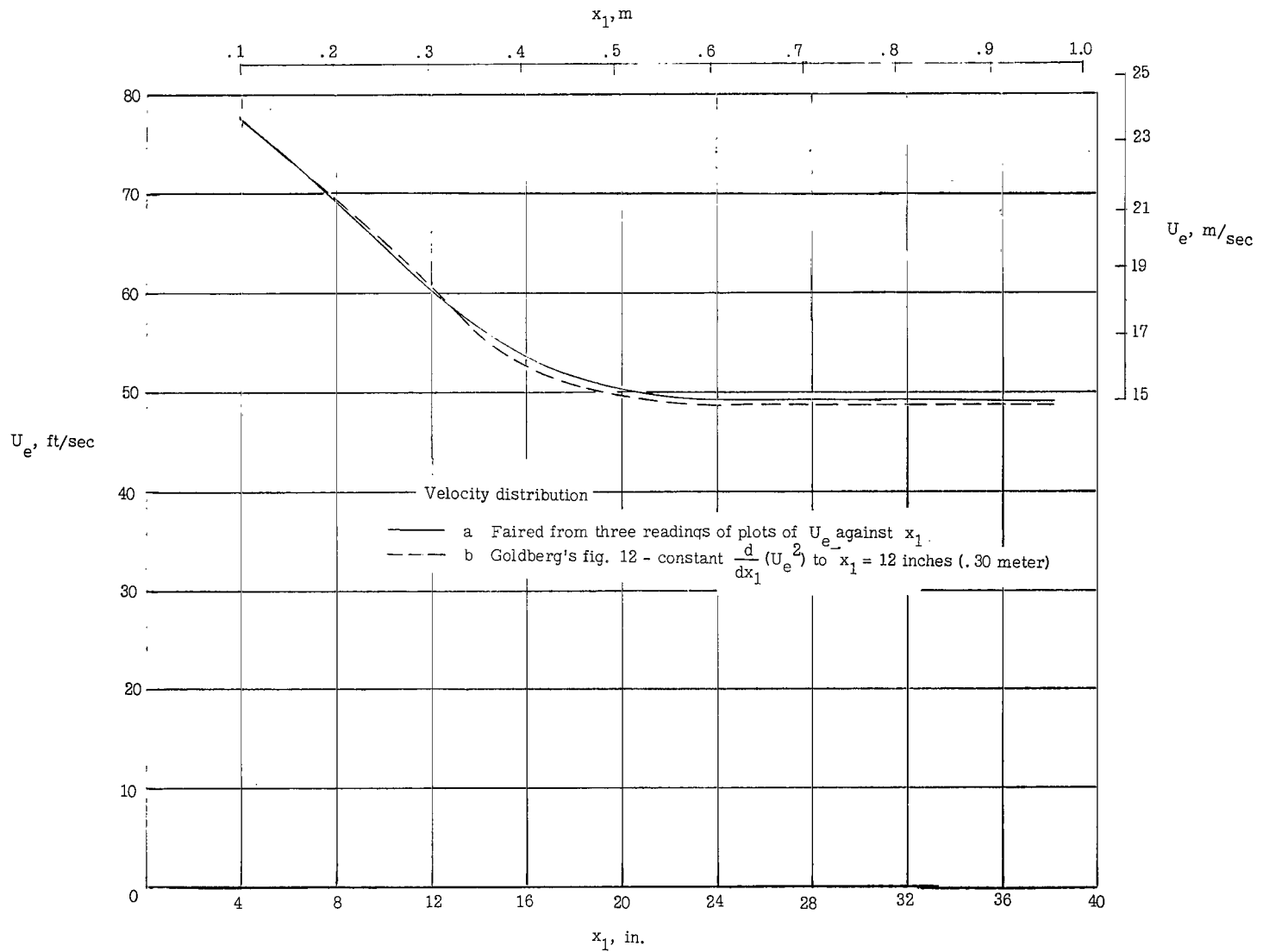
(a) Velocity variation with x_1.

Figure 8.– Free-stream flow distribution from the Goldberg (ref. 43) pressure distribution number 3 as used in the present calculations.
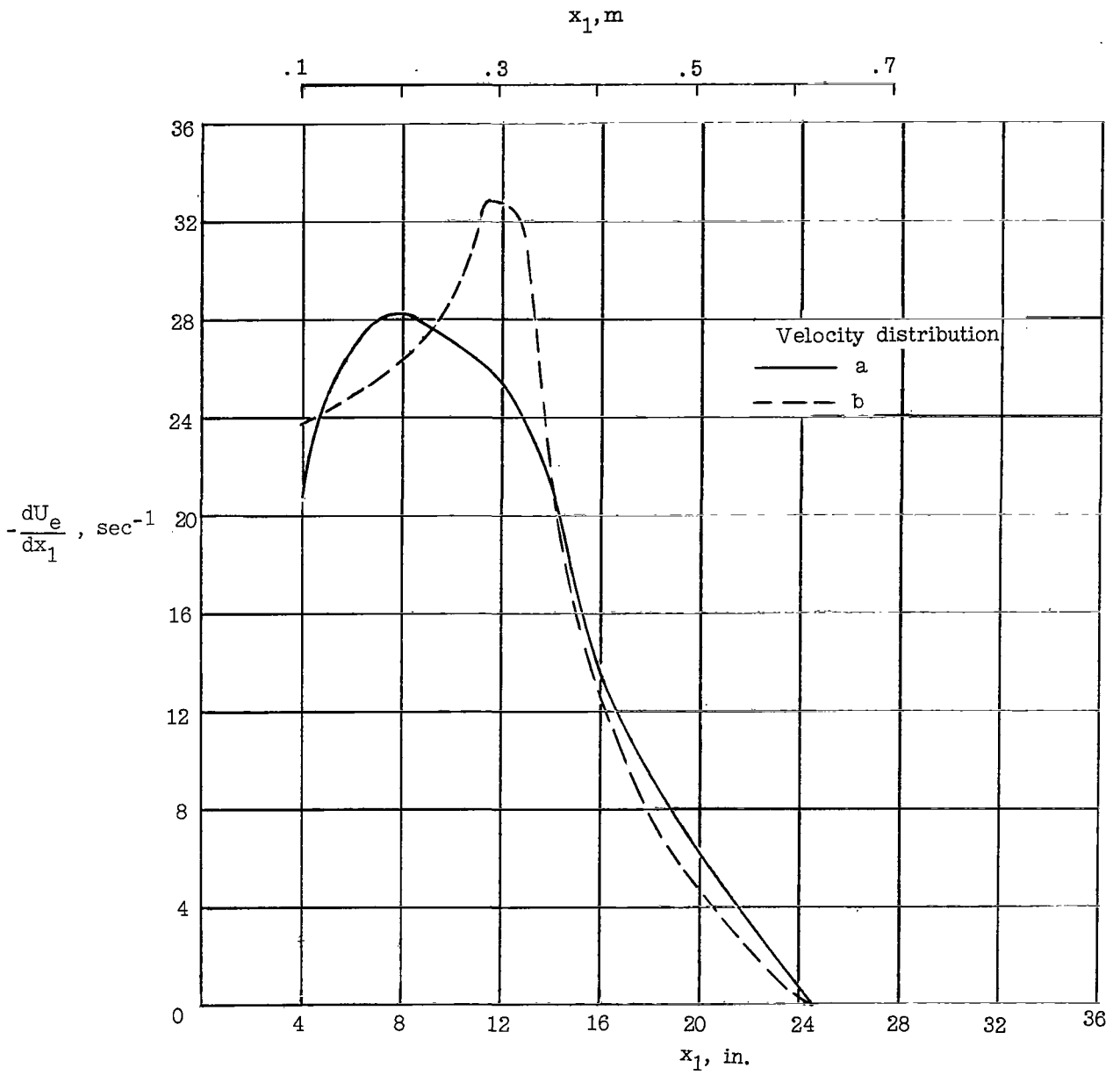
(b) Variation of external velocity derivative.

Figure 8.- Concluded.
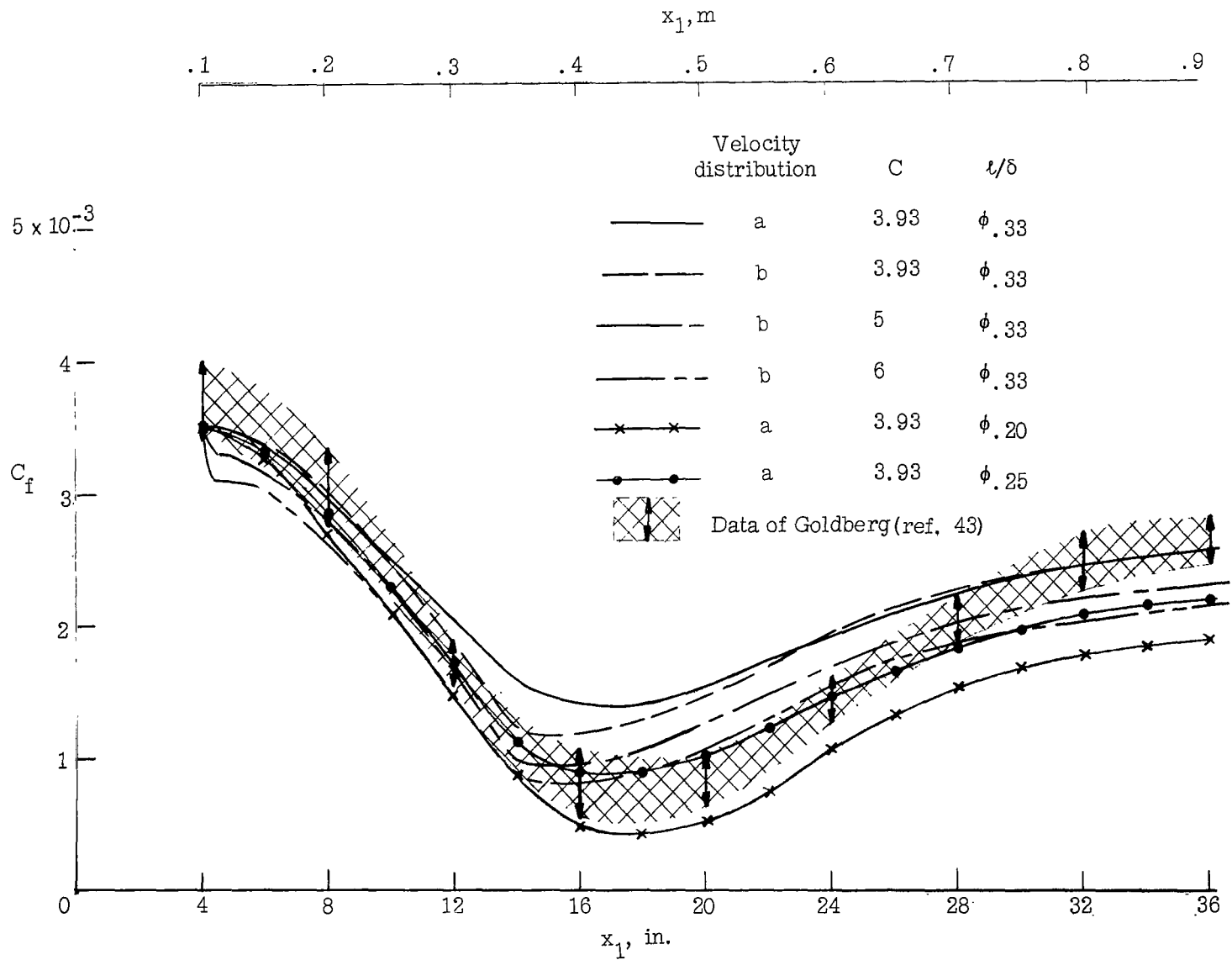
Figure 9.- Comparison of calculated skin friction with measured values of Goldberg (ref. 43) for different velocity distributions, values of C, and ℓ/δ functions. Diffusion is 3 times Glushko diffusion and $\bar{H}(R) = 1$ in outer part of boundary layer.
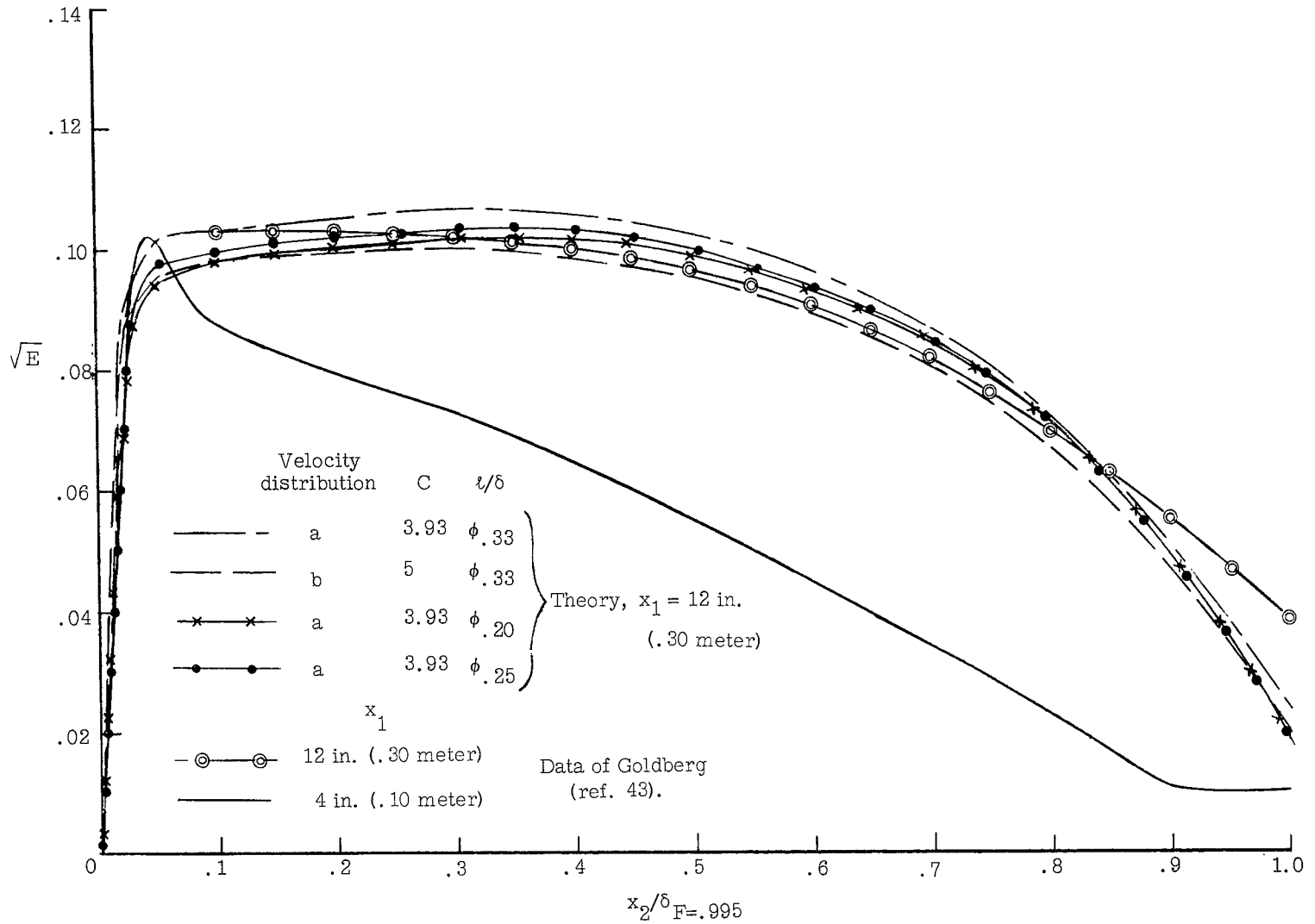
(a) $x_1 = 12$ inches (0.30 meter) and input profile used to start solution at $x_1 = 4$ inches (0.10 meter).

Figure 10.- Calculated distribution of $\sqrt{E}$ compared with distribution obtained from measured longitudinal turbulence intensity of Goldberg (ref. 43). Diffusion is 3 times Glushko diffusion.
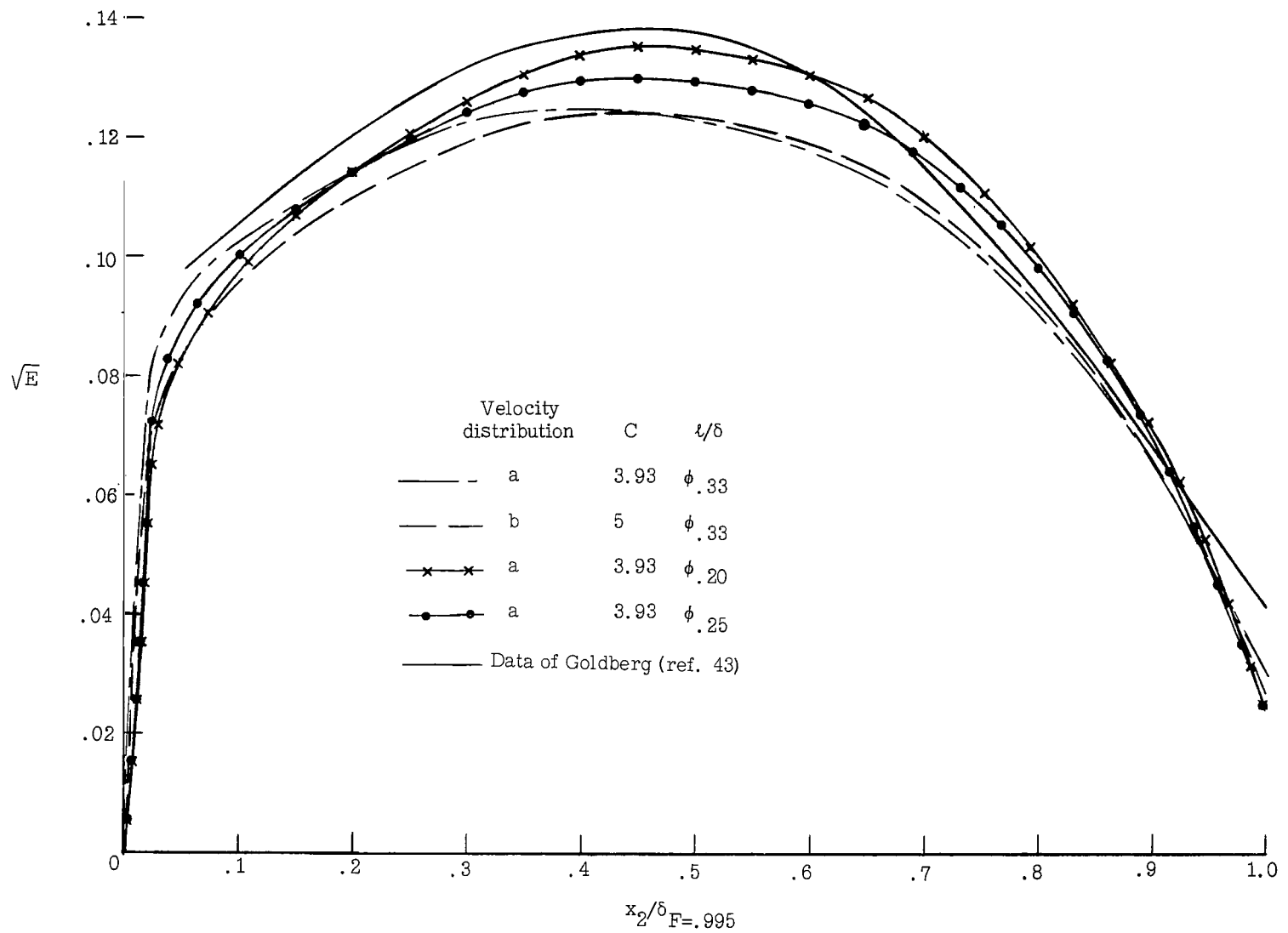
(b) $x_1 = 20$ inches (0.51 meter).

Figure 10.- Continued.
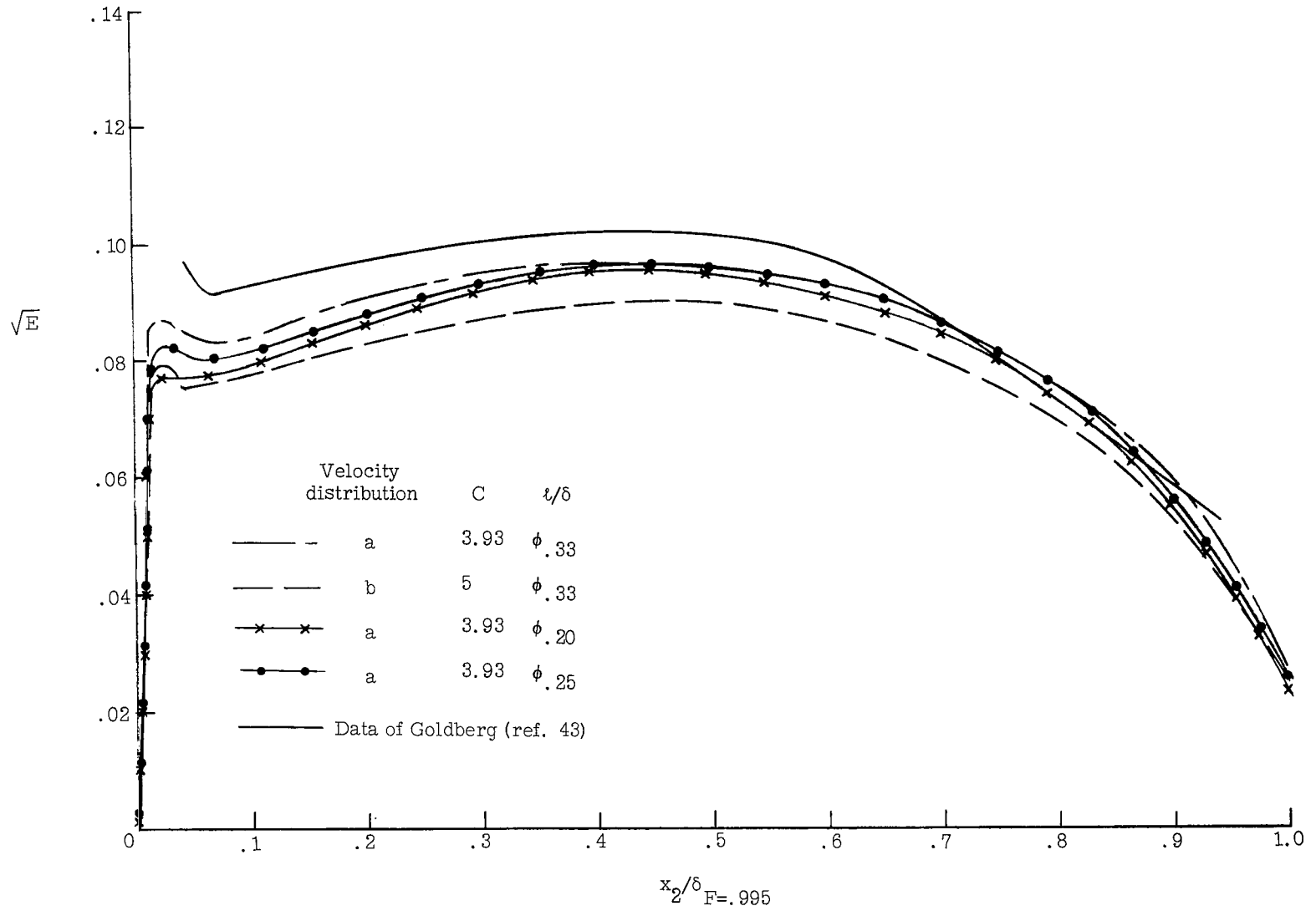
(c) $x_1 = 36$ inches (0.91 meter).

Figure 10.- Concluded.
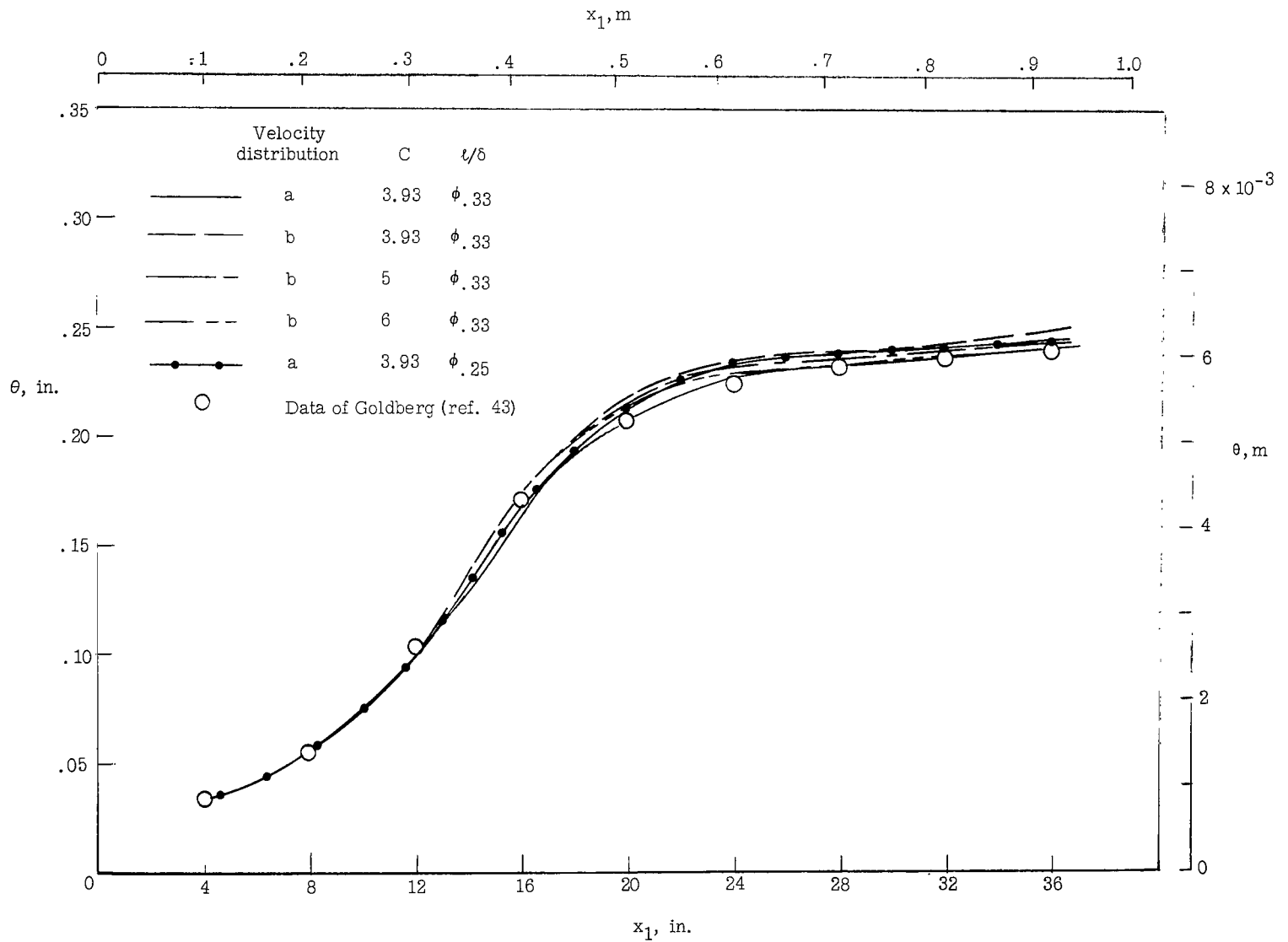
(a) Momentum thickness.

Figure 11.- Effect on momentum thickness of velocity distribution, value of dissipation factor, C, and l/δ function.

x_1, m

Velocity
distribution   C ℓ/δ

——————— a   3.93 $\phi_{.33}$

— — — — b   3.93 $\phi_{.33}$

— —— — b   5 $\phi_{.33}$

— – — – b   6 $\phi_{.33}$

●—●—● a   3.93 $\phi_{.25}$

○   Data from ref. 43

δ, in.

δ, m

Distance along test cylinder, x_1, in.
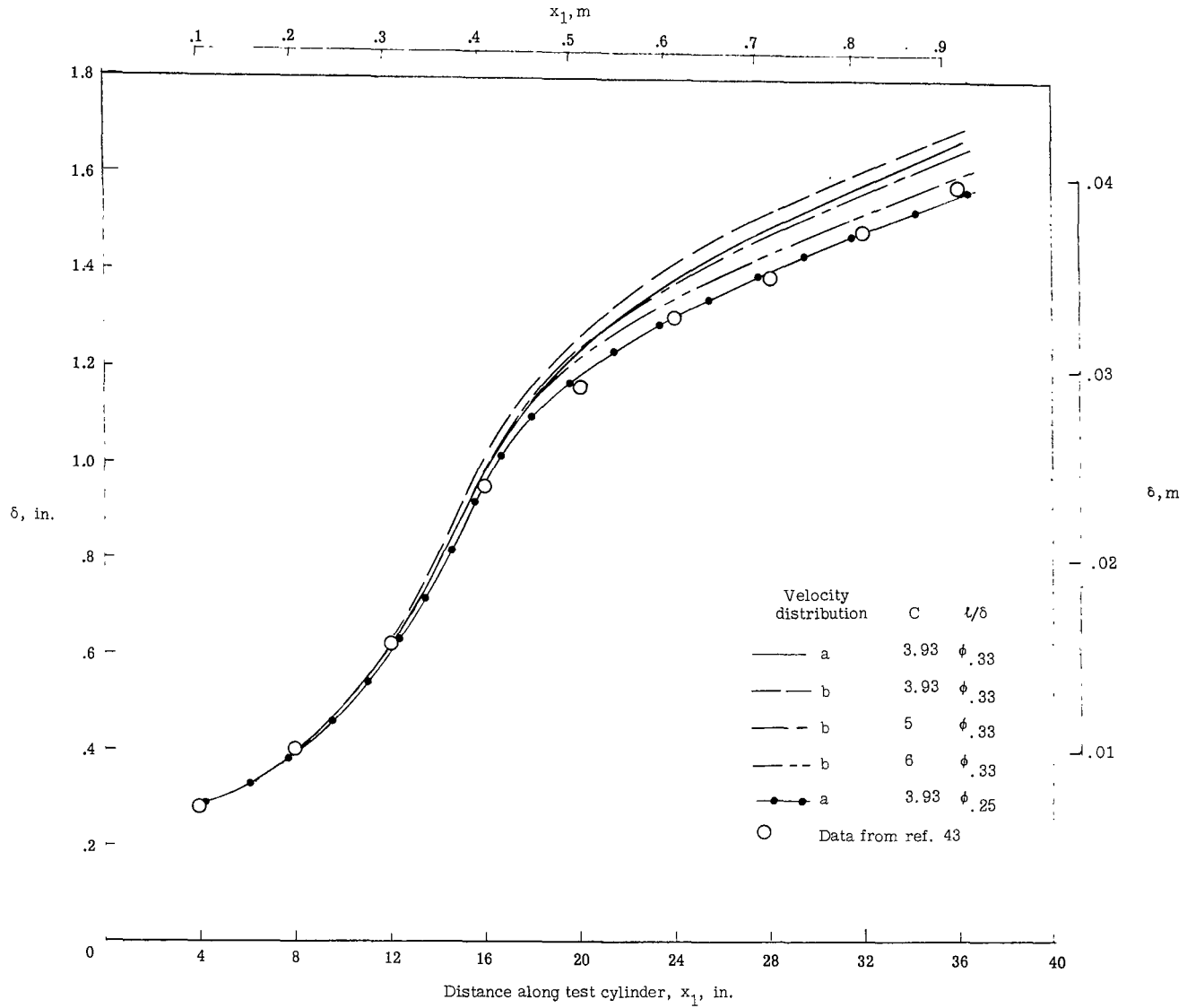
(b) Boundary-layer thickness at point where $F = 0.995$ for theory and according to figure 20 of reference 43.

Figure 11.- Concluded.
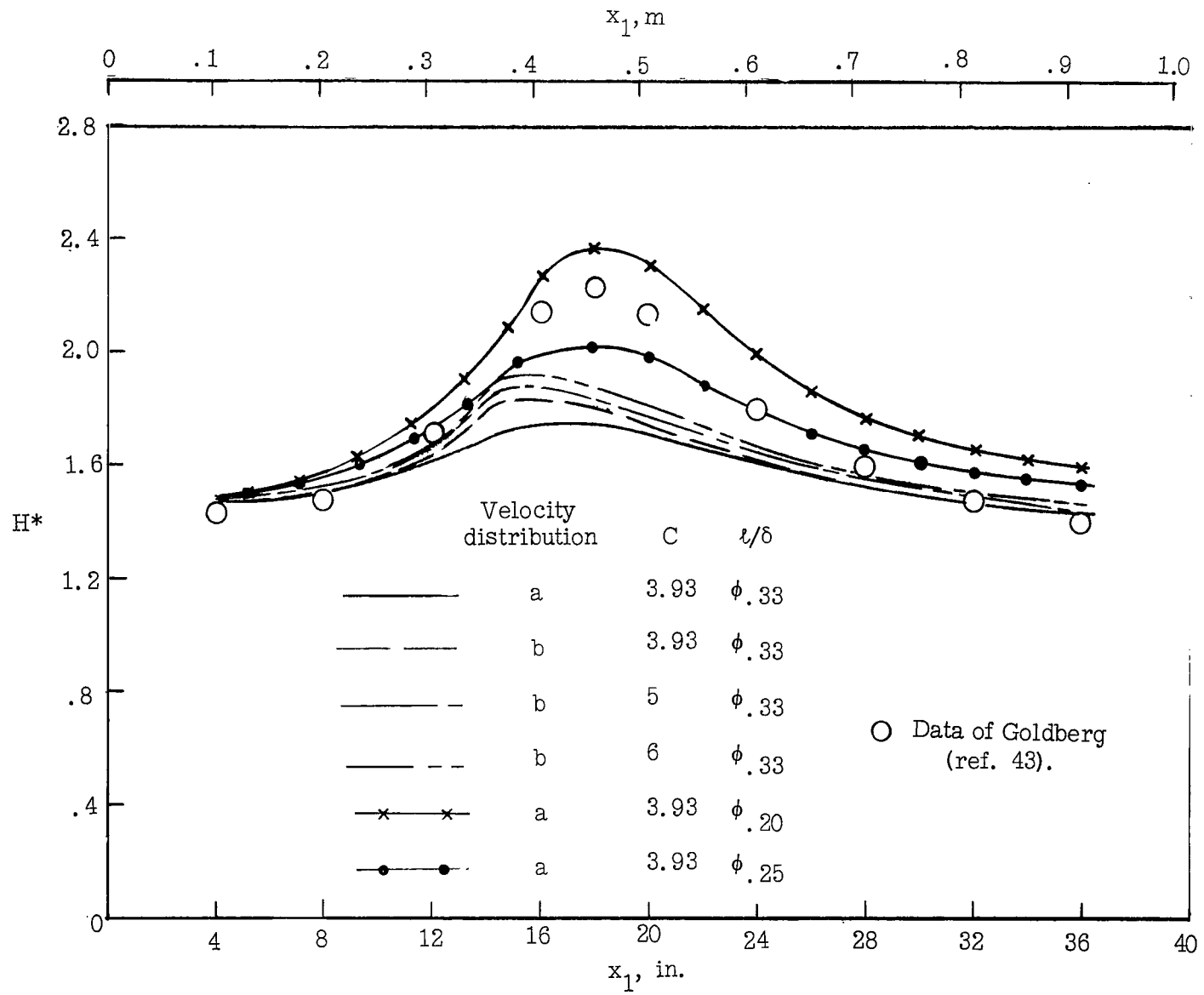
Figure 12.- Comparison of computed values of the shape parameter H^* for velocity distributions a and b, various values of C, and various l/δ functions with data of Goldberg (ref. 43).
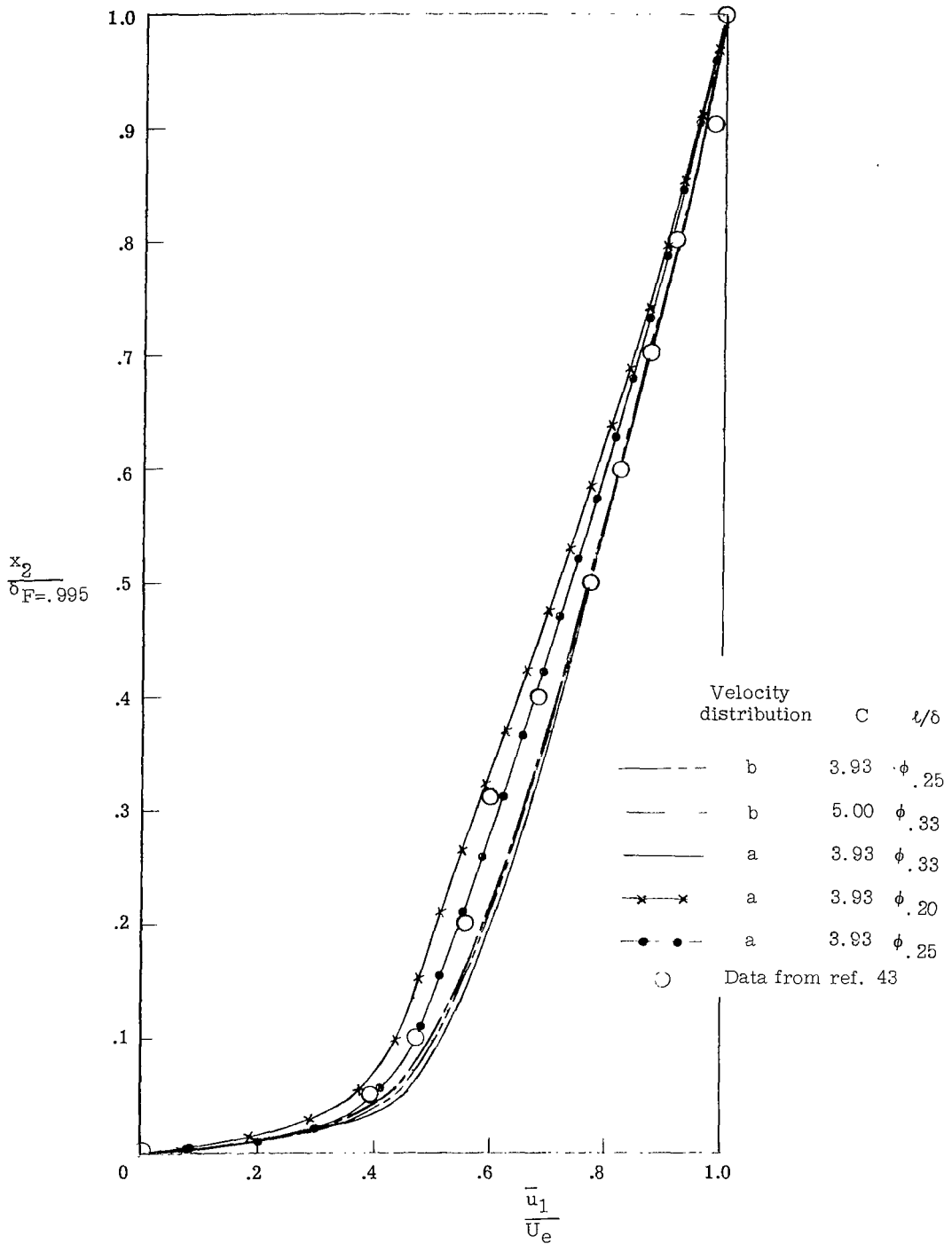
(a) x_1 = 12 inches (0.30 meter).

Figure 13.- Comparison of theoretical velocity profiles with data of reference 43.
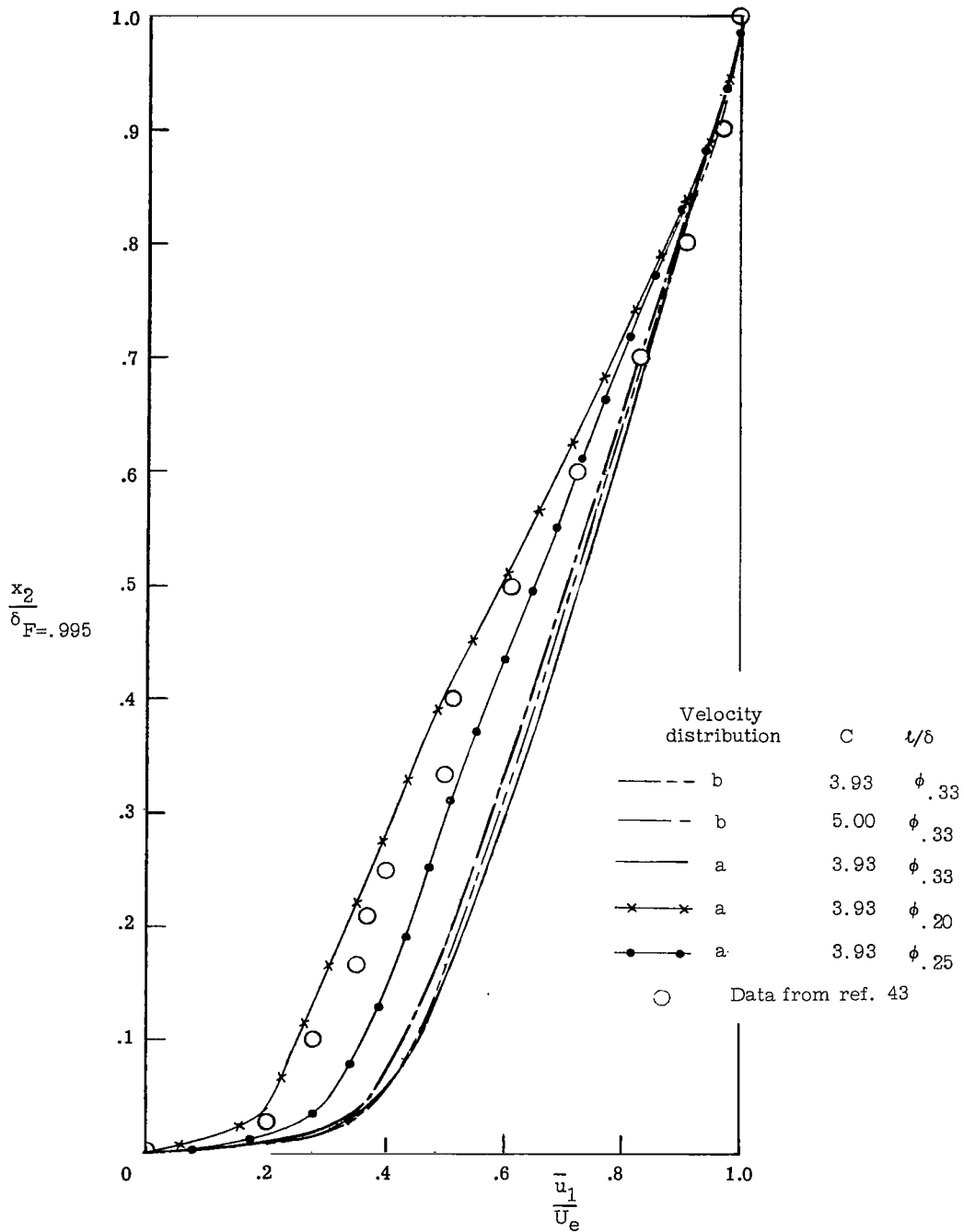
(b) x_1 = 20 inches (0.51 meter).

Figure 13.- Continued.
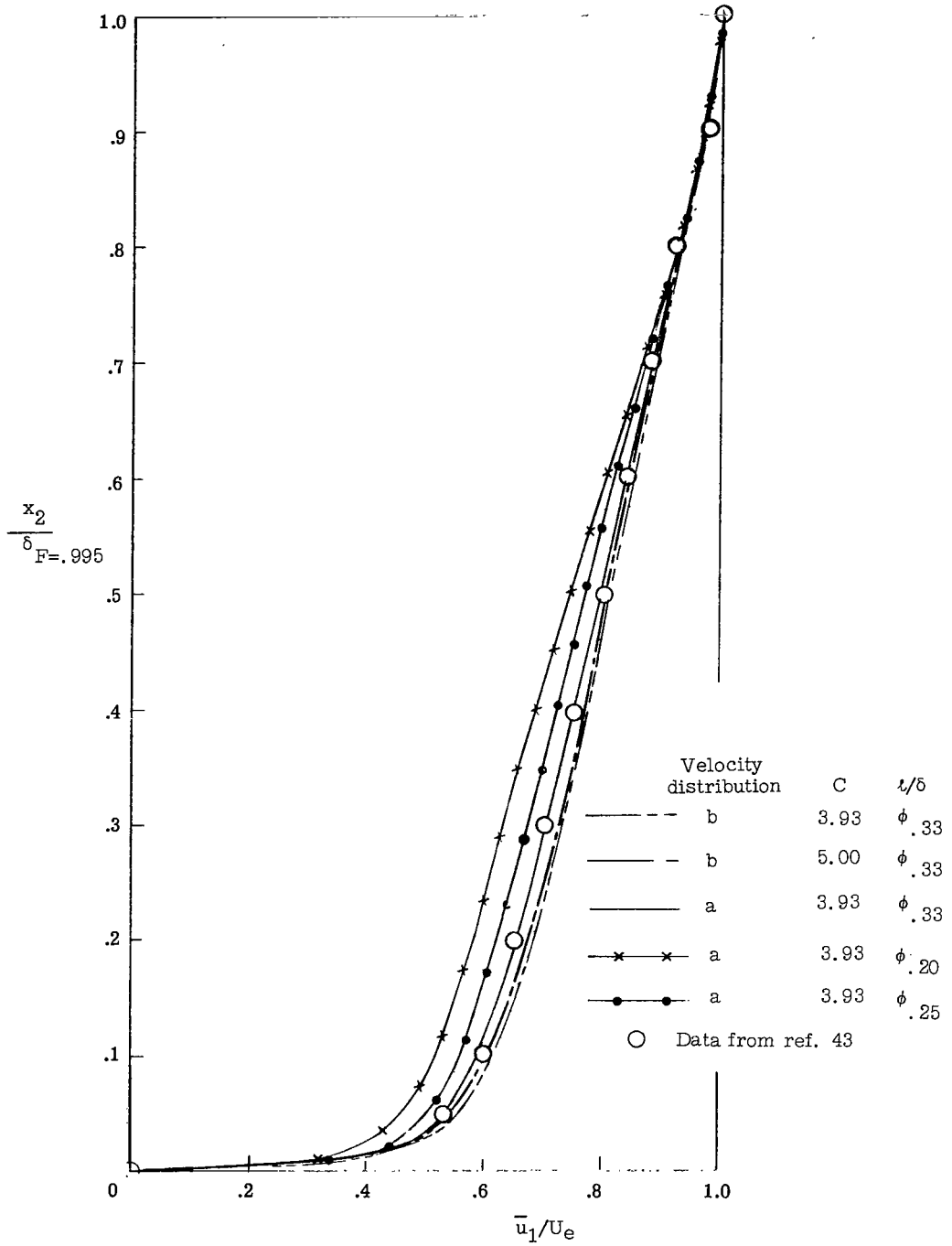
(c) $x_1 = 36$ inches (0.91 meter).

Figure 13.- Concluded.
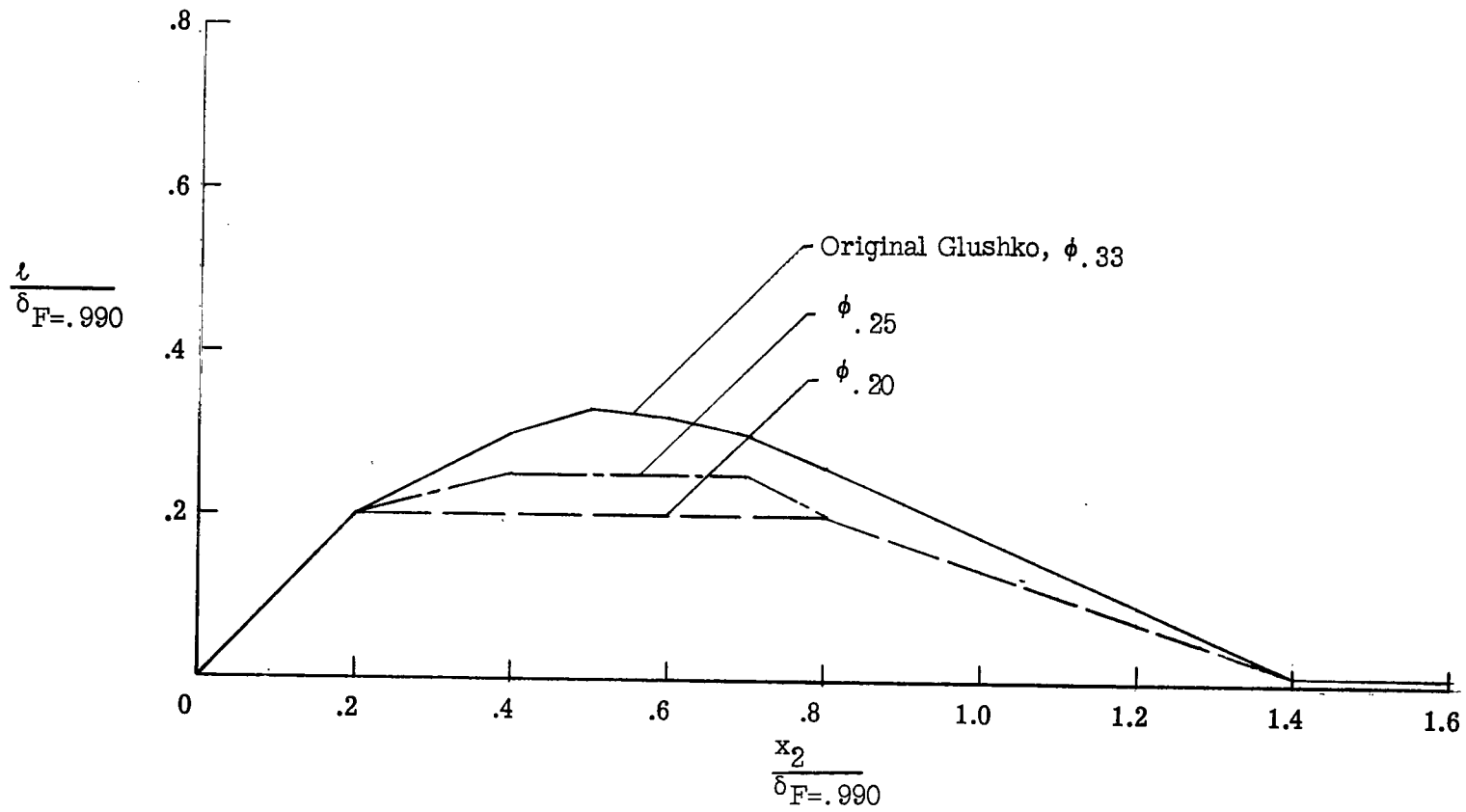
(a) $\frac{l}{\delta}$ functions.

Figure 14.- Turbulence scale and eddy viscosity functions.
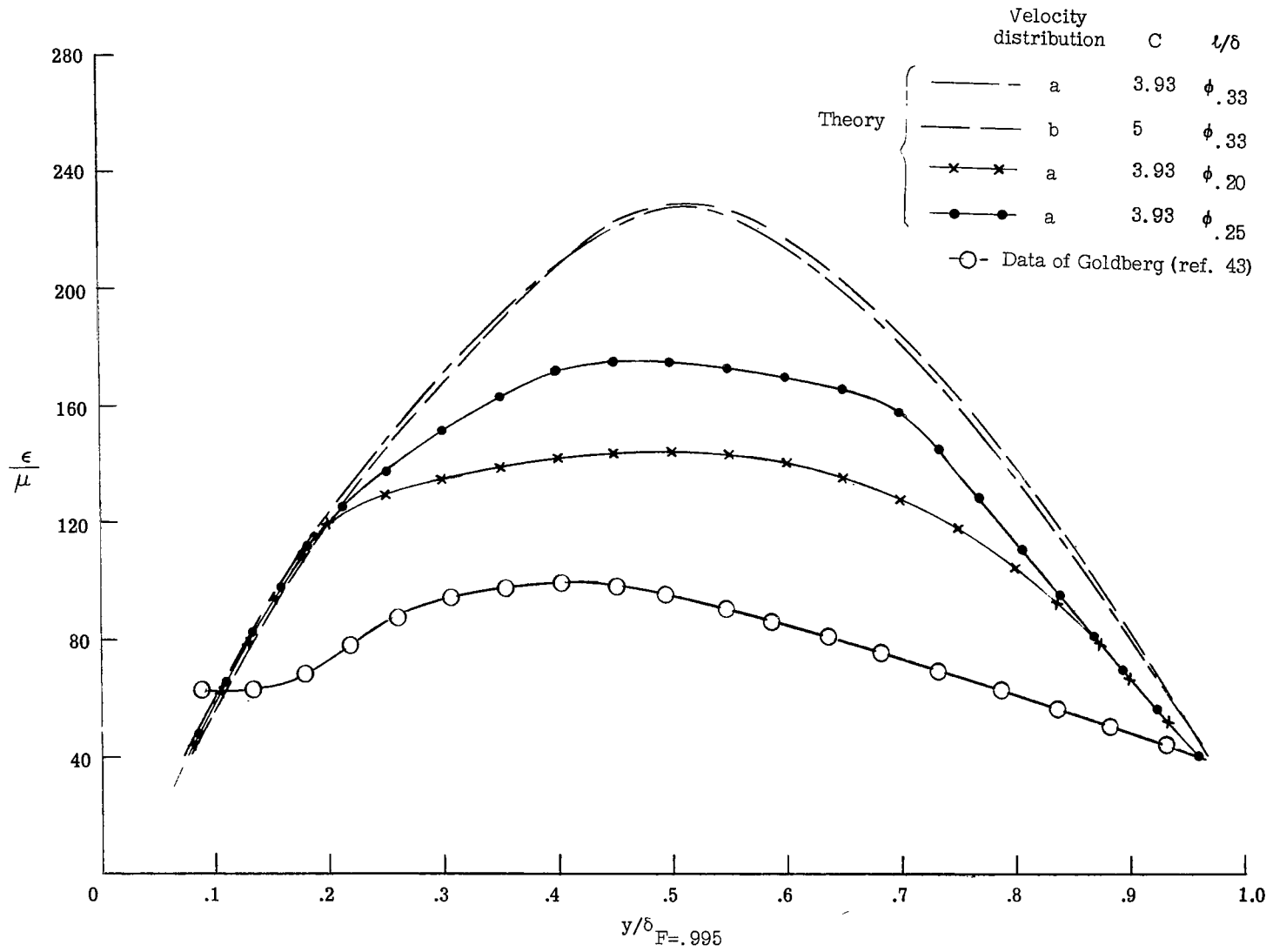
(b) Variation of eddy viscosity at $x_1 = 20$ inches (0.51 meter) compared with values derived by Goldberg from his data.

Figure 14.- Concluded.
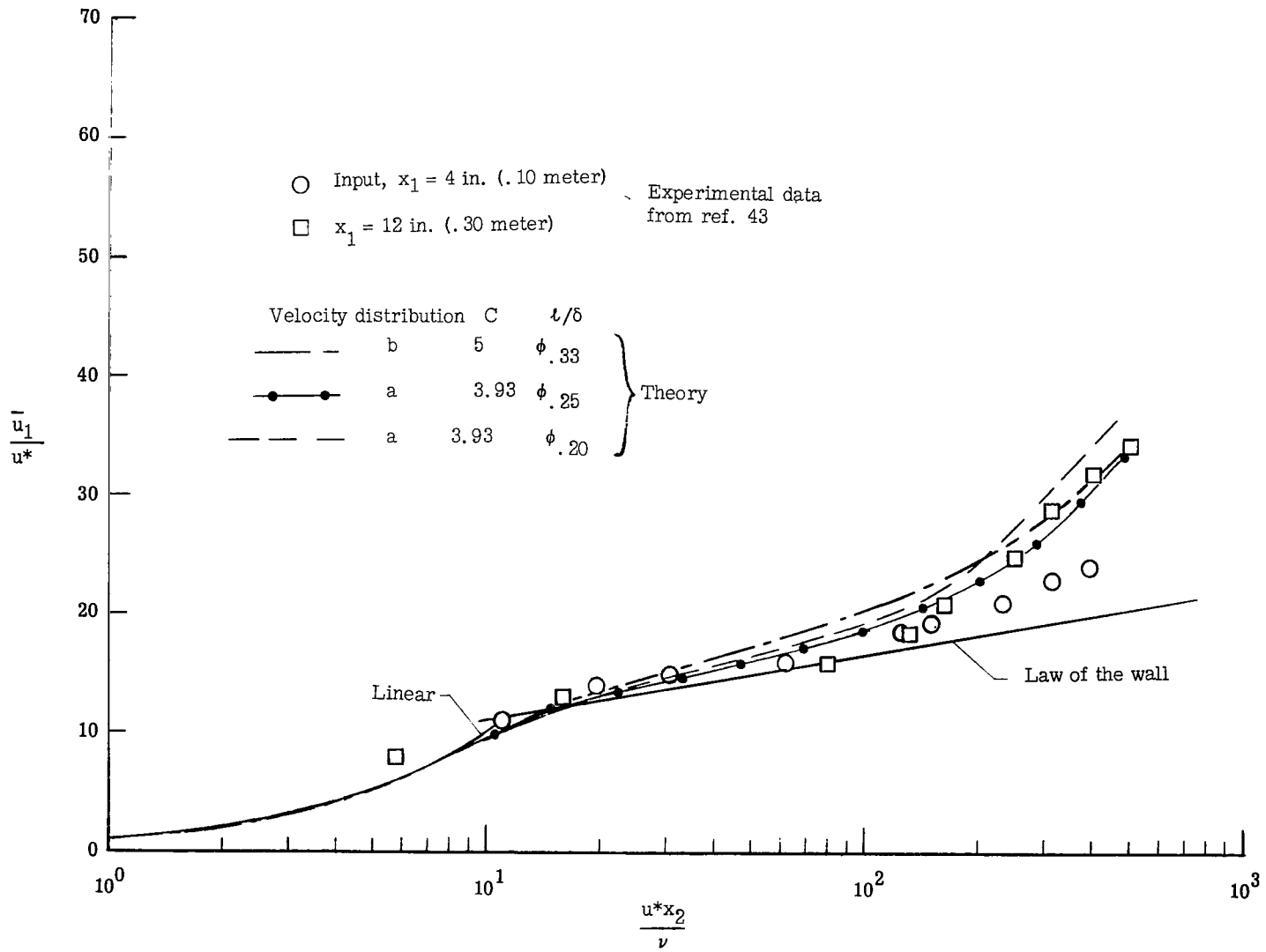
(a) x_1 = 4 inches (0.10 meter) and 12 inches (0.30 meter).

Figure 15.- Comparison of theory-computed and experimental mean velocities in terms of law of the wall.
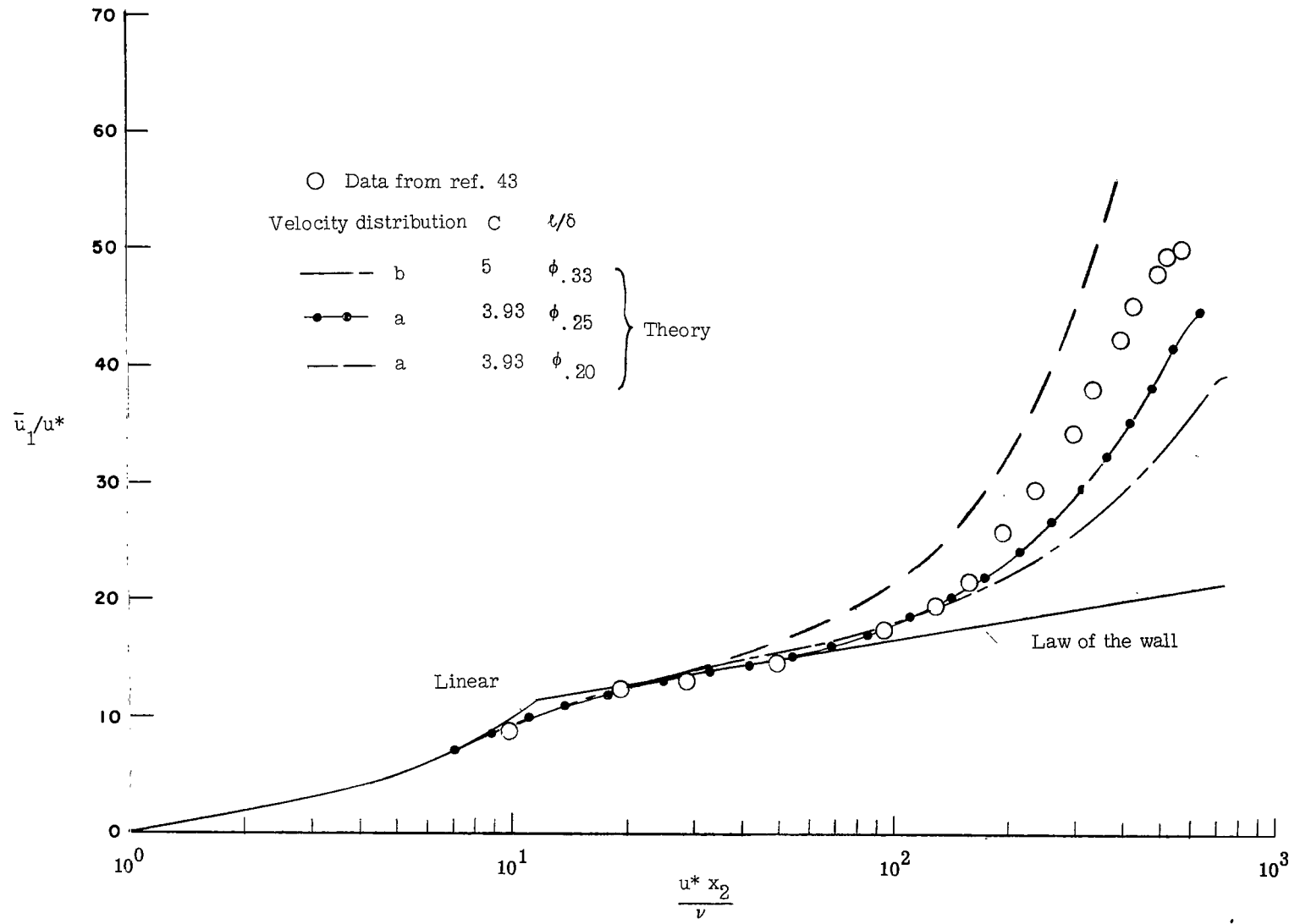
(b) $x_1 = 20$ inches (0.51 meter).

Figure 15.- Continued.
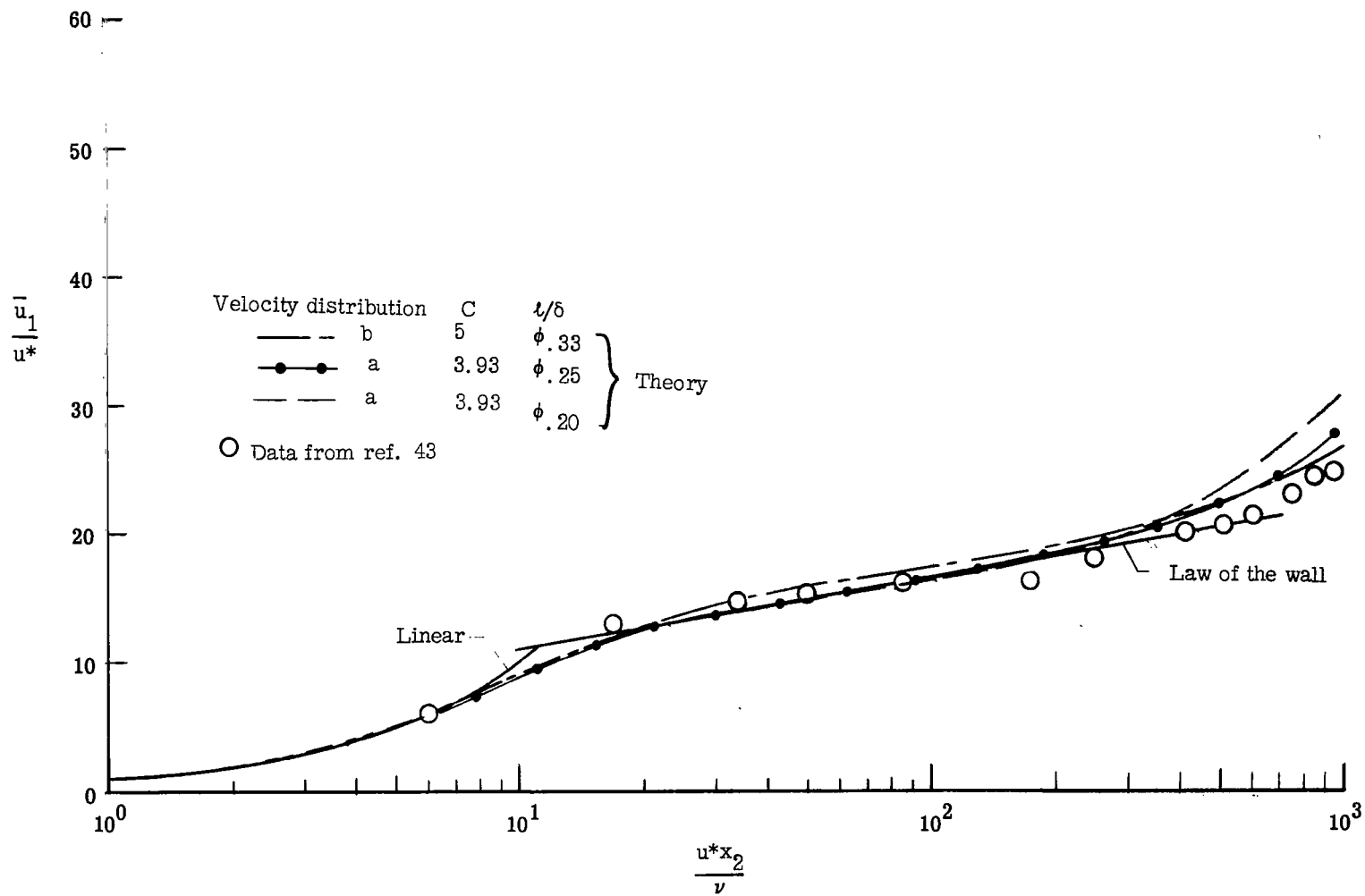
(c) $x_1 = 36$ inches (0.91 meter).

Figure 15.- Concluded.

$$\frac{\tau_T}{2\rho\bar{e}}$$

Experiment

Flow	Ref.	x_1	
Relaxing	43	14 in. (.36 meter)	$\bar{e} \approx \overline{u'_1{}^2}$
○ Relaxing	36	47 in. (1.19 meters)	$\bar{e} \approx \overline{u'_1{}^2}$

Theory
$x_1 = 12$ in. (.30 meter)

| Velocity distribution C	ℓ/δ
a	3.93 $\phi_{.33}$
b	5.00 $\phi_{.33}$
a	3.93 $\phi_{.20}$
a	3.93 $\phi_{.25}$

$x_2/\delta_{F=.995}$
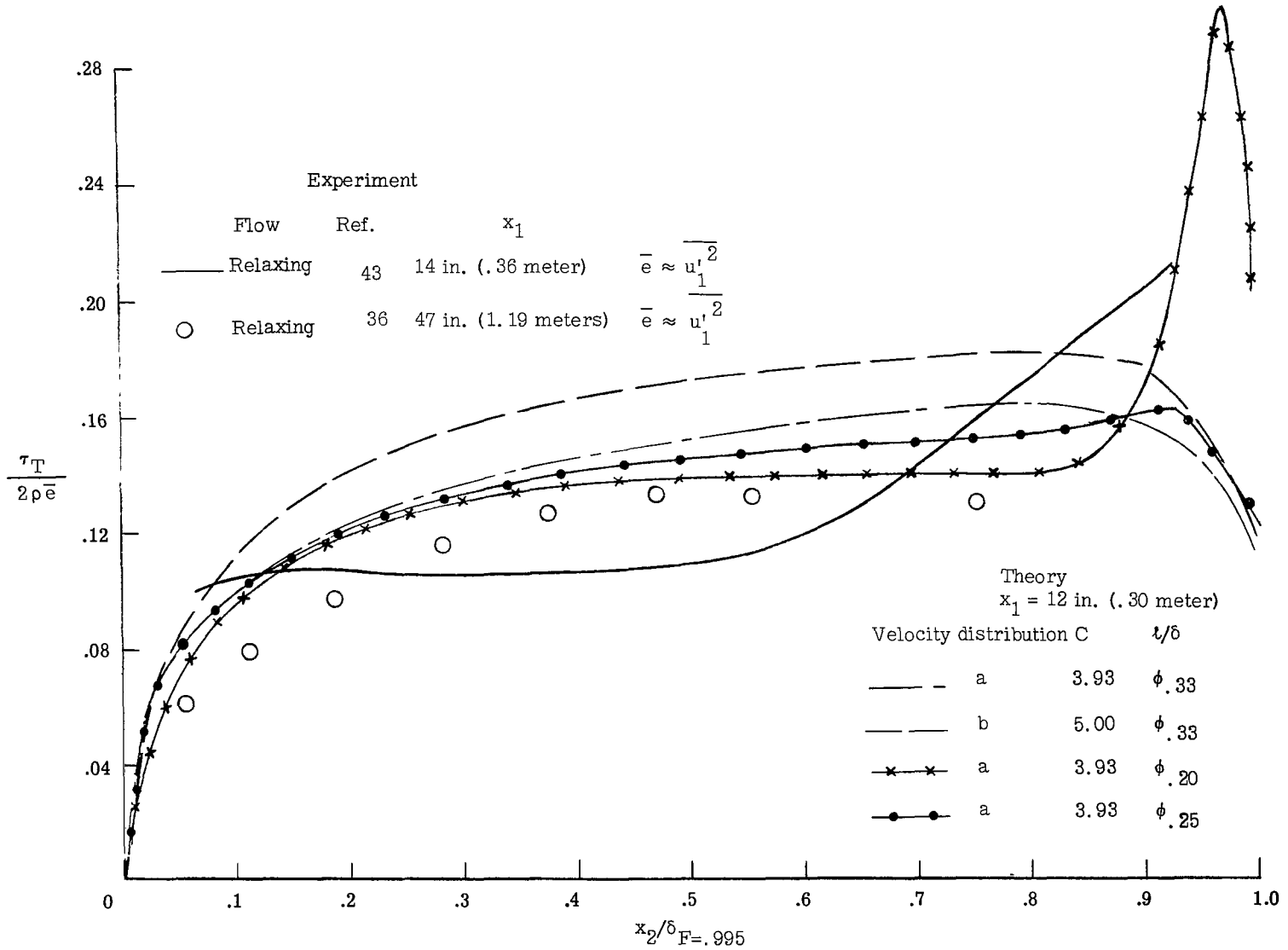
(a) Adverse pressure gradient region.

Figure 16.- Comparison of the ratio of turbulent shear to turbulent kinetic energy from the theory and from the data of references 43 and 36.
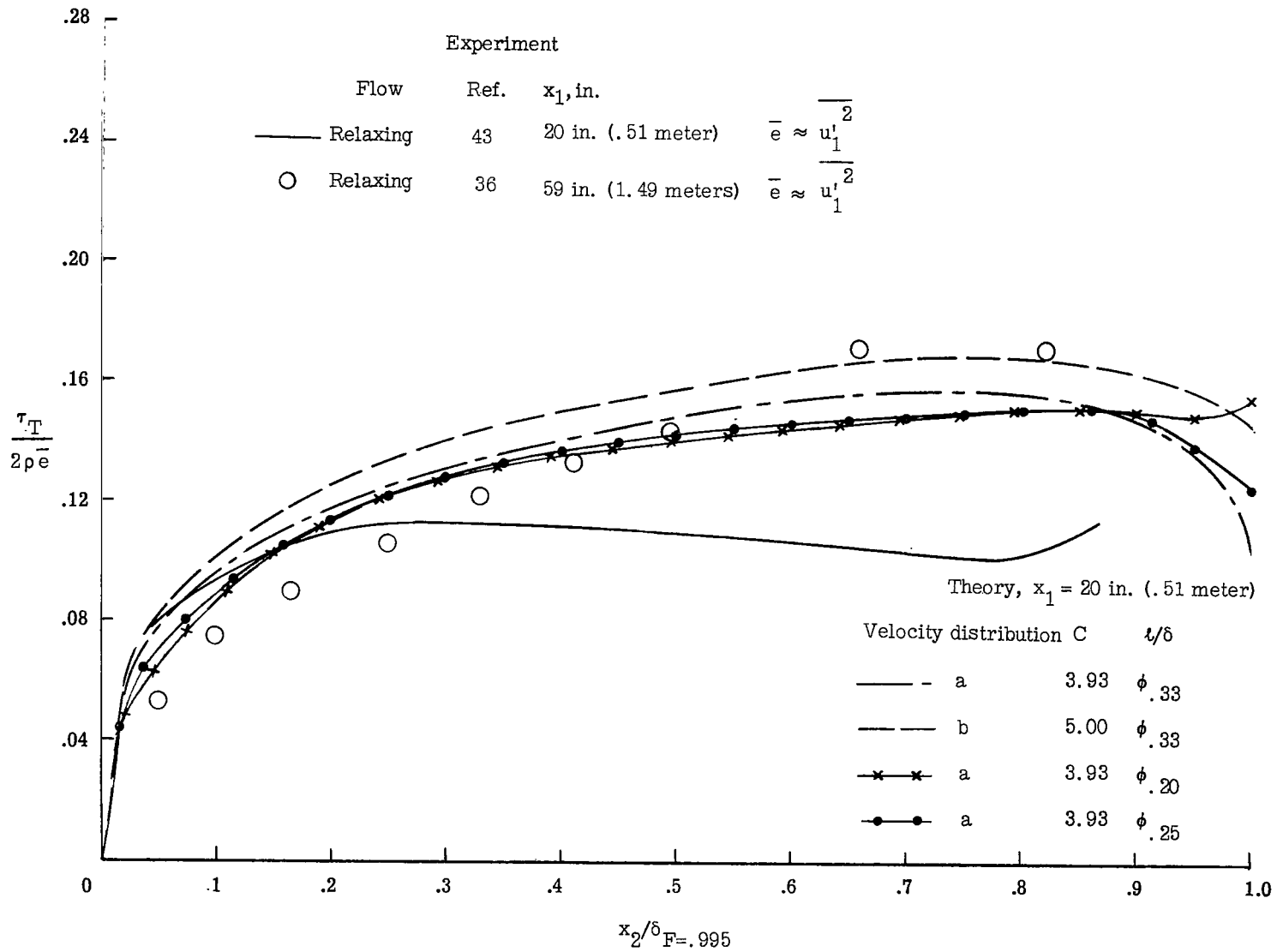
(b) Near end of adverse pressure gradient. x_1 = 20 inches (0.51 meter).

Figure 16.- Continued.

Experiment

Flow	Ref.	x_1	
—— Relaxing	43	36 in. (.91 meter)	$\overline{e} \approx \overline{u_1'^2}$
○ Relaxing	36	95 in. (2.41 meters)	$\overline{e} \approx \overline{u_1'^2}$
□ Flat plate	32		$\overline{e} = \dfrac{\overline{u_1'^2} + \overline{u_2'^2} + \overline{u_3'^2}}{2}$

$$\frac{\tau_T}{2\rho\,\overline{e}}$$

Theory, $x_1 = 36$ in. (.91 meter)

Velocity distribution	C	ℓ/δ
—— a	3.93	$\phi_{.33}$
—— b	5.00	$\phi_{.33}$
—×—×— a	3.93	$\phi_{.20}$
—●—●— a	3.93	$\phi_{.25}$

$x_2/\delta_{F=.995}$
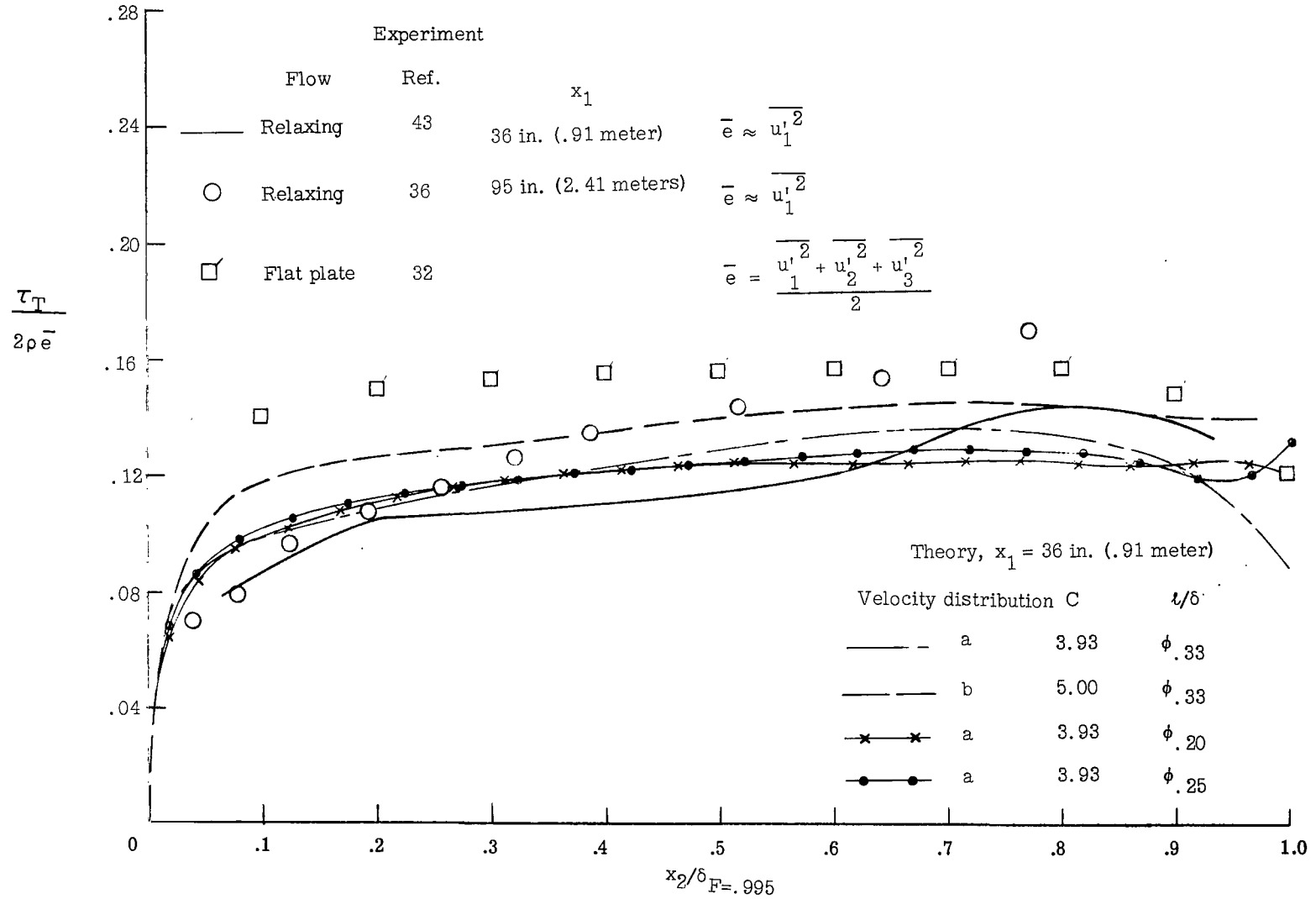
(c) End of constant-pressure run.

Figure 16.- Concluded.

-1.2

-1.0

Loss

-.8   Production $= \left[(M-1)\left(\frac{\partial F}{\partial \eta}\right)^2 \right]$

-.6   Dissipation $= \left[-(2\xi)^{2\bar{n}} C\left(\frac{\nu}{U_e \delta}\right)^2 \frac{DE}{(l/\delta)^2} \right]$

Diffusion $= \left[\frac{\partial}{\partial \eta}\left(D \frac{\partial E}{\partial \eta} \right) \right]$

-.4   Convection $= \left[-\frac{2(2\xi)^{2\bar{n}}}{U_e} \frac{dU_e}{d\xi} EF - V\frac{\partial E}{\partial \eta} - (2\xi)^{2\bar{n}} F \frac{\partial E}{\partial \xi} \right]$

-.2

0

.2

.4

.6

.8

1.0

1.2   Gain

1.4

0   .1   .2   .3   .4   .5   .6   .7   .8   .9   1.0

$x_2/\delta_{F=.995}$
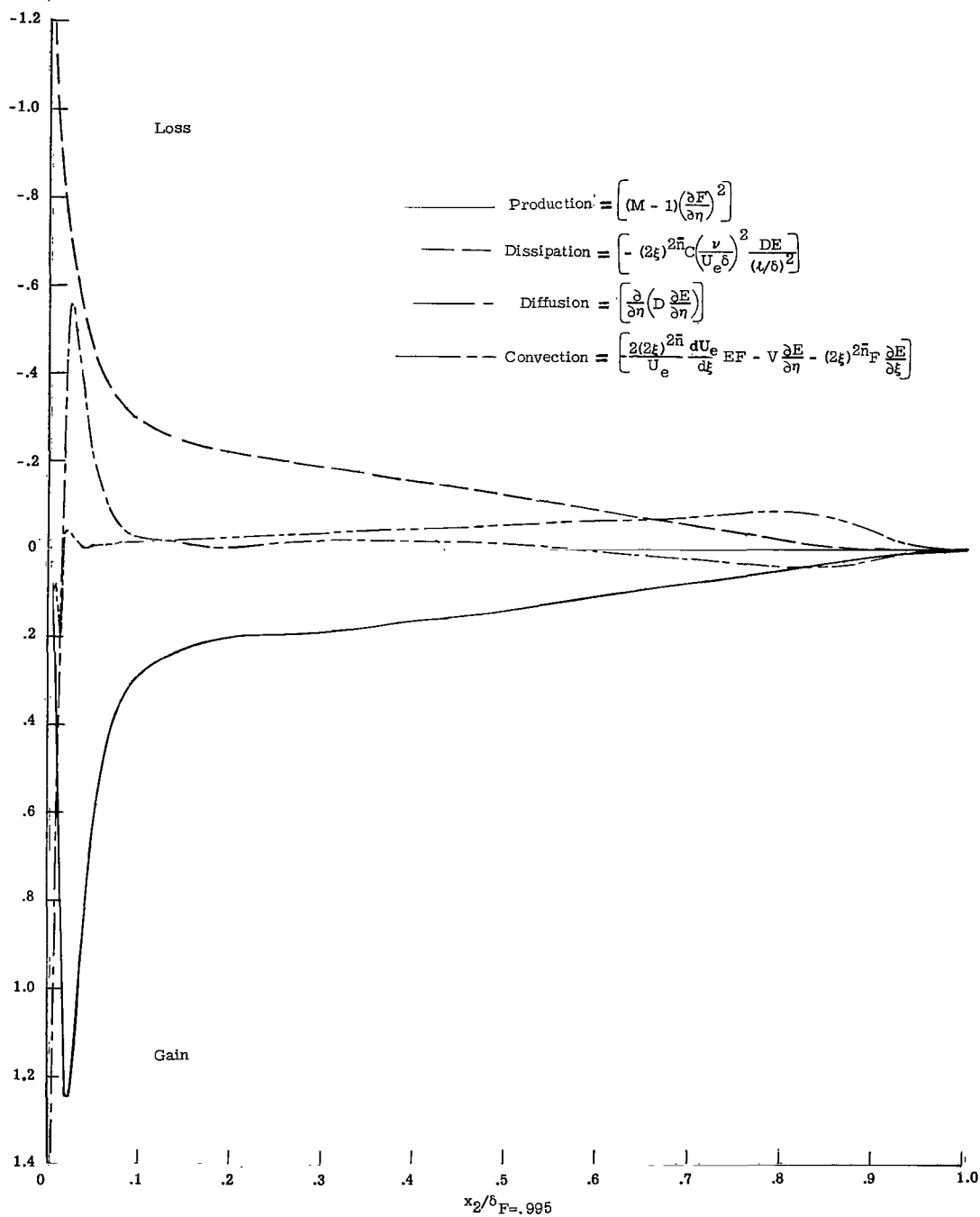
(a) x_1 = 8 inches (0.20 meter).

Figure 17.- Balance of terms in turbulent kinetic energy equation as computed from theory for velocity distribution a (fig. 8). $C = 3.93$ and $\Phi_{0.25}$.

113
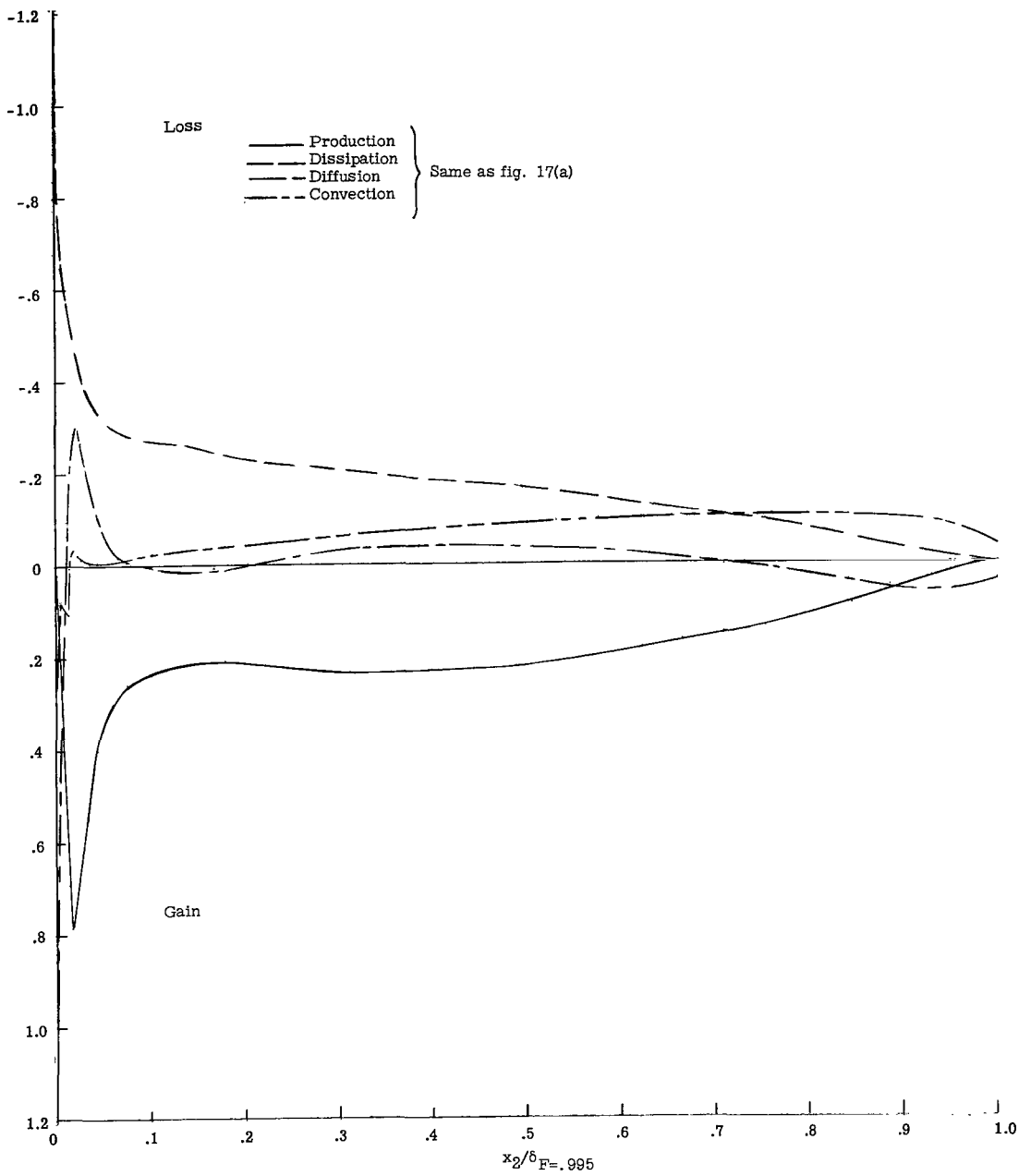
(b) $x_1 = 12$ inches (0.30 meter).

Figure 17.- Continued.
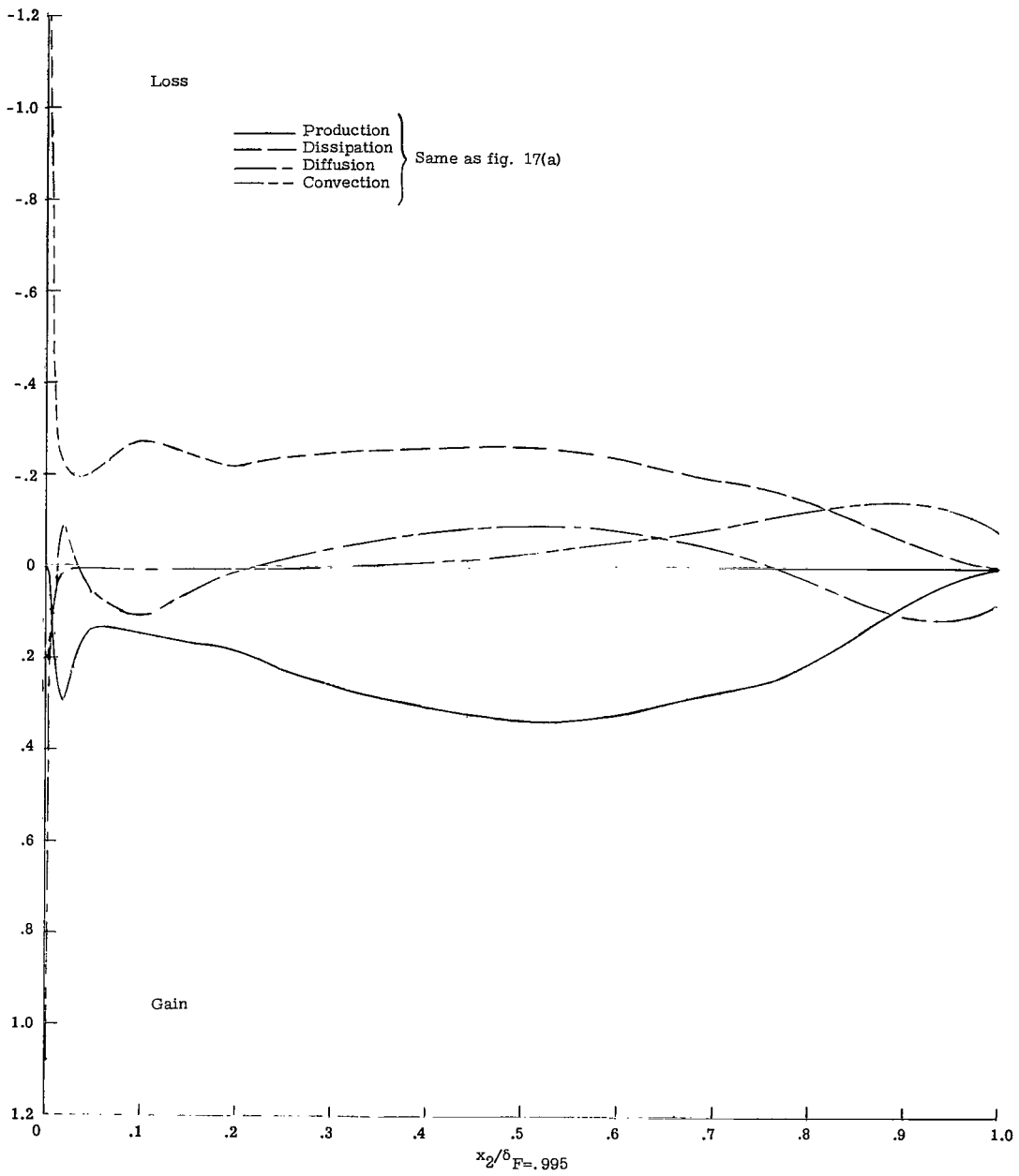
(c) $x_1 = 20$ inches (0.51 meter).

Figure 17.- Continued.
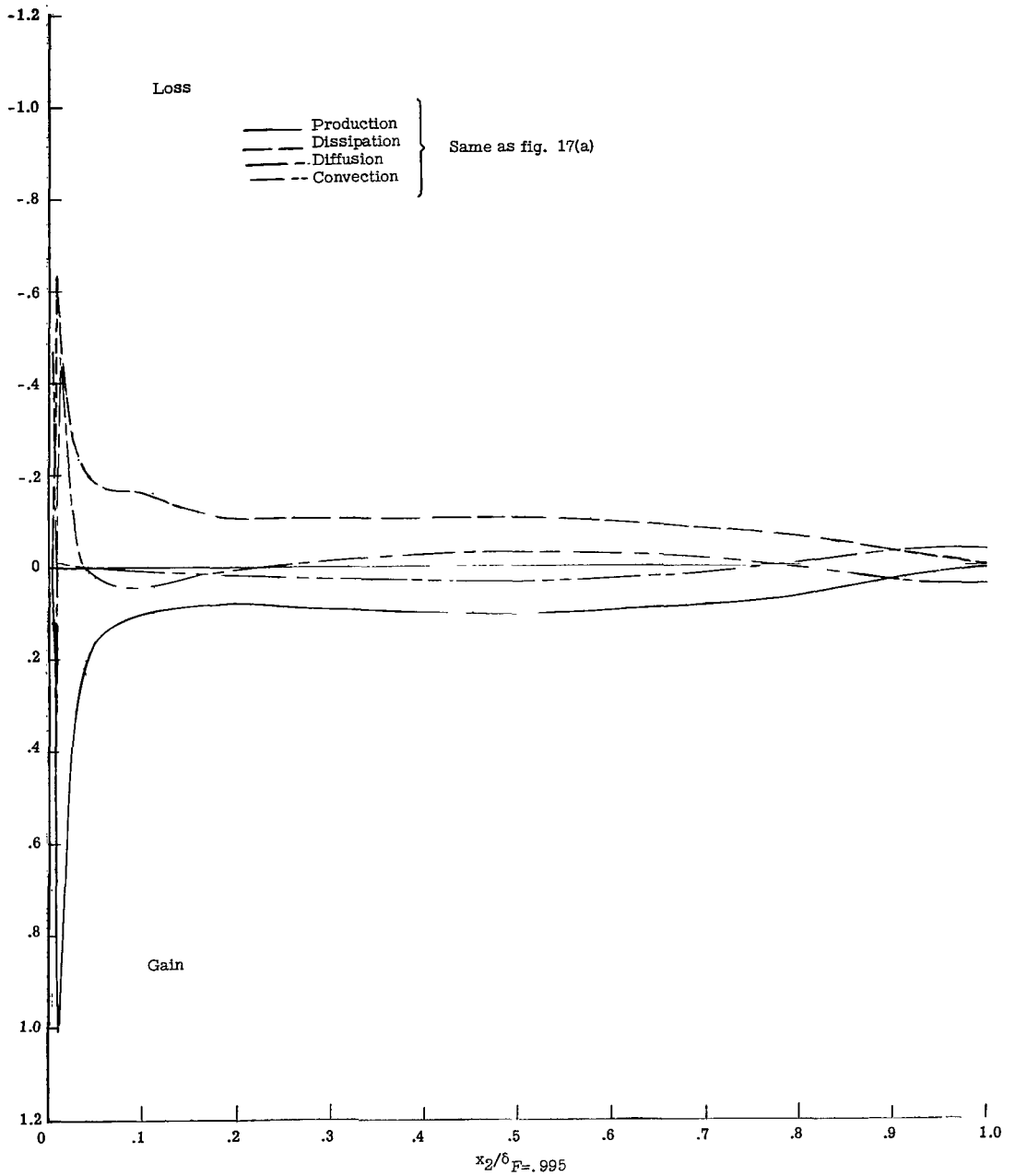
(d) x_1 = 36 inches (0.91 meter).

Figure 17.- Concluded.

"The aeronautical and space activities of the United States shall be conducted so as to contribute . . . to the expansion of human knowledge of phenomena in the atmosphere and space. The Administration shall provide for the widest practicable and appropriate dissemination of information concerning its activities and the results thereof."

— NATIONAL AERONAUTICS AND SPACE ACT OF 1958

NASA SCIENTIFIC AND TECHNICAL PUBLICATIONS

TECHNICAL REPORTS: Scientific and technical information considered important, complete, and a lasting contribution to existing knowledge.

TECHNICAL NOTES: Information less broad in scope but nevertheless of importance as a contribution to existing knowledge.

TECHNICAL MEMORANDUMS: Information receiving limited distribution because of preliminary data, security classification, or other reasons.

CONTRACTOR REPORTS: Scientific and technical information generated under a NASA contract or grant and considered an important contribution to existing knowledge.

TECHNICAL TRANSLATIONS: Information published in a foreign language considered to merit NASA distribution in English.

SPECIAL PUBLICATIONS: Information derived from or of value to NASA activities. Publications include conference proceedings, monographs, data compilations, handbooks, sourcebooks, and special bibliographies.

TECHNOLOGY UTILIZATION PUBLICATIONS: Information on technology used by NASA that may be of particular interest in commercial and other non-aerospace applications. Publications include Tech Briefs, Technology Utilization Reports and Notes, and Technology Surveys.

Details on the availability of these publications may be obtained from:

SCIENTIFIC AND TECHNICAL INFORMATION DIVISION

NATIONAL AERONAUTICS AND SPACE ADMINISTRATION
Washington, D.C. 20546